Phase Transitions and Chemical Reactions in Simple Hydrogen-bonded Molecular Solids under Pressure

（水素結合をもった単純な分子性結晶の圧力誘起相転移と反応）

A Doctoral Thesis

by

Mami Sakashita (Tamaoki)

Submitted to

the Graduate School of Science

Osaka University

November, 2004

Acknowledgments

This research work was carried out at the National Institute of Advanced Industrial Science and Technology, AIST (formerly the National Institute of the Materials and Chemical Research, Agency of Industrial Science and Technology, Ministry of International Trade and Industry). The author would like to express her gratitude to Dr. Katsutoshi Aoki, Japan Atomic Energy Research Institute, Synchrotron Radiation Research Center, Professor Takashi Norisuye and Dr. Fumitoshi Kaneko, Osaka University, for their continuing guidance, discussions, and encouragement throughout the course of this work.

The author also wishes her sincere thanks to Dr. Hiroshi Yamawaki and Dr. Hiroshi Fujihisa, the National Institute of Advanced Industrial Science and Technology, and Professor Hiroyasu Shimizu, Dr. Shigeo Sasaki, and Dr. Tetsuji Kume, Gifu University, for their collaboration and fruitful discussion. Grateful acknowledgement is also made to Dr. Atsuko Nakayama, Advanced Materials Laboratory, National Institute for Materials Science and Ms. Eriko Katoh, for their cordial discussion and encouragement. The author would like to thank her colleagues at the National Institute of Advanced Industrial Science and Technology.

Finally the author thanks her husband for his sincere encouragement in preparing this thesis.

坂下 真実

Mami Sakashita (Tamaoki)

November, 2004

Contents

Chapter 1

General Introduction

Pressure is a thermodynamic parameter of great importance for altering the physical and chemical states of materials as fundamental as temperature. For example, water crystallizes to ice under pressure, as it freezes to ice at low temperature. Because pressure favors the denser state, these ices are not the same; the high-pressure ice has denser structure than low-temperature ice.[1)]

The concept of pressure dates back to Boyle's formulation of his gas laws. Similarly to temperature, pressure has been used routinely to explore the response of chemical systems in varying thermodynamic states, primarily in the gas phase. Much work was done throughout the last century. In 1946 Bridgman[2)] (1882–1961) won the Nobel Prize in Physics for the invention of an apparatus to produce extremely high pressures, and for discoveries in the field of high-pressure physics. He invented the Bridgman anvil apparatus and, over a period of 40 years, he investigated the properties of an enormous variety of materials up to about 3 gigapascals (GPa, equal to 30,000 atomospheric pressures) at room temperature.

In the last few decades, high-pressure experimental techniques have undergone an explosive revolution. [3, 4)] About 30 years ago the static compression data of noble and diatomic gases were limited to several GPa but now the compression of these materials to hundreds of GPa has become common. This advancement has been closely associated with the development of the megabar diamond-anvil cell (DAC),[5)] which has achieved pressures exceeding 5 megabars (500 GPa). The heart of the DAC is a pair of

diamond anvils which squeeze a metal gasket with a hole in which a sample and a ruby (for pressure measurement) are placed in a pressure medium (Figure 1-1). Single-crystal diamonds are used as anvils not only because diamond is the hardest material available, but also because perfect diamonds are transparent to most electro-magnetic radiation over a wide range of wavelength from far infrared to γ-rays. Therefore, diamond anvils are "windows", as well as pressure containers, for *in-situ* measurements of physical properties including X-ray diffraction and optical spectroscopies.[3)]

The number of probing techniques applied for performing *in situ* observations of materials contained in the DAC is continuously growing. Electrical conductivity measurement is well established, providing direct evidence of insulator-to-metal transitions.[6, 7)] Optical studies take advantage of laser beams that can be easily focused on the micrometric samples inside the DAC, and are widely employed. For example, besides or in addition to Raman and Brillouin spectroscopies, both frequency and time resolved laser induced fluorescence have been applied to high-pressure research. Infrared and UV–VIS absorption spectroscopies have become necessary research methods with the DAC, when the access to molecular vibrational and electronic states is required. X-ray diffraction (XRD) is probably the most common investigation approach and is the main source of direct information about the structural changes occurring in the system when the pressure is raised. NMR spectroscopy experiments have also been performed on samples inside the DAC, [8–11)] although the maximum pressure is limited in neutron scattering experiments which still require samples of larger dimensions with respect to those contained in the DAC.[12)]

At present, high pressure provides scientists with a powerful method of tuning the volume of a sample and the consequent properties of that sample

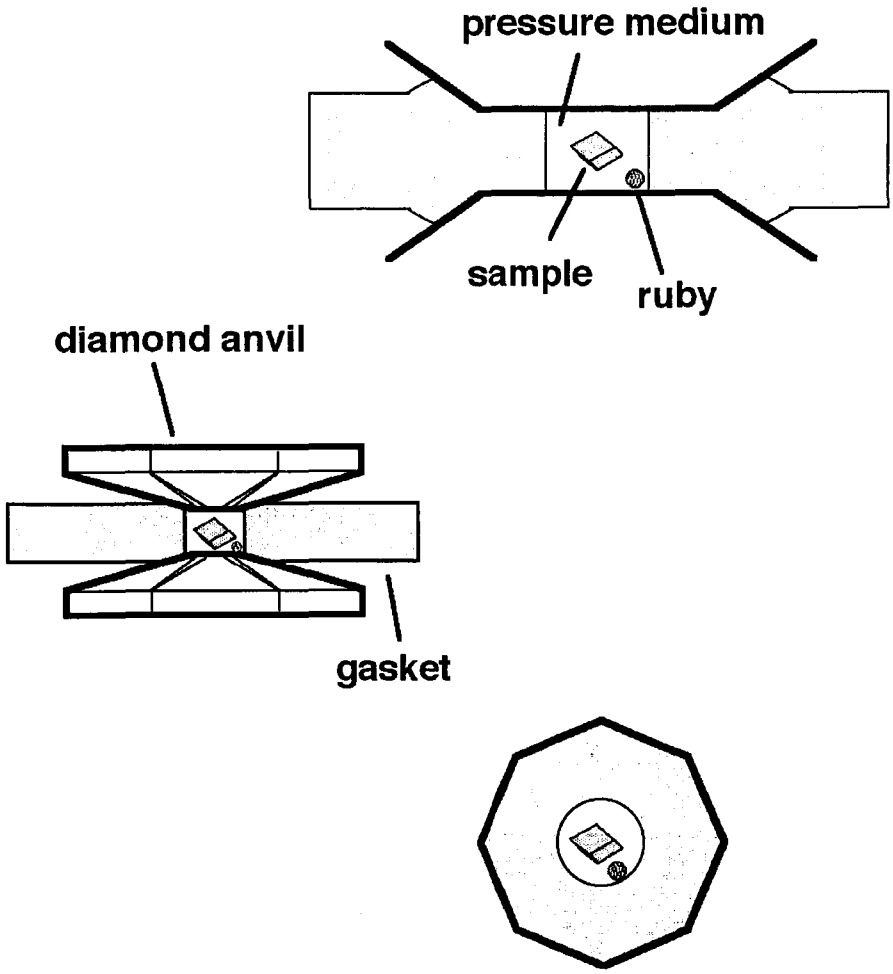

Figure 1-1 The heart of a diamond anvil cell

in a controllable and reversible manner. [2, 3, 13–15] The application of high pressure can produce structural, electronic and other phase transitions, polymerization of organic substances, and many other phenomena. A feature of the modern development of the high-pressure field is the widespread application of high-pressure methods in many branches of physics, chemistry, and biology. The high-pressure techniques, developed in the last few decades, could represent an important tool also for polymer chemistry. As described below, when appropriate conditions are achieved under high pressure a chemical reaction can be induced in crystals or dense fluids of molecules containing unsaturated bonds. The reaction takes place without the use of catalysts, radical initiators or solvents and, in most of the cases, the reactant entirely converts to a product which can be recovered at ambient conditions. The growing need for production methods with a reduced environmental impact invigorates the search for new synthetic approaches in polymer chemistry.

Among a number of high-pressure studies, behavior of molecular materials at high pressure has been one of the most interesting subjects, because large compression can be reached on molecular materials. For instance, in the β phase of solid nitrogen, compression from 0 to 1 GPa results in a volume reduction of 25 %.[16] Moreover, the free-energy change (pressure-volume work) associated with the compression of several hundreds GPa can be more than 10eV, which exceeds the bond energy of the strongest molecular bond. This imparts dramatic changes in chemistry of molecular systems. Because of pressure-induced changes in chemical affinities, the reactivities of otherwise familiar elements and compounds are totally altered, and entirely new classes of materials with unusual combinations of physical properties may be formed.

Molecular materials are characterized by strong intramolecular interactions as opposed to weak intermolecular van der Waals interactions. The compression of a molecular fluid or gas induces phase transitions to a molecular solid. With a further increase in pressure, the intermolecular and intramolecular distances become comparable and typically solid-state reactions take place with accompanying molecular dissociation.

The evolution of molecular bonds towards their ultimate destruction at high density can occur over widely different pressures, depending on bond strengths and intermolecular interactions. For unsaturated bond systems, irreversible reactions generally occur; polymers have been obtained from a number of molecular solids such as carbon disulfide,[17] carbon monoxide,[18] cyanogens C_2N_2,[19] cyanoacetylene H–C≡C–C≡N,[20] and a number of hydrocarbon compounds. For triple- and double-bond aliphatic hydrocarbon molecules, such as acetylene or ethylene, polymerization occurs at relatively low pressures (a few GPa).[21–26] Aromatic compounds are expected to be more stable; pentacene was observed to polymerize around 30 GPa[27, 28] and benzene around 23 GPa.[29–34] On the other hand, for saturated bond systems, transition to atomic structure sometimes occur. For example, iodine undergoes a pressure-induced insulator-metal transition near 16 GPa, [35, 36] and methane breaks down to form diamond at pressures between 10 and 50 GPa and temperatures of about 2000 to 3000 K.[37]

Behavior of hydrogen bond under pressure is a very interesting subject, because high pressure provides a means of controlling the length of the hydrogen bonds in order to investigate the potential energy curves of hydrogen-bonded protons. In other words, pressure is the most important external parameter to examine the effect of hydrogen bond on physical property and crystal structure of molecular materials. A hydrogen bond is a

type of attractive intermolecular force that exists between two partial electric charges of opposite polarity. Although it is stronger than most other intermolecular forces, the hydrogen bond is much weaker than both the ionic bond and the covalent bond. The hydrogen bond possesses some degree of orientational preference, not like a simple attraction between point charges. It can exist between two parts of the same molecule and figures as an important constraint on such molecules' overall shape within macromolecules such as proteins and nucleic acids.

High-pressure behavior of ice is fundamental to a number of problems in chemistry and physics for a long time. In particular, much works has focused on the behavior of hydrogen bond in ice under compression. For example, Pauling suggested that the shrinkage of the distance between oxygens in an O–H–O linkage to 2.35 Å would produce symmetric hydrogen bonding.[38] In the symmetric state the proton lies midway between the two oxygens. Extending Pauling's earlier conjecture, Holzapfel provided a simple model based on a double Morse potential, estimating a transition pressure of 35–80 GPa, or a critical O–O distance of 1–2.44 Å.[39] Recent development of high-pressure technique enables us to observe directly hydrogen-bond symmetrization of ice.

The purpose of the present work is to clarify the nature of chemical bonds, especially the reactivity of covalent bonds and the role of intermolecular hydrogen bonds under pressure. As previously mentioned, the development of the diamond-anvil cell enables us to reach more than 100 GPa and to provide crucial information on the behavior of hydrogen-bonded materials. In this thesis, three systems having strong or weak hydrogen bonds, ice (H_2O), hydrogen sulfide (H_2S), and acetylene (C_2H_2), were selected (Table 1-1), and the phase transitions and chemical reactions of these systems

are examined under pressure. Simple molecular systems were selected, because the simple systems are useful to characterize the reaction processes and to compare experimental results with theoretical calculations. One system was ice, the most typical hydrogen-bonded molecular solid. As mentioned above, there has been considerable interest in the hydrogen-bond in ice under pressure. In ice, every H_2O molecule is H-bonded with four other molecules (two through its two lone pairs, and others through its two hydrogen atoms). In high-pressure ice, the hydrogen-bond symmetrization was expected to observe using megabar DAC. Another system is hydrogen sulfide, a sister molecule of ice having weaker hydrogen bonds than ice. The high-pressure behavior of hydrogen sulfide was compared with that of ice. An understanding of the differences in high-pressure behavior between H_2O and H_2S will provide insights into the nature of chemical bond. Still another is acetylene, the simplest molecule having C≡C triple bond and very weak hydrogen bond. Acetylene was chosen because it was reported that hydrogen bond plays an important role in chemical reaction of acetylene under pressure.[21)]

Most of the experimental information concerning the reaction of simple molecular systems under pressure has been gained by vibrational spectroscopy.[40)] Thus, infrared absorption spectroscopy with DAC was mainly used in this thesis. Infrared spectroscopy is often preferable to Raman spectroscopy since the measurement technique does not interfere with the reaction. In Raman spectroscopy the strong excitation light source can drastically affect the reaction evolution and the kind of reaction products. Furthermore, in constant pressure experiments the sample thickness is assumed to be fixed, and the measurement of the intensity of the absorption bands offers a direct determination of the amount of transformed material.

Table 1-1 Comparison among H_2O, H_2S, and C_2H_2

	Hydrogen bond	Number of unsaturated bond
H_2O	strong	zero
H_2S	weak	zero
C_2H_2	weak	one (C≡C triple bond)

This thesis is constructed with the following chapters concerning pressure-induced phase transitions and chemical reactions of the simple molecular materials.

In Chapter 2, Infrared spectroscopy with a large optical-aperture diamond anvil cell will be presented. The DAC for Infrared spectroscopy should be designed to meet precise requirements simultaneously, regarding its optical characteristics and its high-pressure performance.[41] The design of DAC, the characteristics of diamond anvils, the monitoring method of high pressure, and the infrared and Raman systems will be explained in this chapter.

In Chapter 3, hydrogen-bond symmetrization of ice will be surveyed using Infrared spectroscopy. Identification of such a transition has been inconclusive because of the difficulty of the H sublattice at the requisite pressures.[42, 43] Fortunately, vibrational spectroscopy provides crucial information on the behavior of ice at ultra-high pressure, in particular, the evolution of hydrogen bonds. The transition was finally identified by infrared spectroscopy near 60 GPa.

In Chapter 4, high-pressure behavior of hydrogen sulfide will be explained. Hydrogen sulfide, H_2S, is a chemical analogue of H_2O ice, but in spite of this basic similarity, there are significant difference in features such as the strength of hydrogen bonding and the phase diagram. For example, H_2O molecules are packed tightly via hydrogen-bonded networks, while H_2S exhibits rotational molecular disorder at low pressure solid phase.[29] Moreover, molecular dissociation instead of hydrogen-bond symmetrization was observed in H_2S under pressure.

In Chapter 5, molecular dissociation of deuterium sulfide under pressure will be discussed. The D_2S sample enables us to assign vibrational

peaks through the isotopic shift and to get further information about molecular dissociation. The experiments suggest that H_2S and D_2S have the tendency toward decomposition to the elements and that sulfur plays an important role in molecular dissociation.

In Chapter 6, the high-pressure behavior of sulfur was investigated by infrared spectroscopy in comparison with H_2S and D_2S. In the sulfur study, Infrared spectroscopy takes an advantage of avoiding the laser-induced phase transitions. Sulfur is a molecular material consisting of puckered S_8 molecules at ambient and low pressures. The ring structures remain essentially undistorted to 10 GPa, but progressively larger rings form with increasing pressure, and metastable amorphous phases and photochemically induced structures may be produced.[44] The investigation of H_2S and D_2S suggested that new S–S bonds will form under pressure, thus, pressure-induced polymerization reaction would be expected for sulfur.

In Chapter 7, phase transitions and chemical reactions of acetylene under pressure will be discussed. The high-pressure polymerization of acetylene was firstly reported by Aoki *et al.* monitoring the room temperature reaction by Raman spectroscopy.[21] However, the Raman spectra of polyacetylene are very sensitive to resonance enhancement and this could make the identification of the reaction products uncertain. To cope with this problem the reaction was investigated by infrared spectroscopy.

In Chapter 8, summary and conclusions will be presented.

References

1) V.F. Petrenko and R.W. Whitworth, "*Physics of Ice*", Oxford University Press. NY (1999).

2) P.W. Bridgeman, "*Physics of High Pressure*", G. Bell and Sons Ltd. (1949).

3) M.I. Eremets, "*High Pressure Experimental Methods*", Oxford Unversity Press (1996).

4) J.D. Barnett, S. Block, and G.J. Piermarini, *Rev. Sci. Instrum.*, **44**, 1 (1973).

5) H.K. Mao and P.M. Bell, *Science*, **200**, 1145 (1978).

6) M.I. Eremets, E.A. Gregoryanz, V.V. Struzhkin, H.K. Mao, R.J. Hemley, N. Mulders, and N. M. Zimmerman, *Phys. Rev. Lett.*, **85**, 2797 (2000).

7) K. Shimizu, K. Suhara, M. Ikumo, M.I. Eremets, and K. Amaya, *Nature*, **393**, 767 (1998).

8) A.S. Balchan and H.G. Drickamer, *J. Chem. Phys.* **34**, 1948 (1961).

9) K. Syassen, K. Takemura, H. Tups, A. Otto, "*Physics of Solids under Pressure*," edited by J.S. Schilling and R.N. Shelton, Amsterdam, North-Holland, 125 (1981).

10) L.R. Benedetti, J.H. Nguyen, W.A. Caldwell, H. Liu, M. Kruger, and R. Jeanloz, *Science*, **286**, 100 (1999).

11) K. Aoki, H. Yamawaki, and M. Sakashita, *Phys. Rev. Lett.* **76**, 784 (1996).

12) P.F. McMillan, *Nat. Mater.*, **1**, 19 (2002).

13) S.M. Sharma and S.K. Shikka, *Prog. Mat. Sci.*, **40**, 1 (1996).

14) R.J.Hemley, *Annu. Rev. Phys. Chem.*, **51**, 763 (2000).

15) V. Schettino and R. Bini, *Phys. Chem. Chem. Phys.*, **5**, 1951 (2003).

16) T. A. Scott, *Phys. Rep.*, **27**, 89 (1976).

17) H.J. Jödl, F. Bolduan, and H.D. Hochheimer, *J. Chem. Phys.* **84**, 6997 (1986).

18) A.I. Katz, D. Schiferl, and R.L. Mills, *J. Phys. Chem.* **88**, 3176 (1984).

19) C.S. Yoo and M. Nicol, *J. Phys. Chem.* **90**, 6726, 6732 (1986).

20) K. Aoki, Y. Kakudate, M. Yoshida, S. Usuba, and S. Fujiwara, *J. Chem. Phys.*, **91**, 778 (1989).

21) K. Aoki, S. Usuba, M. Yoshida, Y. Kakudate, K. Tanaka, S. Fujiwara, *J. Chem. Phys.*, **89**, 529 (1988).

22) K Aoki, Y. Kakudate, M. Yoshida, S. Usuba, K. Tanaka, and S. Fujiwara, *Sol. State Commun.* **64**, 1329 (1987).

23) M. Sakashita, H. Yamawaki, and K. Aoki, *J. Phys. Chem.*, **100**, 9943 (1996).

24) M. Ceppatelli, M. Santoro, R. Bini, and V. Schettino, *J. Chem. Phys.*, **113**, 5991 (2000).

25) C.C. Trout and J.V. Badding, *J. Phys. Chem.* **104**, 8142 (2000).

26) H. Wieldraaijer, J.A. Schouten, and N.J. Trappeniers, *High Temp.–High Press.* **15**, 87 (1983).

27) H.G. Drickamer and C.W. Frank, "Electronic Transitions and the High Pressure Chemistry and Physics of Solids," Chapmann and Hall, London (1973).

28) H.G. Drickarmer, *Science*, **156**, 1183 (1967).

29) Ph. Pruzan, J.C. Chervin, M.M. Thiery, J.P. Itié, J.M. Besson, J. P. Forgerit, and M. Revault, *J. Chem. Phys.*, **92**, 6910 (1990).

30) J.M. Besson, M.M. Thiery, and Ph. Prizan, "*Molecular Systems Under High Pressure*," edited by R. Pucci and G. Piccitto, Elsevier, Amsterdam, 341 (1991).

31) M. Gauthier, J.C. Chervin, and Ph. Pruzan, "*Frontiers of High Pressure Research*," edited by H.D. Hochheimer and R.D. Etters, Plenum, New York, 87 (1991).

32) F. Cansell, D. Fabre, and J.P. Petitet, *J. Chem. Phys.*, **99**, 7300 (1993).

33) L. Ciabini, M. Santoro, R. Bini, and V. Schettino, *J. Chem. Phys.*, **116**, 2928 (2002).

34) L. Ciabini, M. Santoro, R. Bini, and V. Schettino, *Phys. Rev. Lett.*, **88**, 085505 (2002).

35) A.S. Balchan and H.G. Drickamer, *J. Chem. Phys.* **34**, 1948 (1961).

36) K. Syassen, K. Takemura, H. Tups, A. Otto, "*Physics of Solids under Pressure*," edited by J.S. Schilling and R.N. Shelton, Amsterdam, North-Holland, 125 (1981).

37) L.R. Benedetti, J.H. Nguyen, W.A. Caldwell, H. Liu, M. Kruger, and R. Jeanloz, *Science*, **286**, 100 (1999).

38) L. Pauling, "*The Nature of the Chemical Bond*" Itaca, NY: Cornell University Press (1960).

39) W.B. Holzapfel, *J. Chem. Phys.*, **56,** 712 (1972).

40) R. Bini, in High Pressure Phenomena, ed. G. L. Chiarotti, M. Bernasconi, L. Ulivi, and R. J. Hemley, International School of Physics "Enrico Fermi" IOS press, Amsterdam, 2002, vol. 147, p. 455.

41) J.C. Chervin, B. Canny, J.M. Besson, and Ph. Pruzan, *Rev. Sci. Instrum.* **66**, 2595 (1995).

42) A. Polian and M. Grimsdich, *Phys. Rev. Lett.*, **52**, 1312 (1984).

43) K.R. Hirsh and W.B. Holzapfel, *J. Chem. Phys.*, **84**, 2771 (1986).

44) B. Eckert, R. Schumacher, H. J. Jodl, and P. Foggi, *High Pressure Research*, **17**, 113 (2000).

Chapter 2

Infrared Spectroscopy with a Diamond Anvil Cell

2-1. Introduction

Infrared spectroscopy is an immense field of study of low-energy excitation in matter. Primarily it concerns phonons and molecular vibrations. Low-energy electron states such as impurity levels in semiconductors, inter-band transitions, superconductor gap transitions, and many other phenomena are studied by infrared spectroscopy. This is a very important technique complementary to Raman scattering, which has different selection rules. A combination of infrared and Raman studies has clearly shown that the phase transition of hydrogen at 150 GPa is connected with discontinuous change occurring in the intramolecular vibration.[1, 2)]

Infrared spectroscopy was comparatively less used than other methods in very high-pressure studies until 1990s. For instance, Ferraro[3)] and Johannsen[4)] discussed the problems of interfacing a diamond anvil cell (DAC) with an infrared spectrometer, or an interferometer. The main cause of the difficulty is the low efficiency of incident infrared radiation. The standard beam diameter at a commercial spectrometer is several mm at the sample stage, whereas the gasket hole of the DAC measures 300 μm or less in diameter. Hence, the gasket hole acts like a diaphragm and the most part of the incident beam is stopped by it without being used for infrared measurements. There are several attempts to carry out infrared study without any focusing optics.[5-7)] However, it is necessary for the infrared measurement using a 50-μm or less diameter gasket hole at high pressures, say, at 100GPa, to use a focusing device that improves vastly the signal-to-noise ratio.

Various devices have been used as focusing optics: KBr, CaF_2, NaCl lenses and beam condensers consisting of aspherical mirrors[3] or on-axis Cassegrain-type beam condensers.[8] This latter device, which is used in the present work, is the most convenient for optical adjustments. Contrary to the lenses, the Casegrain-type beam condenser consisting of mirrors is free from the refractive index dispersion, and therefore, it gives access to a wide spectral range. However, such condenser optical system requires sufficiently large optical apertures which are unfavorable for the DAC with respect to its mechanical strength. Namely, the DAC used for infrared spectroscopy is designed so as to make the best compromise between the two opposite requirements, large optical aperture and good mechanical stability. Recently, the membrane diamond anvil cell with an internal membrane unit and other kinds of miniature cells have also been designed for infrared spectroscopy.[9,10]

This chapter is allocated to the description about the instrumentation that the author used for vibrational spectroscopy under high pressures. The DAC, the characteristics of diamond anvils and the monitoring method of high pressure will be described. Then, the infrared and Raman systems with this cell will be presented. The performances and possibilities of the systems will be described in Chapters 3 to 7.

2-2. Diamond Anvil Cell for Infrared Spectroscopy

2-2-1. Small Diamond Anvil Cell

The pressure cell described here was designed and built to meet precise requirements simultaneously, regarding its optical characteristics and its high-pressure performance. The following are the requirements for the DAC

by the optical path of the Cassegrain optics (see Figure 2-8).

(1) The optical aperture of both sides of the DAC must be greater than or equal to that of the Cassegrain mirror; it is 2 × 23.5° here.

(2) The thickness of the DAC must be less than twice the working distance of the Cassegrain, here: 2x20 mm.

(3) The sample-side faces of two diamond anvils must be kept parallel to each other under a load. This is required to achieve high pressure.

The above requirements can be solved using a small diamond anvil cell (Figures 2-1 and 2-2) and a gearbox (Figure 2-3). The cell has a piston-cylinder assembly, combined with the hemispherical tungsten carbide seats as diamond mount plates on the body. The total height of the cell is 30 mm (or 20 mm) and the optical aperture of the tungsten carbide seat is 50°, which fulfill the requirements (1) and (2). The cell has guiding pins to prevent the piston from rotating and to keep a clearance of 10μm between the fixed and movable pistons. A load is applied with the aid of the gearbox, which fulfill the requirements (3), and it is fixed with three clamping screws of the cell. Owing to the mechanical stability and excellent parallelism between diamond anvils, the pressures up to 100 GPa were easily obtained with this cell and gearbox.

2-2-2. Selection of Diamond Anvils

The diamond anvils are type IIa stones (nitrogen free) whose infrared absorption bands lie in the range 1800–2600 cm^{-1} (two-phonon spectrum of the diamond) as shown in Figure 2-4. For the present studies the anvils had a standard Drukker shape or a beveled cut shape. As shown in Figure 2-5, a standard Drukker shape with culet diameter of 0.3–0.5 mm, 1–1.2 mm height, and 2–3 mm table diameter, was used up to 50 GPa, and a beveled cut shape

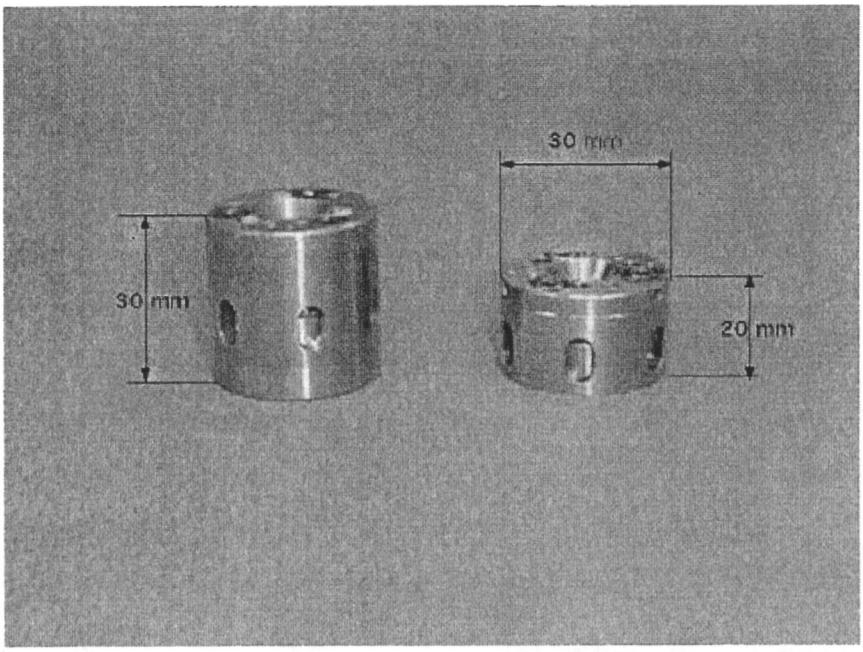

Figure 2-1. Photograph of small diamond anvil cell designed for infrared microspectroscopy. The total height of the cell is 30 mm (left-hand side) and 20 mm (right-hand side).

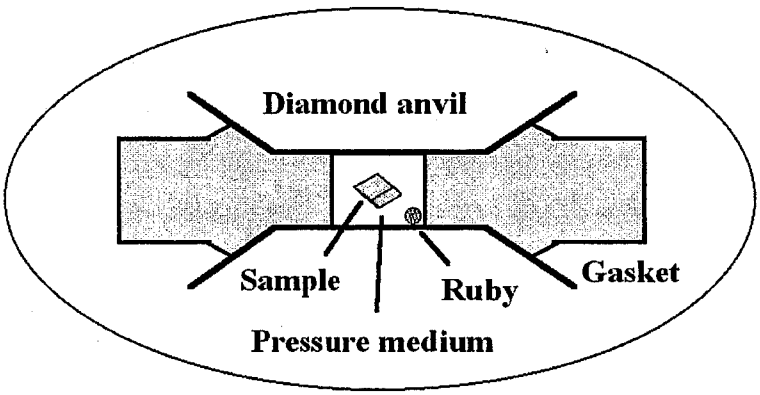

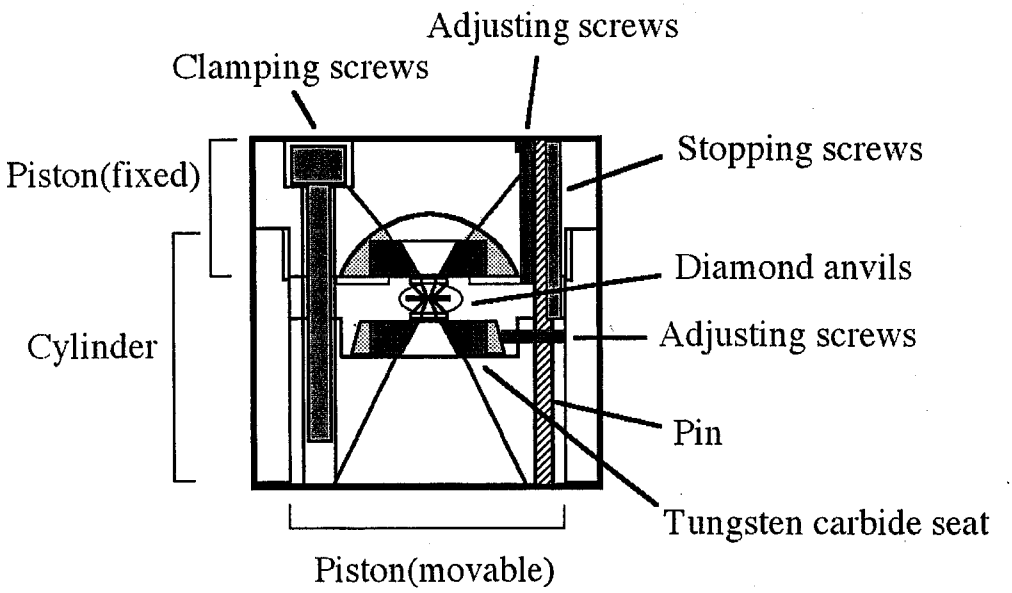

Figure 2-2. A horizontal section view of a small diamond anvil cell designed for infrared microspectroscopy.

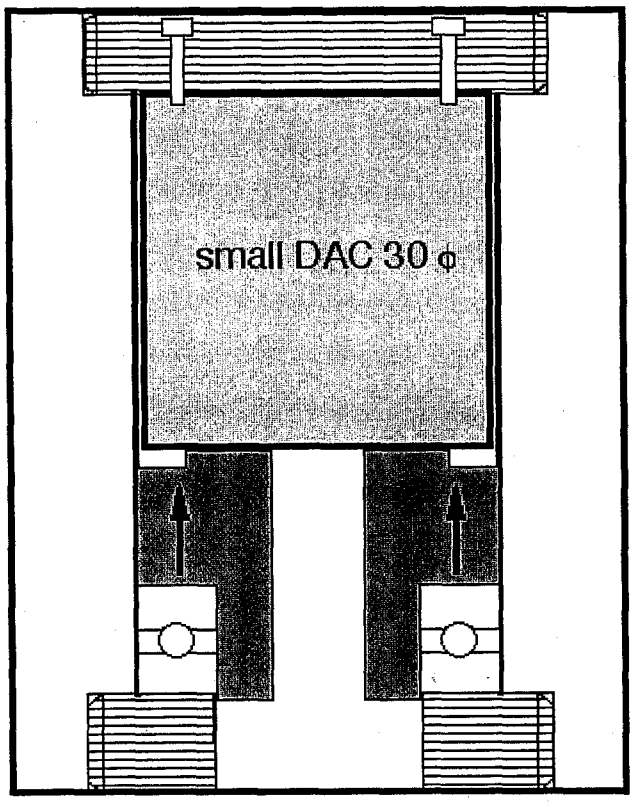

Figure 2-3. Gearbox for loading. The small DAC is set inside this gearbox.

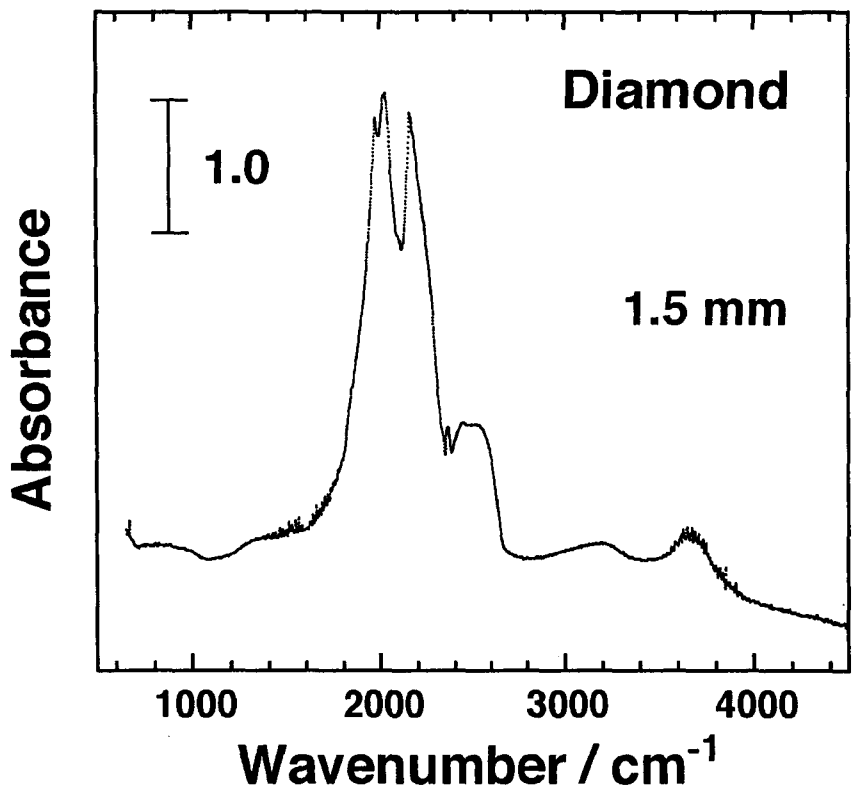

Figure 2-4. Infrared absorption spectra of type IIa diamond anvils.

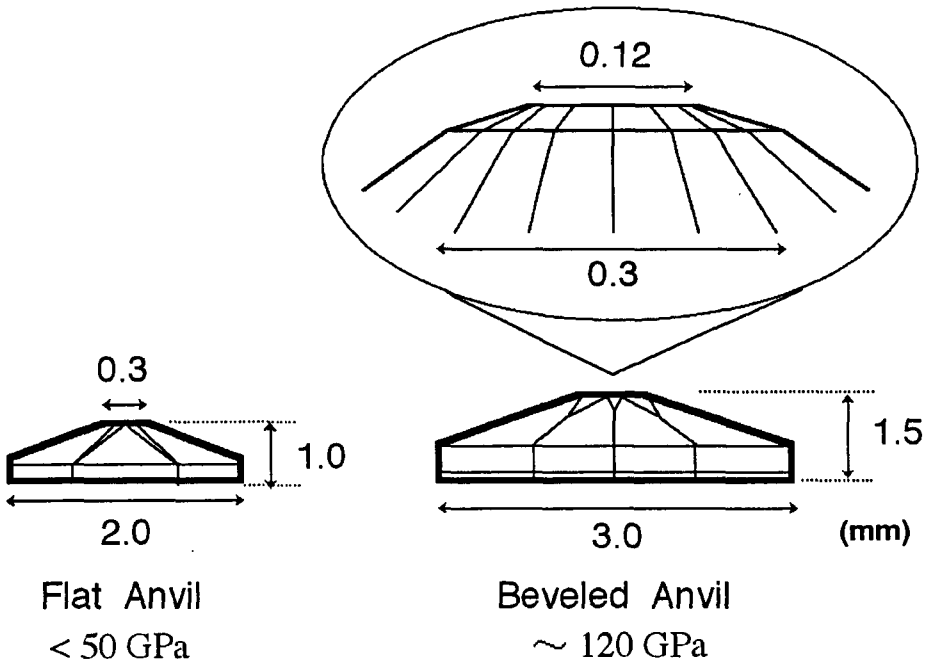

Figure 2-5. Diamond anvils with a standard Drukker shape and a beveled cut shape.

with culet diameter of 0.12 mm (inner) and 0.3 mm (outer), 1.5 mm height, and 3 mm table diameter, was used up to over 100 GPa. The access holes in the tungsten carbide seat are 0.8 mm in diameter. For easy optical adjustments of the sample position with the infrared setup, the cell was designed in such a way that the diamond culets were close to the geometrical center of the DAC main body.

Because the diamond windows are nearly opaque in the frequency range from 1800 to 2400 cm^{-1}, the quality of the spectra was poor in this range. Thus, the reference spectrum of potassium bromide (KBr) in DAC was subtracted from a raw spectrum of sample in DAC. KBr is nearly transparent over the whole infrared region and is used as an ordinal infrared window. In order to improve the spectral quality in 1800 to 2400 cm^{-1} range, the pressure which is nearly equal to the sample pressure was applied to KBr. An example is shown in Figure 2-6.

2-2-3. Monitoring of High Pressures

The most common approach to the measurement of the local pressure in the DAC is the ruby fluorescence method. This measurement is based on the determination of the extremely intense R_1 emission line of ruby. This line is narrow and undergoes a very large frequency shift on varying pressure (see Figure 2-7). A few micrometric ruby grains are added to the sample and their fluorescence can be probed with a blue laser beam through the diamond window.[11] The ruby scale is a kind of secondary standard pressure calibration method and it has been calibrated up to 200 GPa against primary shock-wave standard.[12] The laser power employed to excite the ruby fluorescence ranges from 0.1 to 10 mW depending on the pressure value. In the study of the pressure induced chemical reactions involving conjugated or more generally

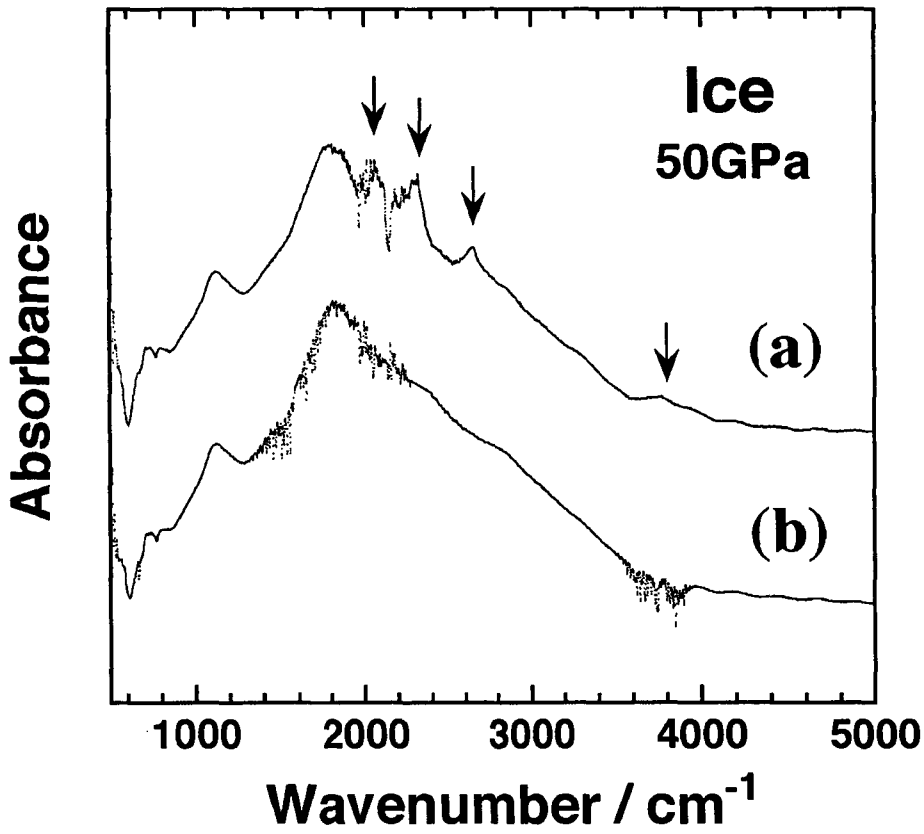

Figure 2-6. Correction for diamond absorption. (a) Reference spectrum of DAC at 1 atm is subtracted from the raw H_2O spectrum at 50 GPa. (b) Reference spectrum of KBr at 50 GPa is subtracted from the raw H_2O spectrum at 50 GPa. Arrows indicate the remainders of the subtraction.

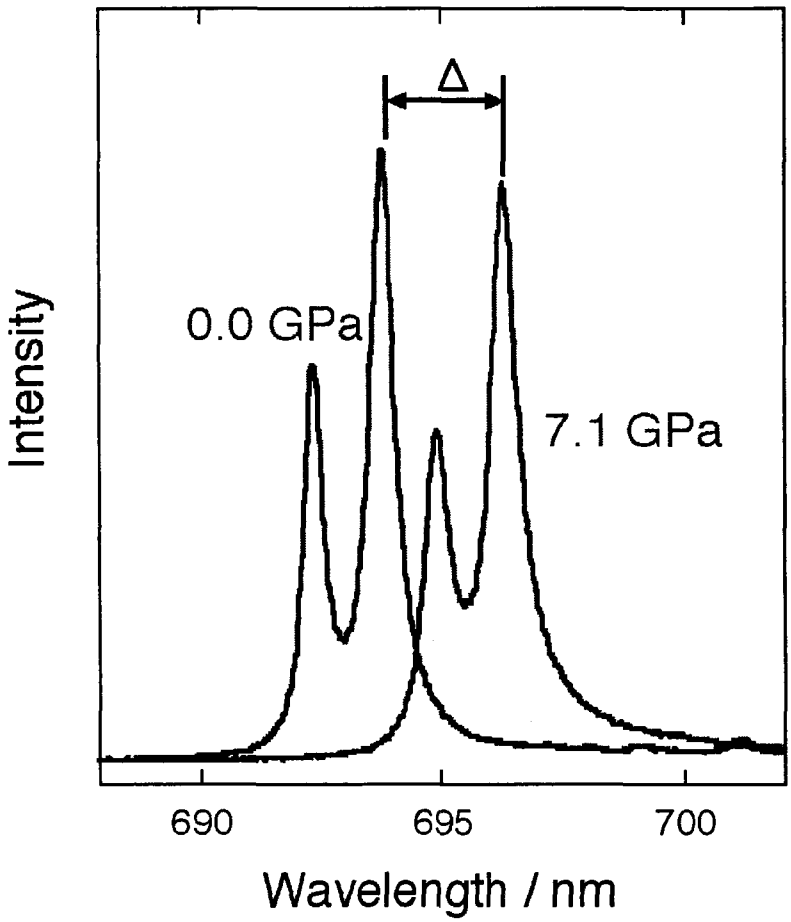

Figure 2-7. Ruby fluorescence spectra for pressure calibration.

unsaturated molecules, even low laser power less than 0.1 mW was used to prevent the chemical reaction.

2-3. Description of the Infrared System

As mentioned above, the DAC described in the previous section was designed for use with beam condensers consisting of on-axis Cassegrain mirrors. We used a commercial system, HORIBA FT-530 micro FT-IR spectrometer equipped with a liquid nitrogen cooled MCT (HgCdTe) photoconductive detector as shown in Figure 2-8. The opposed Cassegrain mirrors of this system have 16× magnifications, a 0.4 numerical aperture, and a working distance of 2×20 mm. With this system the diameter of the infrared beam spot on the sample is 0.1 mm. A variable knife-edge targeting aperture, which is placed at the conjugate point (see Figure 2-8) of the sample after the output Cassegrain mirror, allows us to select a desired area (25×25 μm or more) of the sample for infrared analysis. The DAC was mounted on an X, Y, and Z-axis sample stage. The spectral range of the system extends from 450 to 4400 cm^{-1} (with a wide-band MCT detector) or from 700 to 4400 cm^{-1} (with a narrow-band MCT detector). Each spectrum was measured after about one hour on pressurization. It should be noted that a similar microscope, equipped with a bolometer is very efficient for investigation in the far infrared region. Specifically, the use of a synchrotron radiation source [1, 13] would be very powerful in this case.

2-4. Description of the Raman System

Figure 2-9 shows the schematic diagram of the experimental system for *in situ* Raman scattering measurement for a DAC. The Raman scattering is measured using a single monochromator SPEX 270M, which is a 270 mm

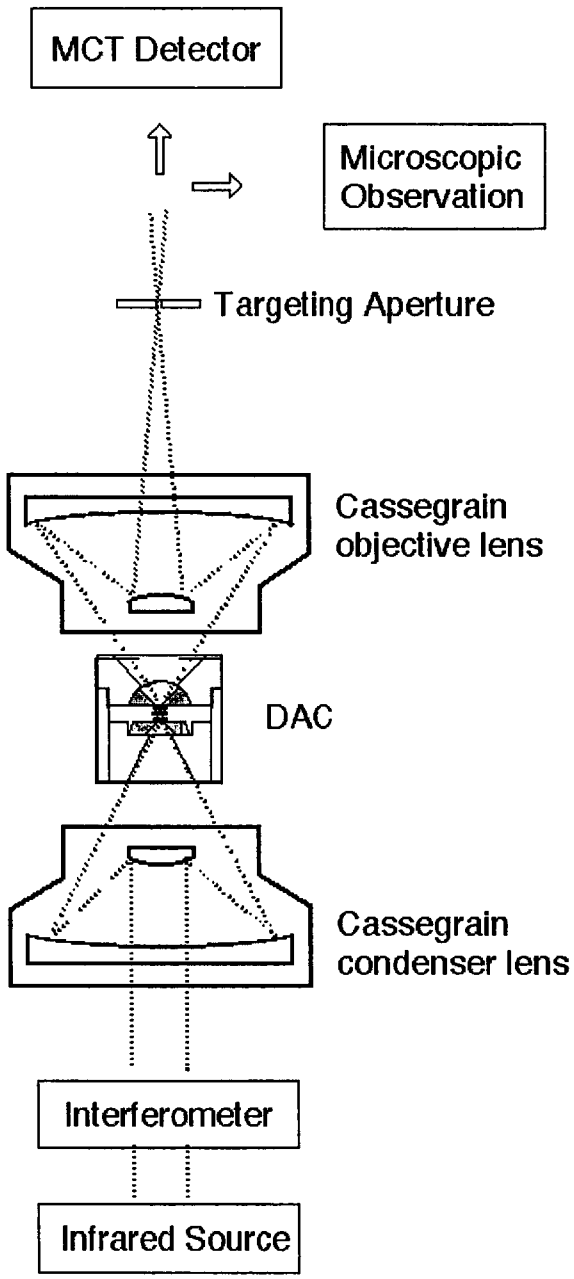

Figure 2-8. Optical system for infrared microspectroscopy.

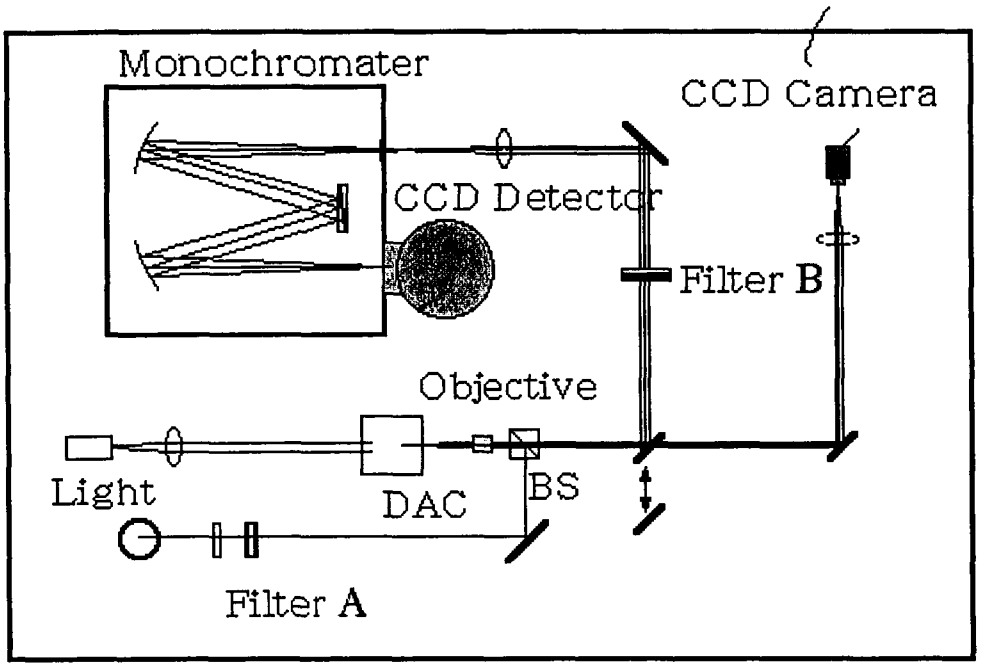

Figure 2-9. Optical system for Raman spectroscopy. Laser beam comes from the circle at left below and go through BS (beam splitter) and Objectives to DAC. The backscattered light is collected through the same Objectives and is detected with CCD Detector. Filter A is a band-pass filter to cut the emission line of argon ion laser and Filter B is a holographic notch filter to weaken the intensity of initial 488-nm beam. Light and CCD camera were used for microscopic observation to align the beam and the sample.

focal length spectrograph with a wavelength resolution of 0.1 nm at 546.07 nm. The excitation laser is a 200 mW argon ion laser at 488.0 nm. The laser beam is focused into the center of the DAC with an objective lens of a 200 mm focal length, a 0.35 numerical aperture, and a 20 fold magnification (Nikon, CF M Plan SLWD 20×). The backscattered light is collected through this lens and two holographic notch filters with an optical density 4.0 (Kaiser Optical Systems, Inc., HSNF-488-1). The optical density 4.0 filter can weaken the intensity of initial 488-nm light to 10^{-4}. The filters were placed in front of the entrance slit of the monochromator to block the laser excitations. Raman spectra were recorded with a liquid nitrogen cooled CCD detector SPEX SPECTRUM ONE (800×2000 pixels) covering a wave-number region of 3000 cm^{-1} at one time with a spectral resolution of 2.3 cm^{-1}. The frequencies of Raman bands were calibrated both with spectral calibration lamps (Xe, Ne, Kr) and with emission lines of the argon laser.

References

1) M. Hanfland, R.J. Hemley, H.K Mao, and G.P. Williams, *Phys. Rev. Lett.* **69**, 1129 (1992).

2) M. Hanfland, R.J. Hemley, H.K Mao, and G.P. Williams, *Phys. Rev. Lett.* **70**, 3760 (1993).

3) J.R. Ferraro, "*Vibrational Spectroscopy at High External Pressures*", the Diamond Anvil Cell (Academic, London, 1984).

4) P.G. Johannsen, in Simple Molecular Systems at Very High Density, edited by A. Polian, P. Loubeyre, and N. Boccara (Plenum, New York, London, 1989).

5) K. Martin; L. Hall, J.R. Ferraro, and A.W. Herlinger, *Appl. Spectrosc.* **38**, 104 (1984).

6) Ph. Pruzan, J. C. Chervin, M. M. Thidry, J. P. Itie, J. M. Besson, J. P Forgerit, and M. Revault, *J. Chem. Phys.* **92**, 6910 (1990).

7) Ph. Pruzan, J. C Chervin, and J. P Forgerit, J. Chem. Phys. 96, 761 (1992).

8) P. J. Miller, G. J. Piermarini, and S. Block, *Appl. Spectrosc.* **38**, 680 (1984).

9) J.C. Chervin, B. Canny, J.M. Besson, and Ph. Pruzan, *Rev. Sci. Instrum.* **66**, 2595 (1995).

10) M.I. Eremets, "High Pressure Experimental Methods", Oxford Unversity Press (1996).

11) H.K. Mao, P.M. Bell, J.V. Shaner and D.J. Steinberg, *J. Appl. Phys.*, **49**, 3276 (1978).

12) P.M. Bell, J. Xu and H.K. Mao, in Shock Waves in Condensed Matter, ed. Y. Gupta, Plenum, New York, p. 125–130 (1986).

13) J. Reffner, G.L. Carr, S. Sutton, R.J. Hemley, and G.P. Williams, Syncbrotron *Radiation News* 7, 2 (1994), and references therein.

Chapter 3

Phase Transitions in H_2O under Pressure

3-1. Introduction

Ice is a typical hydrogen-bonded molecular material and has an exceedingly rich phase diagram as shown in Figure 3-1. The rich phase diagram reduces to two known molecular ice phases, ice VII and VIII, above about 2 GPa.[1)] Ice VII has the body-centered cubic (bcc) structure in which each O atom is bonded to four of the eight nearest neighbors by hydrogen bond in a tetrahedral arrangement (Figure 3-2). The orientation of the water molecules is random, apart from short-range order imposed by obeying the local "ice rules" that "There are two hydrogens adjacent to each oxygens" and "There is only one hydrogen per bond." The low-temperature ice VIII has the same atomic arrangement as ice VII, but the water molecules and the associated dipole moments possess long-range-order.

The symmetrization of hydrogen bond in ice is intimately related to the quantum motion of protons known as tunneling and has been one of the major subjects in the chemistry and physics of water over a half century.[1-7)] The energy potential for the proton motion along the hydrogen bonded O–O axis can be described as a double-minimum potential with an energy barrier on the midpoint. As oxygen atoms are pushed closer by applying pressure, the potential barrier will gradually be depressed and eventually the potential may converge into a single-minimum at a sufficiently high pressure. Hydrogen-bonded protons initially located at asymmetric positions about one third of the O–O distance[8)] will be relocated to the symmetric midpoints (Figure 3-2). Water molecules dissociate to form an "atomic crystal"

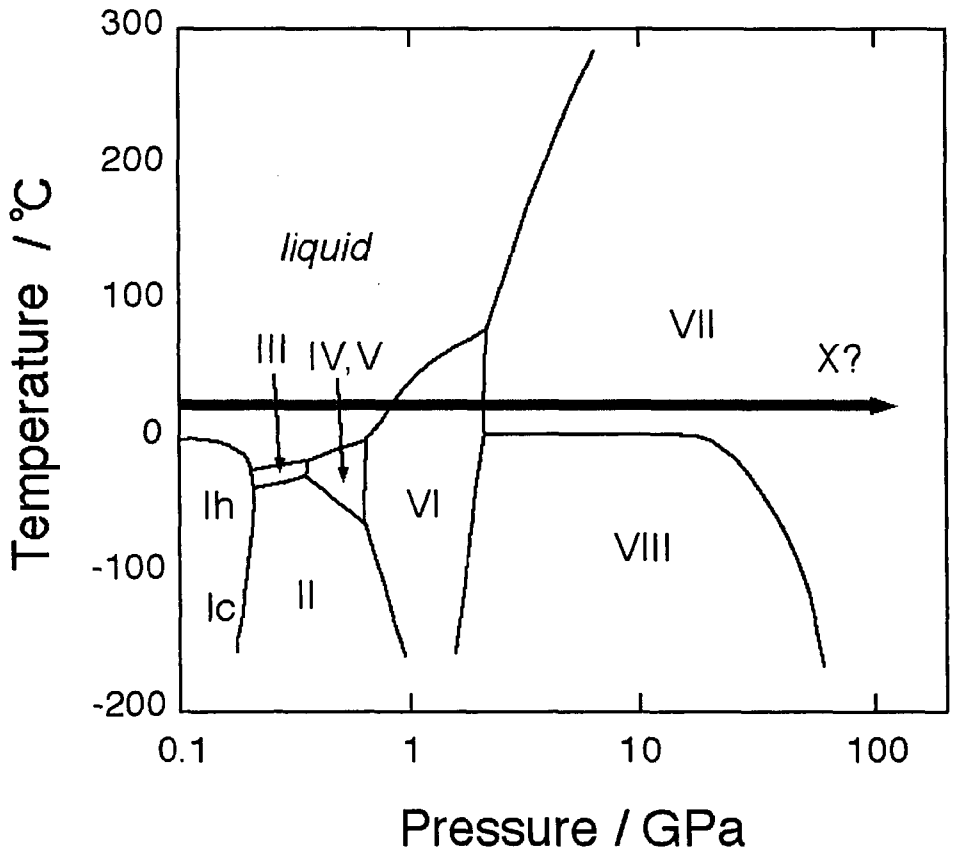

Figure 3-1. Phase diagram of H_2O. A horizontal arrow indicates a loading path at room temperature.

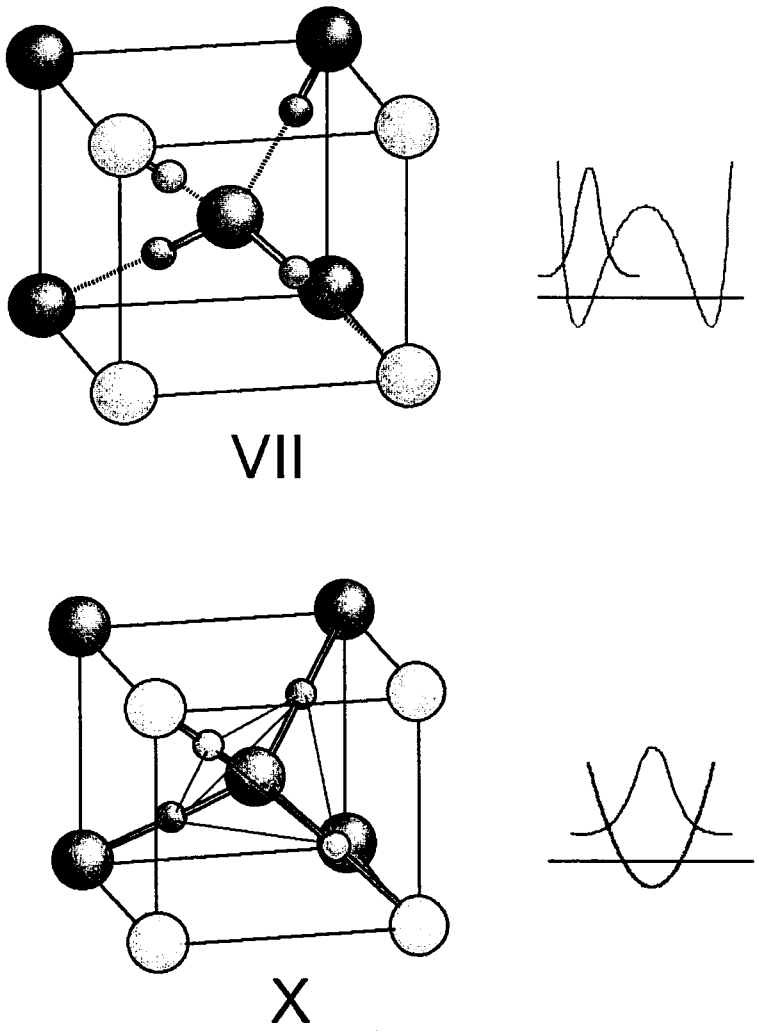

Figure 3-2. Crystal structures of ice VII and symmetric ice (ice X). The corresponding unit cut out from the cubic unit cell of ice VII is also presented for comparison. Energy potentials along the hydrogen bonded O–O axis in each phase is also schematically drawn.

consisting of hydrogen and oxygen atoms, and hence the picture of ice as a molecular crystal breaks down entirely. Here, an "atomic crystal" means that the component pieces of the crystal are not molecules but atoms.

The transition into symmetric ice (ice X) has ambiguously been confirmed in spite of affirmative theoretical results; their predicted transition pressures are below one hundred GPa, which is attainable with the conventional diamond-anvil cell technique. The microscopic transition mechanism has been investigated previously using semiempirical methods [2-5] and very recently using *ab initio* quantum mechanical methods.[6,7] Holzapfel[3] predicted a transition to symmetric hydrogen bonding in ice VII at pressures between 35 and 80 GPa. Lee *et al* [6, 7] calculated the transition pressure into ice X to be 49 GPa, starting from a proton ordered structure of ice VIII. The predicted pressure in ice VIII can be applied to the symmetrization in ice VII without major corrections, because ice VII has a crystal structure very close to that of ice VIII. A number of high-pressure experiments have been performed to explore the symmetric ice and several of them reported some indications of the phase transitions in both ice VII and VIII at about 50 GPa, which were interpreted in relation to the hydrogen-bond symmetrization. It is an anomaly in the Brillouin frequency of ice VII[9] or an appearance of a new lattice vibrational peak in Raman spectra of ice VIII.[10, 11] Very careful Raman measurements, however, revealed recently that the phase transitions associated with the hydrogen-bond symmetrization do not take place either in ice VII at room temperature or in ice VIII at low temperature.[12, 13]

The structural study of ice by X-ray diffraction has provided hopeful results on the hydrogen-bond symmetrization, although the obtained structural information was limited to the compression of oxygen lattice. The

bcc lattice of oxygen atoms in phase VII was found to exist over a very wide pressure range at least to 128 GPa. At this pressure the O–O distance along the hydrogen bonding decreases to 0.228 nm.[14] This value is sufficiently less than 0.24 – 0.25 nm of the threshold distances theoretically predicted[1-6] for the symmetrization transition and slightly shorter than the O–O distances in some molecular crystals in which the hydrogen-bond symmetrization is realized at 1 atm.[15] In fact, X-ray diffraction data provided no information about the proton sublattice. Therefore, it is very likely that the symmetrization would already take place with keeping its bcc lattice in the pressure range explored.

Infrared absorption spectroscopy is one promising method to investigate the hydrogen-bond symmetrization in ice. A water molecule has three fundamental vibrations: the symmetric and asymmetric OH stretching vibrations, ν_1 and ν_3, and the OH bending vibration, ν_2.[16] In molecular solids, all of these vibrational modes are both infrared and Raman active, and their pressure behavior can fundamentally be investigated by either spectroscopy. This biactivity in the vibrational motions should be altered in association with the transition into symmetric ice. These three molecular vibrations are converged into two lattice vibrational modes, one distortional twisting motion of hydrogen atoms (ν_D) and one translational motion of coupled oxygen and hydrogen atoms (ν_T), and both vibrational modes are not Raman active but infrared active.[11, 17] Infrared absorption measurement is expected to give more clear insight into the hydrogen-bond symmetrization. The molecular and lattice vibrational modes of ices VII, VIII, and X are schematically drawn in Figure 3-3. Some infrared measurements of ice were made, and the pressure dependence of the fundamental and combination bands were reported. The measured pressure range, however, was limited to 20 GPa [16, 18]

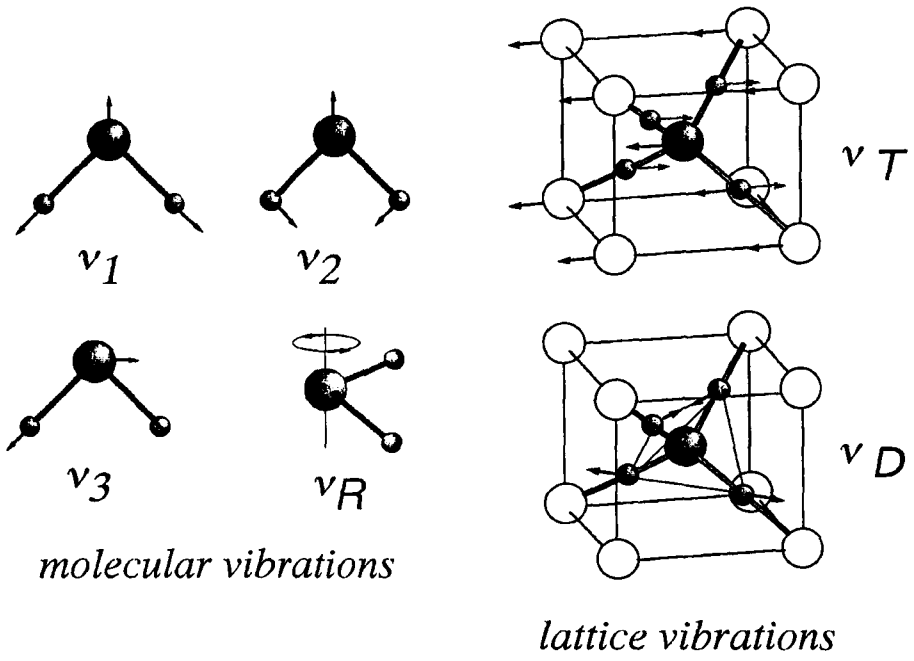

Figure 3-3. Molecular and lattice vibrational modes in phases VII, VIII, and X. Symbols: ν_1, symmetric OH stretching vibrations; ν_3, asymmetric OH stretching vibrations; ν_2, OH bending vibration; ν_R, rotational vibration; ν_D, distortional twisting motion of hydrogen atoms; and ν_T, translational motion of coupled oxygen and hydrogen atoms.

and recently extended to 40 GPa, [19] still below the expected symmetrization pressures. This chapter presents results from infrared measurements on ice beyond 100 GPa and their analysis.

3-2. Experimental

High-pressure infrared spectra were measured at room temperature with a diamond-anvil cell (DAC) (see Chapter 2).[20] Because of very strong absorption from ice, preparation of a thin film in the DAC was required to obtain unsaturated spectra available for quantitative analysis of the spectral profile. The disconnected piston and cylinder of the DAC were cooled with liquid nitrogen in a glove chamber purged with dry nitrogen gas. Ice films were prepared by condensation of evaporated water on the top surface of one diamond anvil with a fixed metal gasket, and successively the gasket hole was filled with pressure transmitting medium. The DAC was quickly assembled and was left in the glove box for a few hours until warming up to room temperature. Xenon (Xe), potassium bromide (KBr), and tetrachloromethane (CCl_4) were used as the pressure media. The former two are transparent over the whole wave-number region measured, while the latter is transparent above 1000 cm^{-1}. The water molecule shows the absorption peaks associated with the molecular vibrations at the high frequency region above 1000 cm^{-1} at modest pressures and hence the spectrum is not significantly disturbed from the absorption of a pressure medium of CCl_4, in particular, at relatively low pressures.

The diamond anvils used were type II-a with a beveled cut shape. The culet diameter was 0.1 mm and the thickness was 1.5 mm. Although diamond itself has strong absorption in the wave-number region of 1800 – 2400 cm^{-1}, such thin anvils allow a few percent of incident light to pass through and

hence collection of the overall spectral profile. The initial thickness of an indented metal gasket was about 25 μm. The sample hole with an initial diameter of 30 μm, which was made on the gasket with an electric discharge machine, was enlarged to 50 – 60 μm in diameter during compression. Transmitted beams were collected through an optical mask typically with a passing area of 25 × 25 μm^2 in order to reduce degradation of spectra due to the pressure gradient in the specimen. A microscope FT-IR spectrometer covering the wave-number region from 700 to 5000 cm^{-1} was used with a spectral resolution of 4 cm^{-1}. The pressure was measured by the ruby fluorescence method.[21)]

3-3. Results and Discussion

3-3-1. Spectral Change and Analysis

Absorption spectra of ice VII were collected with Xe medium up to 86 GPa, with KBr medium up to 112 GPa, and with CCl_4 medium up to 107 GPa. These experiments provided results consistent with each other and ruled out the possibility of the formation of chemical compounds between ice and the pressure media. Typical spectra of ice pressurized with KBr are shown in Figure 3-4. Because the diamond windows of the pressure cell are nearly opaque in the frequency range from 1800 to 2400 cm^{-1}, the quality of the spectra was poor in this range. The symmetric and asymmetric stretching peaks overlapped entirely to form an inseparable broadened peak. The central position of the overlapped peaks shifted from about 2840 to 1700 cm^{-1} when the pressure increased from 27.2 to 50.9 GPa. The peak shift was accompanied with an enormous peak broadening. A new absorption band appeared in the low frequency region around 800 cm^{-1} at 64.7 GPa (see

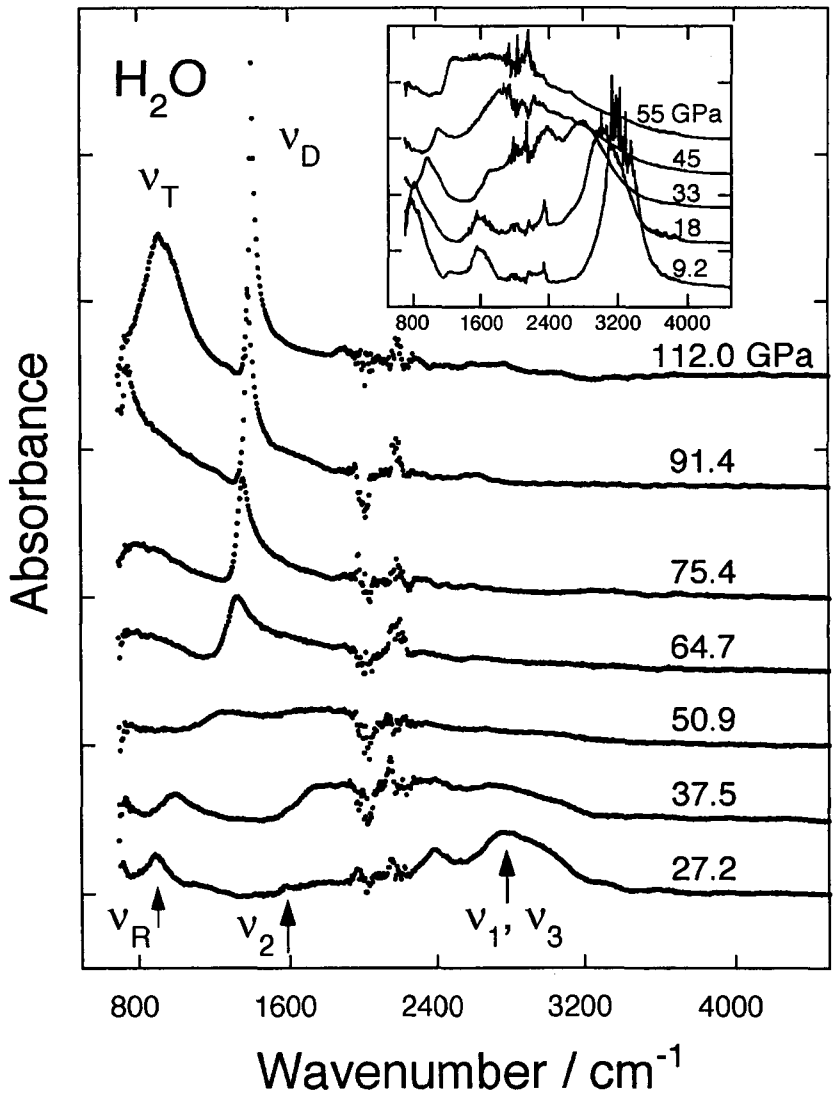

Figure 3-4. Infrared absorption spectra of ice measured with KBr medium. The curves are offset in the vertical direction for clarity. (Inset) Infrared spectra of thick film of ice.

Figure 3-5), growing a definite peak on further compression. As described in detail later, the transition from ice VII to X was observed at 62.1 GPa. Two absorption peaks clearly seen at about 1400 and 1000 cm^{-1} in the top spectrum (measured at 112 GPa) were hence assigned to distortional (ν_D) and translational (ν_T) lattice modes in ice X. The asymmetrically deformed ν_D peak became sharp at pressures above 64.7 GPa, while the OH bending vibrational peak, which stayed at nearly the same position of 1550 cm^{-1}, disappeared at about 45 GPa.

The observed increases in intensity and peak asymmetries may arise from interference, namely Fano interference, between stretching (ν_1 and ν_3) and rotational ν_R modes. The unperturbed spectral features of the stretching mode can be extracted by subtracting an interfered peak shape fitted with a Fano function [22, 23] from an original spectrum. An interfered peak shape is described with a function of frequency ω as

$$I \propto (q+\varepsilon)^2 / (1+\varepsilon^2),$$

where q is a line-shape parameter and ε is a normalized energy given by $(\omega-\omega_0) / \Gamma$, with ω_0 and Γ being an unperturbed frequency and a line width parameter, respectively. Figure 3-5 shows the absorption spectra obtained by this spectral processing. The absorption peak, which was located at 1700 cm^{-1} in the spectrum measured at 50.9 GPa, collapsed to an enormously broadened peak by further compression. The peak position for such a collapsed peak was estimated from a peak-profile fitting with a given peak width on the assumption of a Lorentzian shape. The calculated peak positions were, for example, 1200 and 900 cm^{-1} for the spectra measured at 55.9 and 59.5 GPa, respectively. A remarkable change in spectral profile was observed at 64.7 GPa: a new absorption band appeared around 800 cm^{-1} and showed a gradual increase in intensity and a shift to higher frequencies as pressure

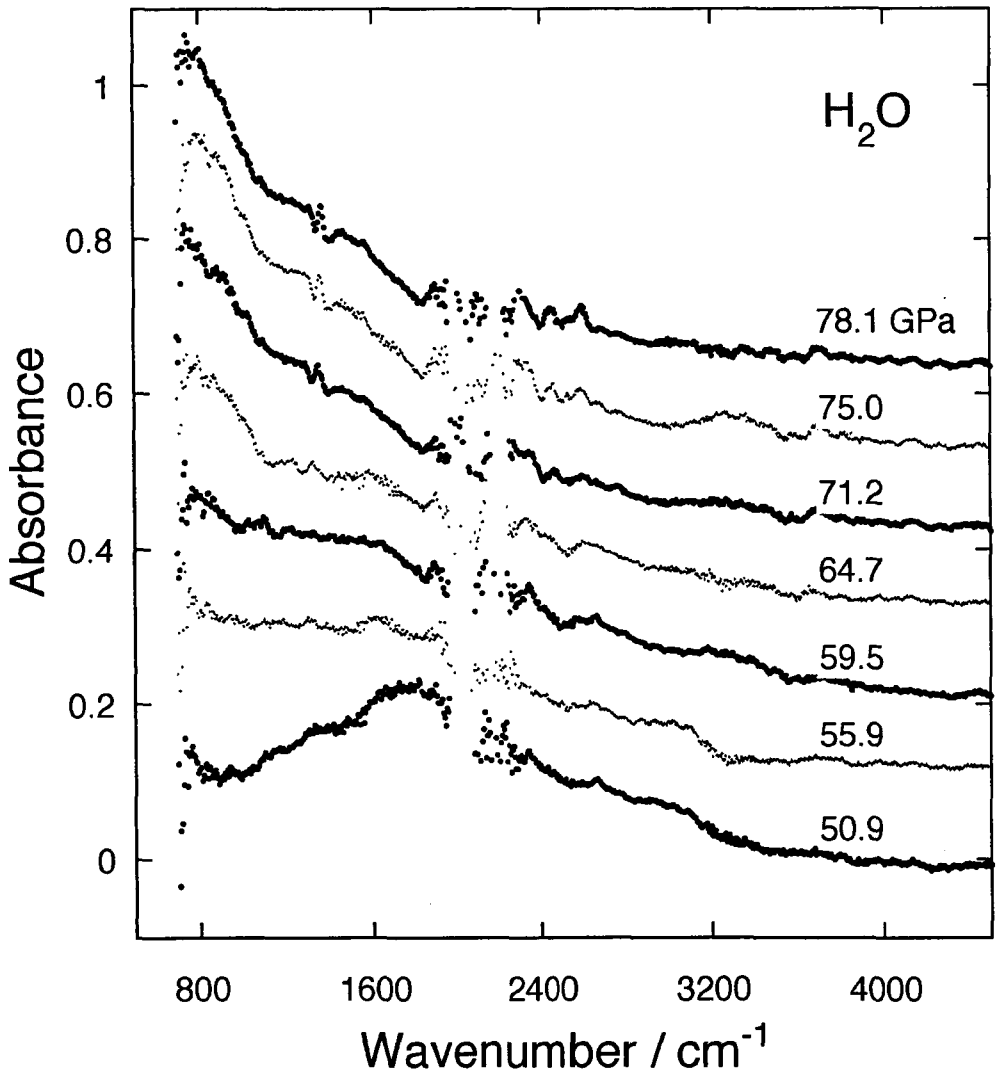

Figure 3-5. Spectral changes associated with the hydrogen-bond symmetrization. An asymmetrically deformed peak of the librational vibration was subtracted from a raw spectrum using fitted Fano parameters.

increased. These spectral changes suggest that a phase transition takes place in the 59.5 to 64.7 GPa pressure range, likely in association with the hydrogen-bond symmetrization.

The observed peak shifts with pressure are plotted in Figure 3-6. The OH stretching frequency (ν_1 and ν_3) decreases at an initial rate of –30 cm^{-1}/ GPa, intersecting the bending ν_2 and rotational ν_R frequencies at about 48 GPa and 56 GPa, respectively. Around 60 GPa the OH stretching frequency went below the measuring limit of 700 cm^{-1}. The frequency at ambient pressure ωo and the pressure coefficient k were obtained as 3549 cm^{-1} and 1.91×10^4 cm^{-2} /GPa, by fitting the observed frequencies with the following phenomenological fuction, $\omega = (\omega_0^2 - k\,p)^{1/2}$, where p is the pressure. The frequencies (ν_T) alternatively measured in the high-pressure region above 90 GPa were fitted with a quadratic form, giving $\omega = -1411 + 33.5p - 0.113p^2$. The OH bending ($\nu_2$) frequency is insensitive to pressure. A slight increase above 30 GPa may be attributed to asymmetric deformation in the peak shape. The bending frequencies plotted were obtained from the apparent peak maxima of the resonant peaks, which were shown to be shifted slightly toward a higher frequency.[23] The rotational frequency (ν_R) shows a monotonic increase from 830 to 1260 cm^{-1} as the pressure increases from 20 to 60 GPa. The variation of the frequency becomes small after the conversion to the distortional lattice mode (ν_D) at 62 GPa.

The width γ and line-shape parameter q, which were obtained for the asymmetrically deformed rotational ν_R peaks, are plotted as a function of pressure along with those of the uninterfered peaks obtained by fitting with a Lorentzian function (Figure 3-7). Thus obtained γ shows a monotonic decrease with pressure from 180 cm^{-1} at 2 GPa to 20 cm^{-1} at 100 GPa. In contrast, q increases with pressure and its values seem to be divided into two

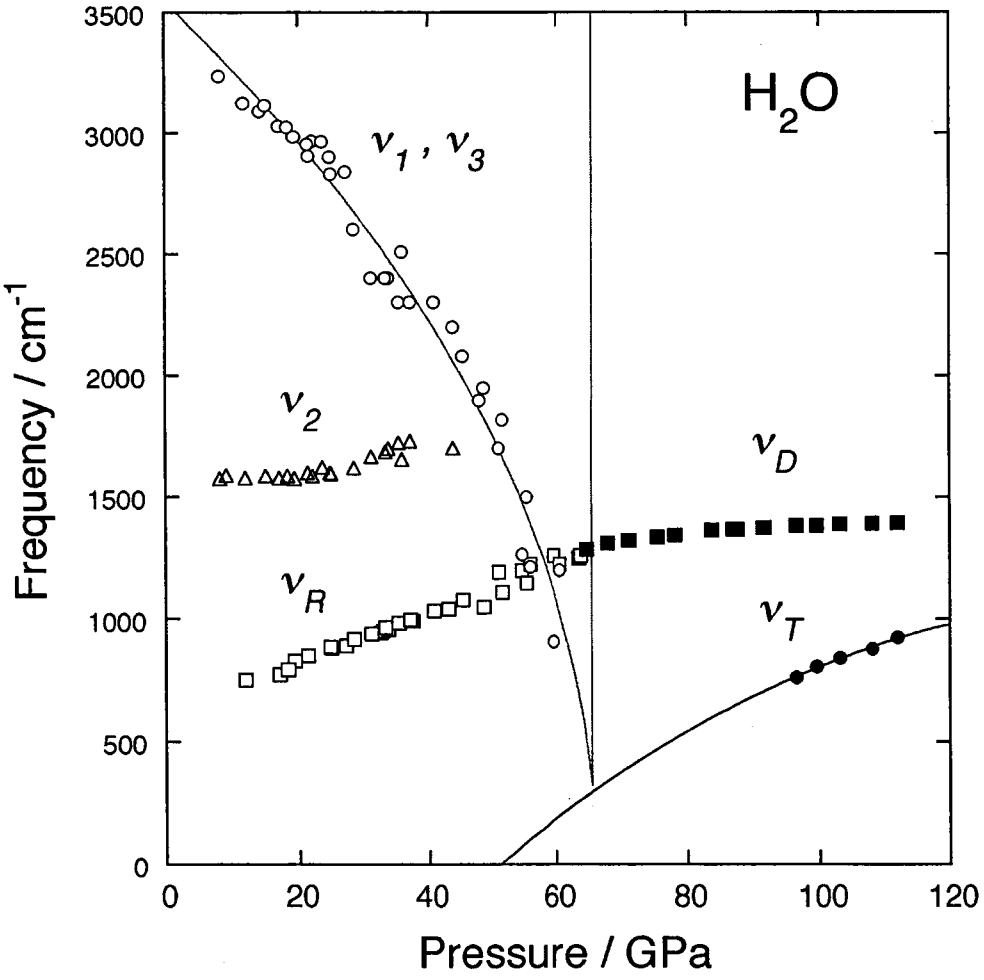

Figure 3-6. Observed peak frequencies plotted as a function of pressure. Symbols: ν_1, symmetric OH stretching vibrations; ν_3, asymmetric OH stretching vibrations; ν_2, OH bending vibration; ν_R, rotational vibration; ν_D, distortional twisting motion of hydrogen atoms; and ν_T, translational motion of coupled oxygen and hydrogen atoms.

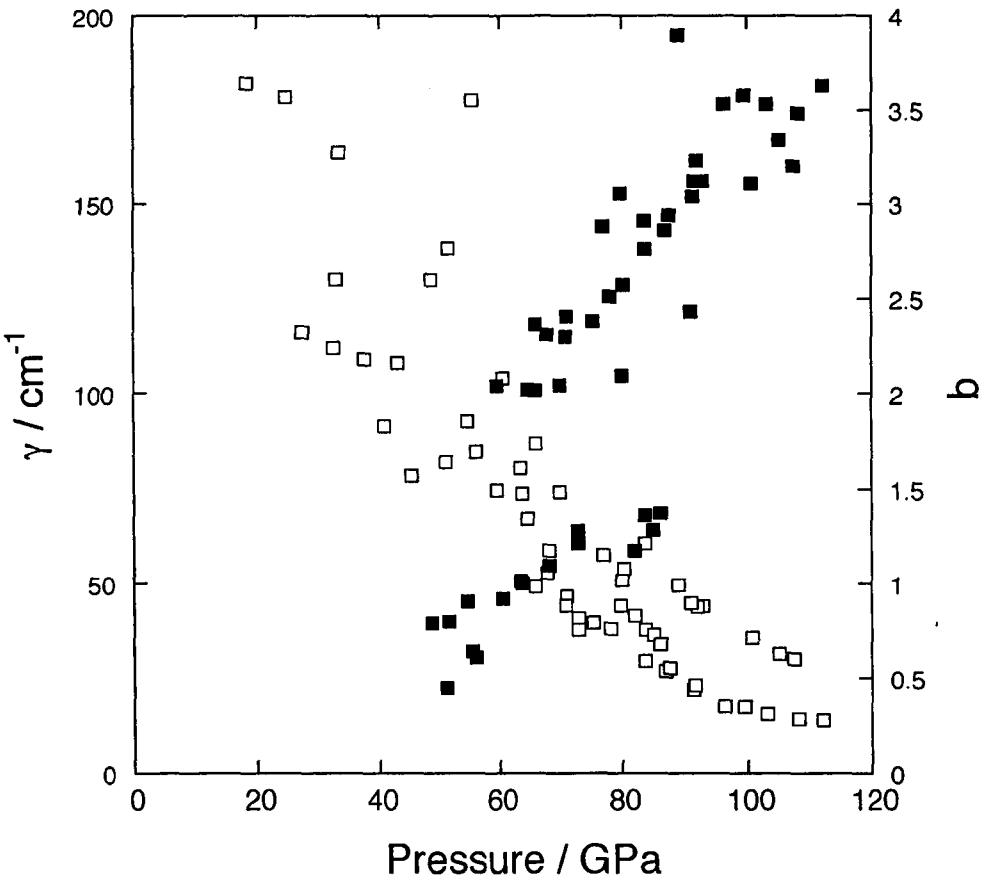

Figure 3-7. Variations in the peak width γ (open squares) and peak shape parameter *q* (closed squares) with pressure.

regions below 1.5 and above 2.0. This increase in q indicates that the asymmetric rotational peak changes gradually into a symmetric peak. At the limit of $1/q=0$ the interference effect vanishes and the asymmetrically deformed peak shape converges into a symmetric Lorentzian shape. This tendency can be seen in Figure 3-4, although the asymmetric shape still remains at 112 GPa. Additional pressure of several tens GPa may be required beyond 100 GPa for complete removal of the asymmetric shape.

3-3-2. Phase Transition and Hydrogen-bond Symmetrization

The observed infrared spectra suggest that a phase transition takes place at about 62 GPa and this transition is associated with the hydrogen-bond symmetrization, as described below.

The phase transition can be detected as a turn in the pressure dependence of the stretching frequency. The stretching frequency decreases sublinearly with increasing pressure, falling toward zero around 60 GPa. The turn to an increase in the stretching frequency was not evidently observed in the spectra because of the peak broadening and the limit of low frequency region measured. However, the appearance of the new peak and its shift to a high frequency with pressure indicated unambiguously a phase transition to the symmetric ice at a pressure between 59.5 and 64.7 GPa. We adopt here the midpoint of the two pressures, that is, 62 GPa. The transition pressure can also be estimated as an intersecting point between the fitted curves for the OH stretching and translational lattice modes, which leads to a slightly high pressure of 65 GPa. The transition pressure of 62 GPa is lower by 10 GPa than that previously estimated from the Raman frequencies in a relatively narrow pressure range up to 25 GPa.[13)]

Disappearance of the OH bending ν_2 peak is another spectral feature

indicating the occurrence of the hydrogen-bond symmetrization. This peak showed a gradual decrease in intensity with pressure and eventually disappeared below 50 GPa. The peak-vanishing pressure was not exactly determined from the observed spectra owing to the very weak peak-intensity. It should be noted that the bending peak once disappeared was not observed again after the phase transition. If the bending peak recovered the intensity at higher pressures, it should appear at a frequency close to 1500 cm^{-1}. As seen in the spectrum measured at 112 GPa in Figure 3-4, such the third peak was not observed. The phase transition is thus accompanied by the disappearance of the OH bending peak.

The vibrational mode analysis has predicted only two infrared-active lattice modes for the symmetric ice.[11, 17] One is a translational (ν_T) vibration associated with opposite displacements of hydrogen and oxygen atoms and the other is a rhombohedral distortion (ν_D) of the tetrahedron of hydrogen atoms with one oxygen atom at the center (see Figure 3-3). The former corresponds to the OH stretching vibration in the molecular phase, while the latter is related to the OH bending and the molecular rotational vibrations which converge into one degenerated lattice mode at the transition point. Only two peaks were observed in the spectra measured above 100 GPa in consistent with the results of the vibrational mode analysis. [11, 17] The peaks located at about 1400 and 1000 cm^{-1} are consequently assigned to the distortional (ν_D) and translational (ν_T) vibrational modes in ice X, respectively.

The transition pressure determined from the present infrared measurement is in good agreement with that obtained from the analysis of the equation of state for ice. The volume compression data obtained by X-ray diffraction was analyzed in detail using a universal eqation of state, and was

found to be divided into three regions with two phase transitions at 40 and 70 GPa.[24] On the basis of previously reported Raman and Brillouin data, [9-11] the lower-pressure transition was interpreted as the hydrogen-bond symmetrization and the higher-pressure transition as a new transition of the symmetric ice. There is great uncertainty about this interpretation. The change in the equation of state at 40GPa is small to such an extent that it can be ignored, but the change at 70GPa is much significant and distinct. A very recent X-ray diffraction measurement of ice VII confirmed a similar anomaly in the equation of state at 66GPa again.[25] Taking the present infrared results into account, it is reasonable to attribute the phase transition at 70 GPa rather than that at 40GPa to the hydrogen-bond symmetrization.

It is interesting to examine the hydrogen-bond symmetrization from the viewpoint of the crystal structure. From the X-ray diffraction data, the hydrogen-bonded O–O distance at 62.1 GPa is calculated to be 0.240 nm; the symmetrized OH distance is 0.120 nm. These values are very close to those of theoretical calculations predicting the symmetrization at the threshold O–O distances of 0.23–0.24 nm. A recent neutron diffraction study of D_2O ice VIII, which is a deuteron ordered phase derived from a slight distortion of the bcc lattice of ice VII, revealed a very small pressure dependence of the OD bonding, 4×10^{-5} nm/GPa.[26] If we adopted the same pressure dependence for ice VII with an initial OH distance of 0.099 nm, the OH distance would extend by about 18 % at the transition pressure of 62.1 GPa. Such an abrupt extension should produce some kinds of discontinuous change in vibrational property, in particular, in the OH stretching vibration. Such discontinuous change does not agree with what actually observed in the present infrared measurement. The latest calculation of the hydrogen bonding in ice shows that the OH bonding distance increases linearly as a result of

potential deformation, being accelerated by higher pressures.[27] In such case a continuous relocation of protons to the symmetric positions may take place. A second-order like nature still remains for the hydrogen-bond symmetrization. Low-temperature infrared measurements of phases VIII and X are required to clarify the transition mechanism in relation to the hydrogen-bond symmetrization.

3-4. Conclusion

Infrared measurements at room temperature have shown that the hydrogen-bond symmetrization occurs at 62 GPa in ice. The OH stretching frequency initially located at 3500 cm^{-1} at ambient pressure falls toward zero around 60 GPa. A new absorption band appears in the low frequency region below 800 cm^{-1} at about 65 GPa, growing a definite peak with a continuous shift to higher frequencies by further compression. Such a turn in the pressure dependence of the stretching frequency is a piece of evidence for the transition from ice VII to symmetric ice X. The OH bending peak disappears before the transition. Two absorption peaks persist above the transition pressure, being assigned to a translational and distortional lattice vibrations in ice X. The transition to ice X can be interpreted as a kind of molecular dissociation, because H_2O molecule did not exist after the transition.

References

1) P.V. Hobbs, "*Ice Physics*", Clarendon Press, Oxford (1974).

2) C. Reid, *J. Chem. Phys.*, **30**, 182 (1959).

3) W. B. Holzapfel, *J. Chem. Phys.*, **56**, 712 (1972).

4) F. H. Stinllinger and K. S. Schweizer, *J. Phys. Chem.*, **87**, 4281 (1983).

5) K. S. Schweizer and F. H. Stinllinger, *J. Chem. Phys.*, **80**, 1230 (1984).

6) C. Lee, D. Vanderbilt, K. Laasonen, R. Car, and M. Parrinello, *Phys. Rev. Lett.*, **69**, 462 (1992).

7) C. Lee, D. Vanderbilt, K. Laasonen, R. Car, and M. Parrinello, *Phys. Rev. B*, **47**, 4863 (1993).

8) J. D. Jorgensen and T. G. Worlton, *J. Chem. Phys.*, **83**, 329 (1985).

9) A. Polian and M. Grimsditch, *Phys. Rev. Lett.*, **52**, 312 (1984).

10) K. R. Hirsh and W. B. Holzapfel, *Phys. Lett.*, **101A**, 142 (1984).

11) K. R. Hirsh and W. B. Holzapfel, *J. Chem. Phys.*, **84**, 2771 (1986).

12) Ph. Pruzan, J. C. Chervin, and B. Canny, *J. Chem. Phys.*, **99**, 9842 (1993).

13) Ph. Pruzan, *J. Mol. Structure*, **322**, 279 (1994).

14) R. J. Hemley, A. P. Jephcoat, H. K. Mao, C. S. Zha, L. W. Finger, and D. E. Cox, *Nature*, **330**, 737 (1987).

15) M. Ichikawa, *Acta Cryst. B*, **34**, 2704 (1978).

16) W. B. Holzapfel, B. Seiler, and M. Nicol, *J. Geophys. Research*, **89**, B707 (1984).

17) K. H. Huang, *Z. Phys.*, **171**, 213 (1963).

18) D. D. Klug and E. Whalley, *J. Chem. Phys.*, **81**, 1220 (1984).

19) K. Aoki, H. Yamawaki, and M. Sakashita, *Science*, **268**, 1322 (1995).

20) K. Aoki, Y. Kakudate, M. Yoshida, S. Usuba, K. Tanaka, and S. Fujiwara,

Jpn. J. Appl. Phys., **26**, 2107 (1987).

21) H. K. Mao, P. M. Bell, J. W. Shaner, and D. J. Steinberg, *J. Appl. Phys.*, **49**, 3276 (1978).

22) U. Fano, *Phys. Rev.*, **124**, 1866 (1961).

23) K. Aoki, H. Yamawaki, and M. Sakashita, *Phys. Rev. Lett.*, **76**, 784 (1996).

24) J. Hama and K. Suito, *Phys. Lett. A*, **187**, 346 (1994).

25) E. Wolanin, Ph. Pruzan, M. Gauthier, J. C. Chervin, B. Canny, M. Hanland, and D. Haüserman, Private communication.

26) R. J. Nelmes, J. S. Loveday, R. M. Wilson, J. M. Besson, Ph. Pruzon, S. Klotz, G. Hamel, and S. Hull, *Phys. Rev. Lett.*, **71**, 1192 (1993).

27) L. Ojamäe, K. Hermansson, R. Dovesi, C. Roetti, and V. R. Saunders, *J. Chem. Phys.*, **100**, 2128 (1994).

Chapter 4

Phase Transitions in H_2S under Pressure

4-1. Introduction

Pressure-induced molecular dissociation provides crucial insights into chemical bonding. Atomic and molecular solids are the extreme structures for the solid state. When molecules consisting of atoms connected by strong covalent bonds condense, van der Waals forces and other weak intermolecular interactions govern the physical properties of the resulting molecular solids. Characteristics of individual atoms are buried in the molecules. Molecular dissociation releases atoms to form an "atomic solid" whose physical properties depend more directly on characteristics of constituent atoms. Thus, atomic and molecular solids with the same composition may behave very differently. The molecular dissociation of solid hydrogen, which is predicted to occur at several hundreds GPa accompanied by metallization, [1, 2] is one representative example of this behavior.

Hydrogen sulfide, H_2S, is a hydrogen-bonded molecular solid at ambient pressure and low temperatures. Hydrogen bonds align the molecules in this solid just as they orient H_2O molecules in the ices. By destroying these hydrogen bonds at high pressures, molecular dissociation should take place with a change in the structure of solid H_2S.

Molecular dissociation in H_2O ice at high pressures was very recently identified by optical reflection [3] and absorption measurement [4] as described in Chapter 3. For water, dissociation coincides with symmetrizing the hydrogen bond. That is, above 60 GPa, the protons in solid H_2O move to the middle between neighboring O atoms, and intact H_2O molecules are no

longer obvious. This dissociation and hydrogen-bond symmetrization is well characterized as a displacive phase transition with soft-mode behavior for the proton-related vibrations. These results for H_2O suggest that its sister molecule, H_2S, should also dissociate at high pressures. However, it is uncertain whether the dissociation mechanisms would be similar and how large pressure would be required for the dissociation.

Phase transitions in solid H_2S have been studied by Raman [5, 6] and Brillouin scattering, [7] X-ray diffraction [8] (see Figure 4-1) and infrared absorption [9] up to 50 GPa from 30 to 300 K. All of the phases studied are molecular solids, differing by arrangements of molecular orientations. No experimental evidence for molecular dissociation has been reported in these studies. However, a dramatic change in the electronic state of H_2S accompanied the IV–V transition, was recently observed at 27 GPa and ambient temperature.[8] The transparent and colorless IV phase becomes black and opaque, suggesting an apparently large decrease of the bandgap energy. This possible precursor of metallization motivated us to study H_2S to 100 GPa, in search of what might be a metallic hydrogen-bonded system.

4-2. Experimental

Infrared spectra of solid H_2S were measured with a diamond-anvil cell.[10] The 30-μm diameter, 20-μm thick sample chamber was machined in the metal gasket by electrical-discharge methods. When the H_2S filled the chamber, the spectra were saturated, which prevents determining the positions and intensities of the peaks. We, therefore, prepared thin films of H_2S by packing most of the sample chamber with potassium bromide, KBr, cooling the cell with liquid nitrogen below 170 K, and condensing gaseous H_2S (purity 99.999%) on the surface of the KBr. These operations were done

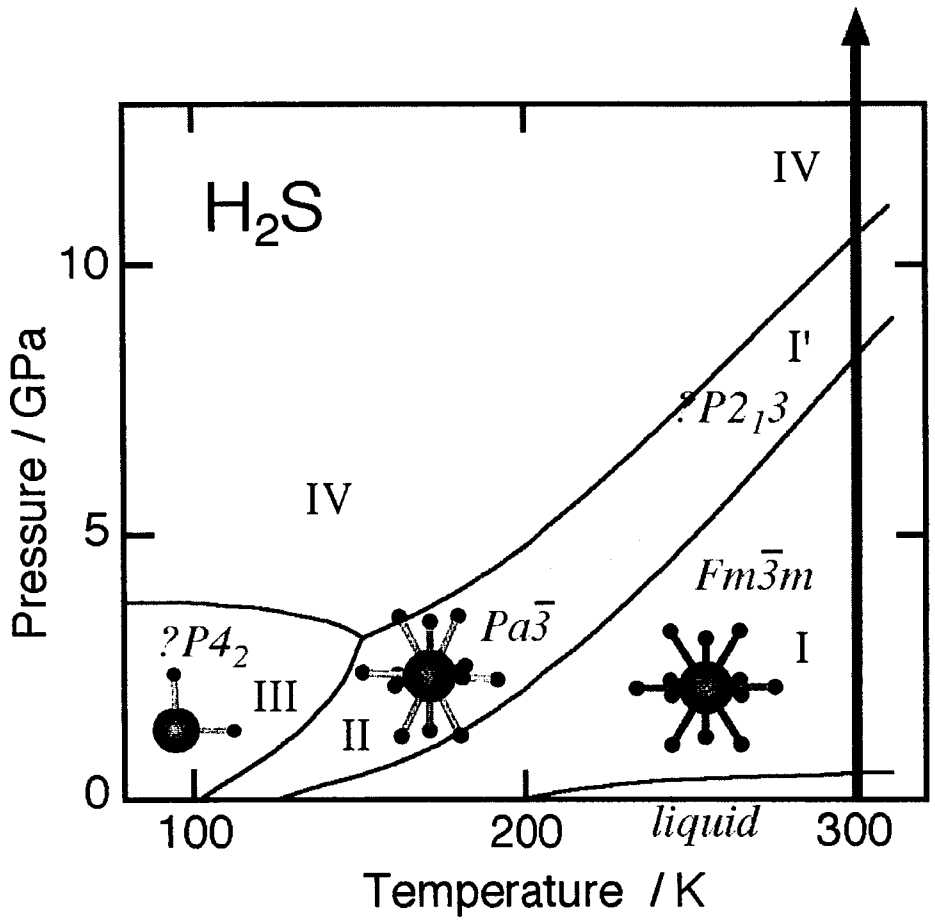

Figure 4-1. Phase diagram of H_2S. A vertical arrow indicates a loading path at room temperature.

in a nitrogen-purged glove box.[11] KBr is transparent from 700 to 6000 cm^{-1} at these pressures.

Infrared spectra were measured with a microscope FT-IR spectrometer with 4 cm^{-1} spectral resolution. The reference spectra of potassium bromide (KBr) in DAC under pressures corrected absorption by the diamond anvils. Pressures were determined from fluorescence spectra of a ruby chip buried in the KBr.[12] A thin film was studied to 100 GPa and 297 K, and a rather thick film was examined to 50 GPa.

4-3. Results and Discussion

All three fundamental vibrational modes of the H_2S molecule are infrared active. In the gas phase, the infrared bands due to ν_1 (symmetric stretch), ν_2 (bending), and ν_3 (antisymmetric stretch) modes are observed at 2615 cm^{-1}, 1183 cm^{-1}, and 2623 cm^{-1}, respectively. Hydrogen bonding and other solid phase effects slightly modify the wavenumbers of these bands; for instance, at 140 K and ambient pressure, ν_1, ν_2, and ν_3 modes appear at 2550, 1770, and 2562 cm^{-1}, respectively.

Figure 4-2-a and Figure 4-2-b show spectra of a thin film of H_2S. At pressures below 42 GPa, the strong ν_1 and ν_3 peaks appeared between 2300 to 2500 cm^{-1} while the weak ν_2 bending peak was missing. The ν_1 and ν_3 peaks disappeared at higher pressures, and a new broad peak appeared around 1300 cm^{-1}. We interpret the disappearance of the SH stretching peaks as showing a phase transition involving dissociation of H_2S molecules. Above the transition pressure, an absorption band starting around 6000 cm^{-1} (0.74 eV) also developed gradually. The absorption extended toward lower energies as the pressure increased and it covered the entire infrared spectral region at 90 GPa. This phenomenon suggests band-gap closure or metallization. This

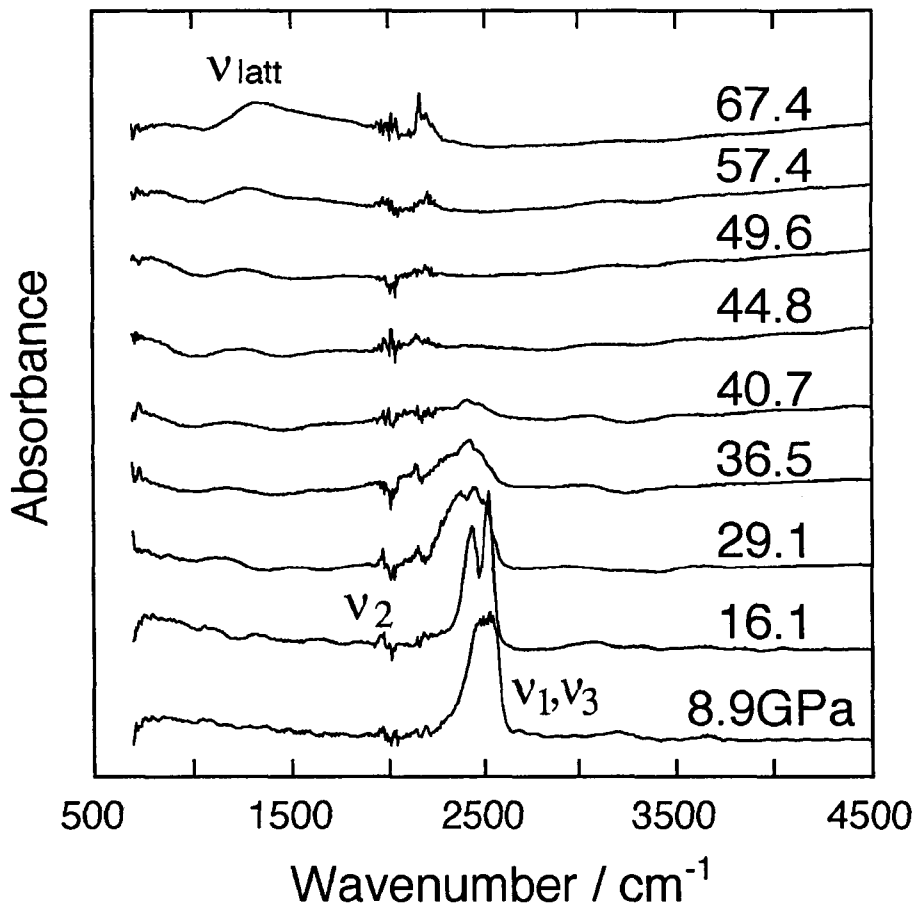

Figure 4-2-a. Absorption spectra measured for a thin film of H_2S to 67 GPa. The curves are offset in the vertical direction for clarity.

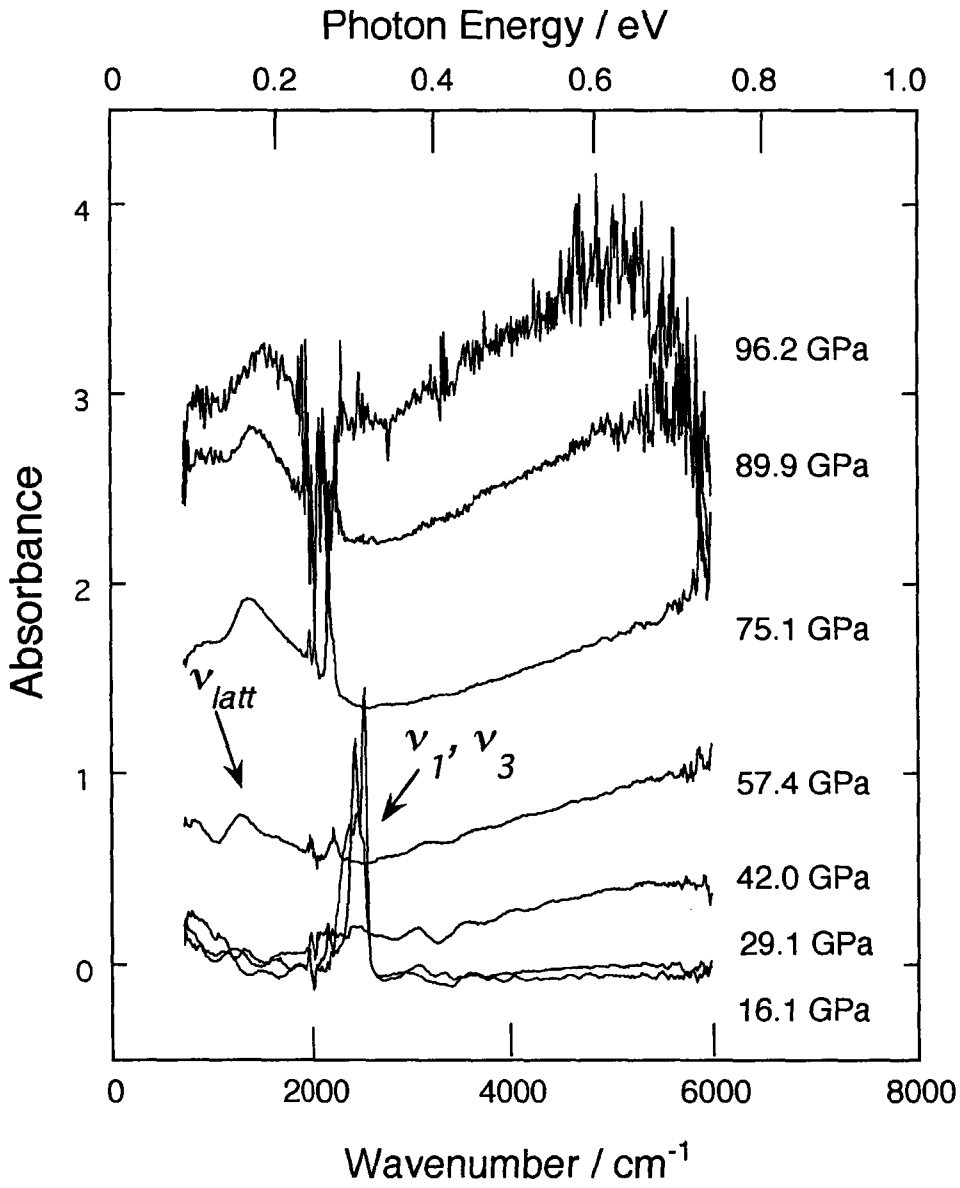

Figure 4-2-b. Absorption spectra measured for a thin film of H_2S to 100 GPa. The curves are **not** offset in the vertical direction.

phenomenon suggests band-gap closure or metallization. The specimen transmited no light at pressures above 96 GPa.

Spectra of a thick H_2S film (Figure 4-3) to 50 GPa more clearly showed the character of the transition near 40 GPa. The ν_1 and ν_3 stretching peaks occurred near the absorption of diamond windows of the high-pressure cell and were saturated. They provided little useful information about the phase transition pressure. We used the appearance of the new peak at lower wavenumbers than the stretching peaks in the spectrum at 46 GPa to locate the V–VI phase boundary.

Figure 4-4 shows the pressure dependences of the vibrational frequencies of H_2S. The frequencies ν_1 and ν_3 decreased at the ratio of -3.5 to -5.3 cm^{-1} GPa^{-1}, suggesting that the SH covalent bonds weaken slightly and the hydrogen bonds become slightly stronger as the molecules approach each other. The frequency of the ν_2 bending mode increased slightly up to 46 GPa.

The 46 GPa transition can be interpreted in terms of molecular dissociation. The disappearance of the SH stretching vibrations implies that the SH bonds have ruptured, and that the molecules have been dissociated into H and S atoms which probably have significant ionic character. We interpret the new strong broad band near 1300 cm^{-1} as a lattice vibrational mode of the atomic solid, although we cannot assign this mode more definitely until the crystal structure of phase VI is known. However, this mode may correspond to the distortional vibration of the OH_4 tetrahedron in symmetric ice [3, 4] which derives from the OH bending mode when OH ··· O hydrogen bonds symmetrize. In parallel with the H_2O case, the ν_2 mode of H_2S seems to convert to a lattice mode without changing frequency at the V–VI transition. However, both the intensity and width of this peak changed

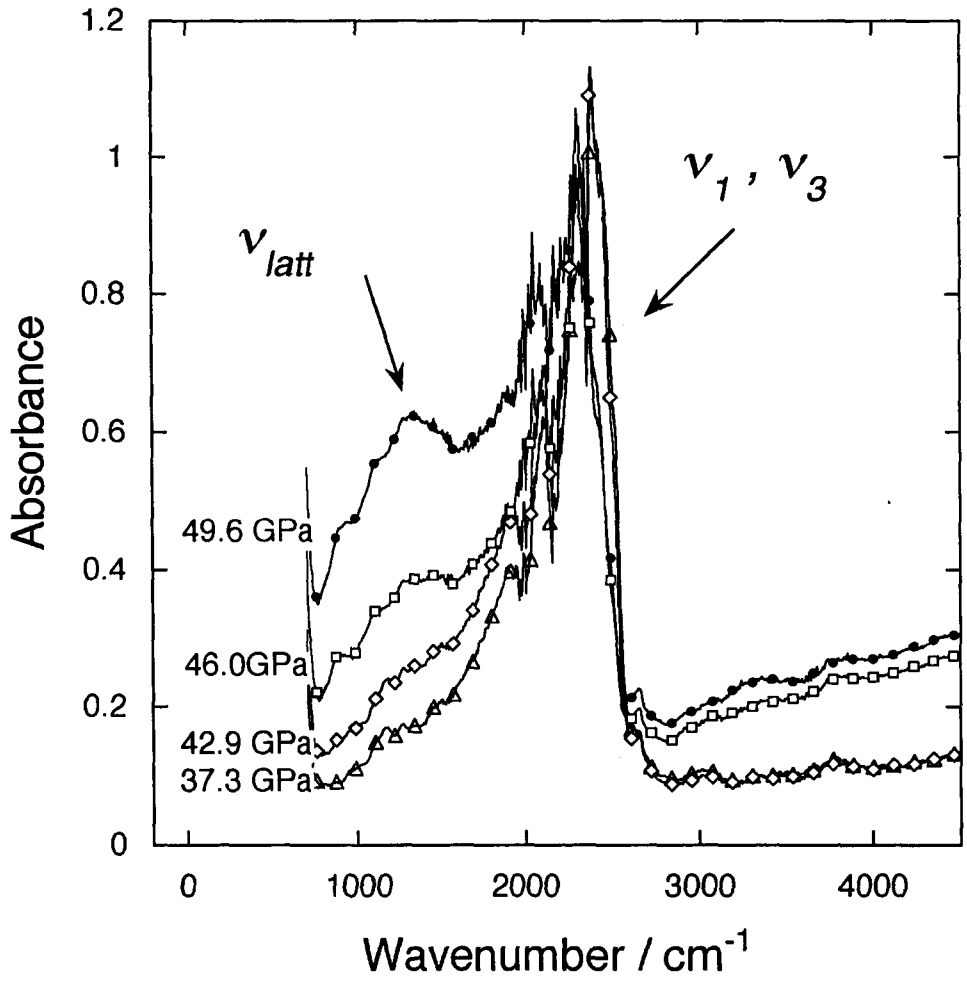

Figure 4-3. Infrared absorption spectra measured for a thick film of H_2S to 50 GPa. The curves are **not** offset in the vertical direction.

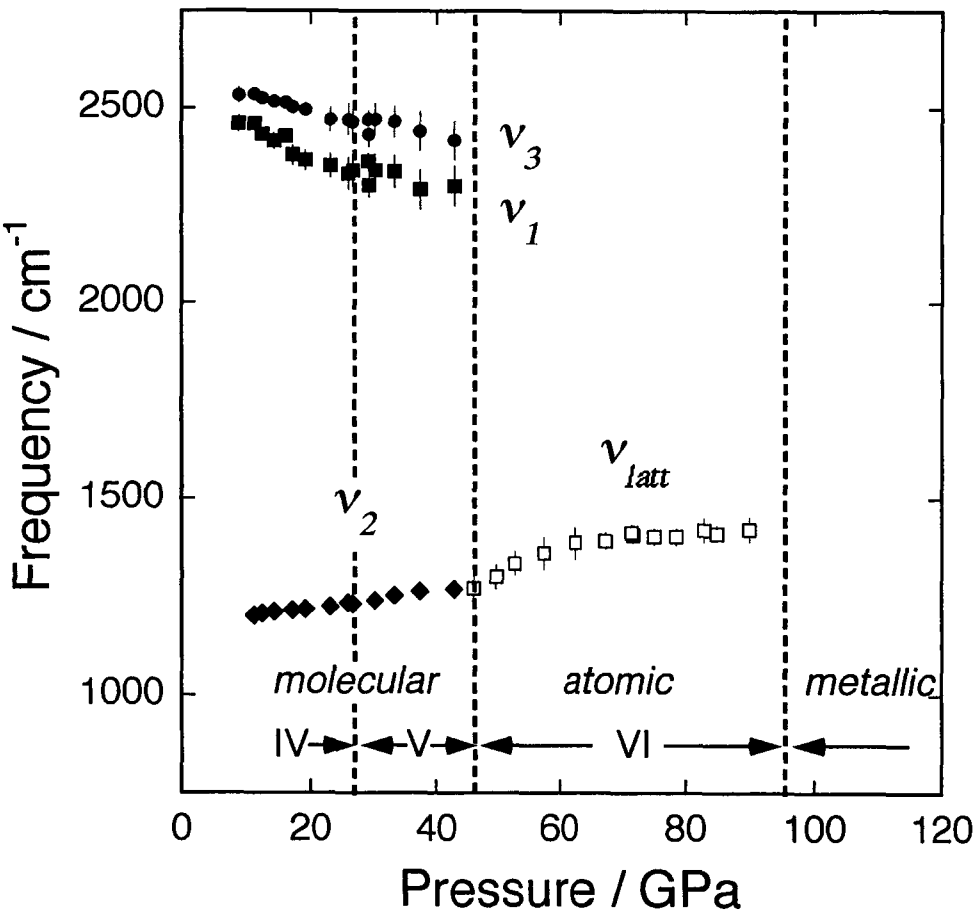

Figure 4-4. Frequencies of the peaks of the infrared spectrum of solid H_2S plotted vs. pressure to 96 GPa.

at the phase boundary. The ν_2 mode of the molecular phase is very weak and narrow,[9] while the lattice mode of the dissociated phase is broad and strong.

At about 96 GPa, the entire specimen became opaque, even in the infrared region, and no vibrational spectrum was able to be detected. We interpret this change as a transition to a metallic phase. Because there is no definite information on the location and bonding state of the H atoms in the metallic state, it is difficult to identify whether segregation into atomic hydrogen and sulfur phases take place.

A likely mechanism for the molecular dissociation transition of H_2S is displacement of the protons from the original hydrogen bonded axes, as depicted in Figure 4-5-(a). In the molecular phase V, H atoms lie on the line joining S atoms by hydrogen bonds. Beyond 46 GPa, the H atoms move from the hydrogen-bond axes in forming an atomic solid. Because H atoms are much smaller than S atoms (the ratio of atomic radii r_H / r_S is roughly 0.3), the H atoms can occupy the interstices among the S atoms. This atomic arrangement in the dissociated solid phase brings each S atom in contact with most neighboring S atoms, forming S–S bonds. This mechanism differs from the dissociative transition in H_2O which proceeds continuously without deviation of H atoms from the line of hydrogen bond. The H atoms remain in the middle between neighboring O atoms in the atomic phase of H_2O, as shown in Figure 4-5-(b). Similarities of the optical properties between solid H_2S and sulfur at very high pressures also support the proposed interpretations of the 46 and 96 GPa transitions of H_2S. The absorption edge of solid sulfur decreases linearly with pressure from 1.1 eV at 40 GPa to 0.65 eV at 70 GPa, and the reflectivity of sulfur suddenly increases at 95 GPa, where it metallizes.[13] Solid H_2S was already black at 40 GPa, with an absorption edge well below 1 eV. As shown in Figure 4-2-b, the electronic

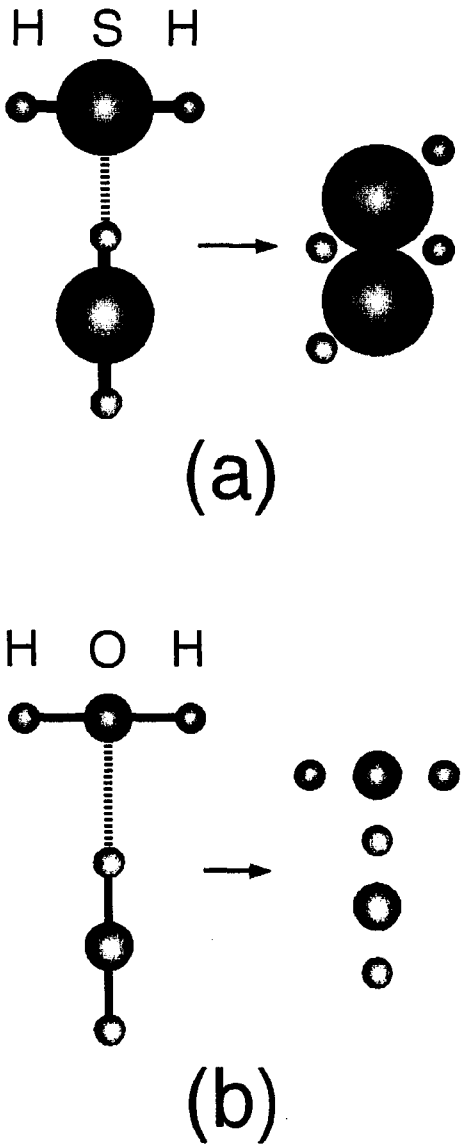

Figure 4-5. Schematic representation of the molecular dissociation processes for (a) H_2S and (b) H_2O, shown as simple linear species.

absorption spectrum of H_2S extended across the infrared region at about 96 GPa. The parallel behavior suggests that S–S bonds form in the dissociated phase of H_2S just as they do for the high-pressure atomic phase of S. That is, S–S bonds may determine the electronic states of both solids with the H atoms having only a slight influence on the electronic states of H_2S near 100 GPa.

The vibrational spectra of H_2O and H_2S also behave differently near their dissociation transitions. For ice, the frequencies of the ν_1 and ν_3 stretching modes decrease very rapidly from 3000 cm^{-1} to nearly 0 just below the transition pressure, about 60 GPa. Beyond the transition, the frequency of the lattice mode of the dissociated phase which develops from these stretching modes gradually increases from zero. That is, for H_2O, the proton-related vibrations show soft-mode behavior during this second-order like dissociation process. H_2S showed no similar soft-mode behavior. The ν_1 and ν_3 modes of H_2S decreased by less than 300 cm^{-1} up to the pressure of the abrupt, first-order like dissociation transition.

In the pressure region below 46GPa, hydrogen atoms determine the molecular arrangements in solid H_2S through forming hydrogen bonds. On the contrary, S atoms govern the electronic properties and crystal structure of the atomic phase, above 46 GPa. The continuous metallization of H_2S, which follows this molecular dissociation transition at higher pressures, presents a new aspect of dissociation-metallization processes in simple molecular solids. The behavior of H_2S differs from the (nearly) continuous changes of structure and electronic states observed for ice [3,4] and halogens.[14-16] Precise structural studies, including atomic positions and even electron densities, will be required to clarify the mechanisms of molecular dissociation and metallization.

4-4. Conclusion

Infrared spectra at high pressure and room temperature reveal that molecular dissociation and metallization occur in solid H_2S near 46 and 96 GPa, respectively. The disappearance of SH stretching bands in the 2300–2500 cm^{-1} region and simultaneous appearance of a lattice vibrational mode around 1300 cm^{-1} indicate the molecular dissociation. Above 46 GPa, a low-energy electronic absorption band develops and eventually extends throughout the infrared region studied (700–6000 cm^{-1}). Thus, metallization of solid H_2S seems to occur by closing a band gap originating from S–S bond formation in the dissociated phase. The molecular dissociation of H_2S is a first-order transition with the protons moving from the axes of the hydrogen bonds. This differs from the second-order like dissociation of H_2O molecules that occur in ice when those hydrogen bonds symmetrize.

References

1) Russel J. Hemley and Neil W. Ashcroft, *Nature*, **380**, 671 (1996).

2) S. T. Weir, A. C. Mitchell, and W. J. Nellis, *Phys. Rev. Lett.*, **76**, 1860 (1996).

3) A. F. Goncharov, V. V. Struzhkin, M. S. Somayazulu, R. J. Hemley, H. K. Mao, *Science*, **273**, 218 (1996).

4) K. Aoki, H. Yamawaki, M. Sakashita, H. Fujihisa, *Phys. Rev. B*, **54**, 15673 (1996).

5) H. Shimizu, Y. Nakamichi, S. Sasaki, *J. Chem. Phys.*, **95**, 2036 (1991).

6) H. Shimizu, H. Yamaguchi, S. Sasaki, A. Honda, S. Endo, and M. Kobayashi, *Phys. Rev. B*, **51**, 9391 (1995).

7) H. Shimizu and S. Sasaki, *Science*, **257**, 514 (1992).

8) S. Endo, A. Honda, S. Sasaki, H. Shimizu, O. Shimomura, T. Kikegawa, *Phys. Rev. B*, **54**, R717 (1996).

9) H. Shimizu, T. Ushida, S. Sasaki, M. Sakashita, H. Yamawaki, K. Aoki, *Phys. Rev. B*, **55**, 5538 (1997).

10) K. Aoki, Y. Kakudate, M. Yoshida, S. Usuba, K. Tanaka, S. Fujiwara, *Jpn. J. Appl. Phys.*, **26**, 2107 (1987).

11) K. Aoki, H. Yamawaki, and M. Sakashita, *Phys. Rev. Lett.*, **76**, 784 (1996).

12) H. K. Mao, J. Xu, P. M. Bell, *J. Geophysical Res.*, **91**, 4673 (1986).

13) H. Luo, S. Desgreniers, Y.K. Vohra, and A.L. Ruoff, *Phys. Rev. Lett.*, **67**, 2998 (1991).

14) K. Takemura, S. Minomura, O. Shimonura, and Y. Fujii, *Phys. Rev. Lett.*, **45**, 1881 (1980).

15) Y. Fujii, K. Hase, Y. Ohishi, H. Fujihisa, N. Hamaya, K. Takemura, O. Shimomura, T. Kikegawa, Y. Amemiya, and T. Matsushita, *Phys. Rev. Lett.*, **63**, 536 (1989).

16) H. Fujihisa, Y. Fujii, K. Takemura, and O. Shimomura, *J. Phys. Chem. Solids*, 56, 1439 (1995).

Chapter 5

Phase Transitions and Chemical Reactions in D_2S under Pressure

5-1. Introduction

Deuterium sulfide (D_2S), a deuterium isotope of H_2S, is also a hydrogen-bonded molecular material. Its sample enables us to assign vibrational peaks through the isotopic shift and to get further information about molecular dissociation of H_2S. When hydrogen atoms are replaced by deuterium atoms, the frequencies of vibrations are altered because of the two-fold increase in mass. In addition, the detection of the presence or absence of the similar isotope effect on the transition behavior will provide us a criterion for the phase transition mechanism of solid H_2S. In the case of ice, the transition pressures relating to hydrogen-bond symmetrization are found to be higher in D_2O by 10–15 GPa than in H_2O.[1-3)]

As described in Chapter 4, the disappearance of S–H stretching peaks and the simultaneous appearance of a lattice vibrational peak near 46 GPa indicate molecular dissociation of H_2S.[4)] Although the mechanism of molecular dissociation in H_2S is yet to be fully described, recent reports have provided useful information. X-ray powder diffraction revealed that the structure of phase IV (11–28 GPa) is tetragonal D_{4h}^{20} - $I4_1$ /acd, and that its first nearest S–S distance is shorter than twice the van der Waals radius of sulfur.[5)] This suggests the possibility of the formation of S–S covalent bonds above 28 GPa, because the first nearest S–S distance is expected to become much shorter with increasing pressure. In addition, Raman studies of H_2S have found that lattice vibrational peaks change notably at IV–V transition.[6)] It is considered that molecular dissociation begins around 27–35 GPa on the

basis of the Raman data. This dissociation pressure is about 15 GPa lower than that found from infrared measurements in Chapter 4.

To clarify the mechanism of molecular dissociation in solid H_2S, We asked ourselves (1) what happens in the chemical bonds above 28 GPa; (2) whether S–S covalent bonds form above 28 GPa; (3) what initiates molecular dissociation. This chapter describes infrared and Raman studies on solid D_2S undertaken with a diamond-anvil cell in the hope of answering these questions. As is well-known, Raman and infrared spectroscopy plays complementary roles, and the following remarks may be pertinent here.

Raman measurement is helpful to confirm the formation of S–S bonds, if the S–S stretching modes appear in the frequency region below 600 cm^{-1}, which is difficult to observe by infrared spectroscopy. However, the information provided by Raman measurement concerns mainly the surface region of a sample of solid H_2S. On the contrary, infrared spectroscopy can detect changes in the bonding state, occurring not only on the surface but also in the inner part of a sample.

5-2. Experimental

Commercially available gaseous D_2S (97 atom% D) was used without further purification. A 100-μm diameter and 50-μm thick sample chamber was drilled in a metal gasket (PK). The chamber was filled with solidified D_2S. Infrared absorption spectra were measured with a microscope FT-IR spectrometer. The spectral resolution was set to 1 cm^{-1}, and each spectrum was accumulated 400 times. A reference spectrum of KBr in DAC at high pressure was used to compensate for the absorption by the diamond anvils. The 488 nm line of an argon ion laser was used for Raman excitation. Back-scattered light from the sample was analyzed using a single

monochromator and two holographic notch filters. The apparatus to perform infrared and Raman experiments has been extensively described in Chapter 2. Pressures were measured from shifts of fluorescence line from ruby chips embedded in the sample.[7)]

5-3. Results and Discussion

Figure 5-1 shows changes in infrared absorption spectra of D_2S measured up to 54 GPa. Because the diamond windows of the pressure cell are nearly opaque in the frequency range from 1800 to 2400 cm^{-1}, the quality of the spectra was poor in this range. Deuterium substitution reduced the fundamental frequency by a factor of about $1/\sqrt{2}$. Broad peaks observed around 1700 cm^{-1} were assigned to the fundamental S–D stretching modes (ν_1 and ν_3), and the peaks at 842 cm^{-1} and 3590 cm^{-1} at 8.8 GPa were assigned to a bending ν_2 and the overtone of the stretching modes ($2\nu_{SD}$), respectively. Peaks around 2500 cm^{-1} originated from S–H stretching modes of impurity HDS. On increasing pressure to 10 GPa, the ν_2 peak became sharp, the $2\nu_{SD}$ peak split into two peaks, and a combination peak ($\nu_2 + \nu_L$, ν_L: lattice vibrational peak) appeared at 1160 cm^{-1}. These spectral changes correspond to an orientational disorder–order phase transition (I'–IV) noted in earlier studies.[8, 9)]

On further compression to 27 GPa, a new shoulder peak appeared at 3585 cm^{-1}, the high-frequency side of the original $2\nu_{SD}$. Furthermore, in the region of the bending mode, another peak appeared at 32 GPa at 870 cm^{-1}, 25 cm^{-1} lower than the position of the original ν_2. These new peaks gradually grew in intensity as the pressure increased and coexisted with the peaks belonging to phase IV up to 54 GPa. Deuterium substitution also reduced the frequencies of the new peaks: the peaks of D_2S are at 847 and 3537 cm^{-1} at

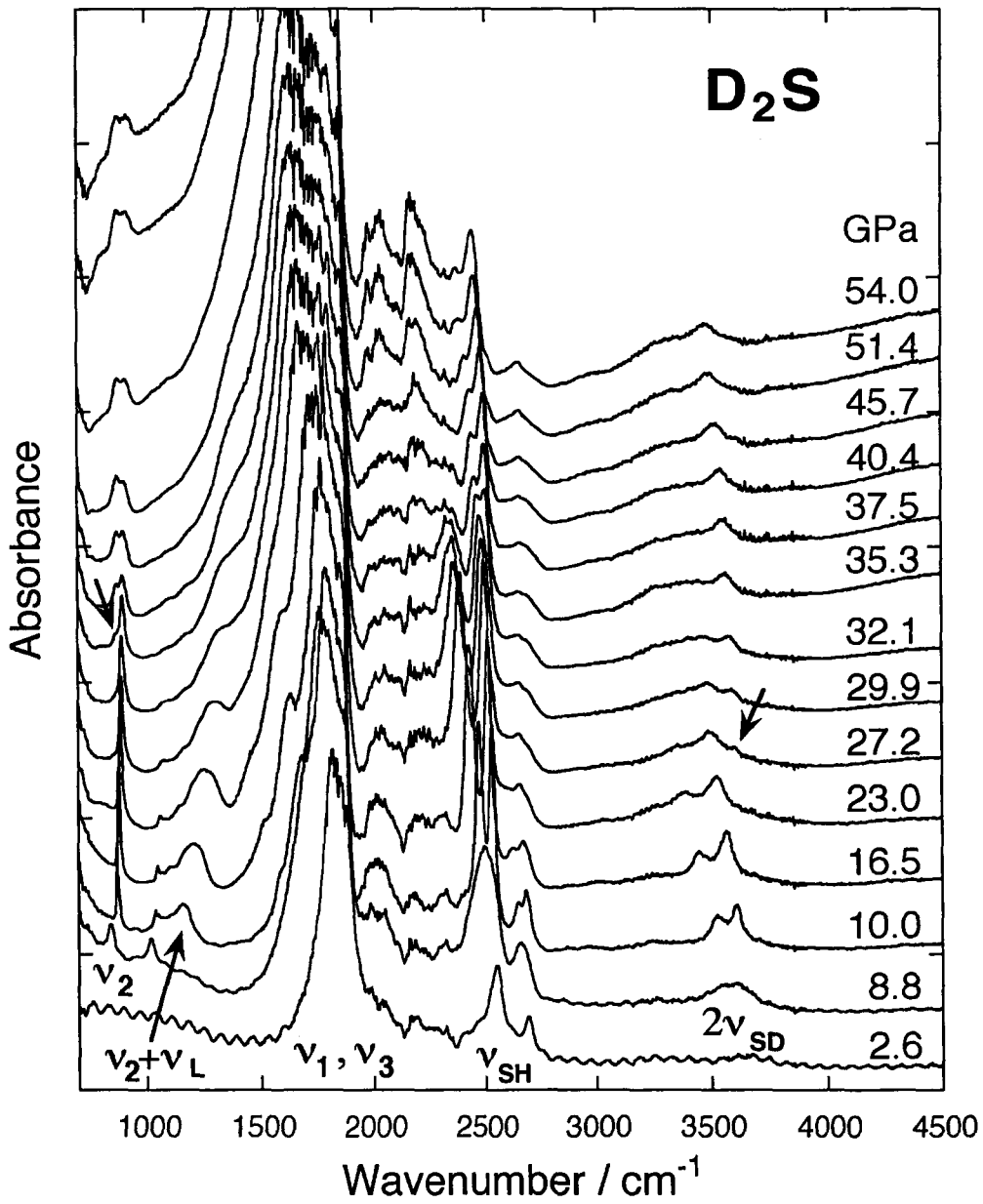

Figure 5-1. Infrared absorption spectra of solid D_2S up to 54 GPa at room temperature. The initial thickness of the sample was about 50μm. New infrared peaks marked with arrows appeared around 3580 cm^{-1} and 870 cm^{-1} above 27 GPa. The curves are offset in the vertical direction for clarity.

40 GPa, while those of H_2S are at 1176 and 4768 cm^{-1} at the same pressure. The ratio ν_{H2S} / ν_{D2S} was close to $\sqrt{2}$ (1.39 and 1.35), indicating that these peaks originate from the vibrational modes involving S–D stretching, probably ν_2 and $2\nu_{SD}$. Figure 5-2 shows the Raman spectra of D_2S measured up to 35 GPa. The stretching peak split into two narrow peaks, ν_1 and ν_3, and the ν_L peak appeared at 10 GPa. These spectral changes indicate that an order–disorder transition takes place at 10 GPa, which is consistent with previous work.[8, 9] Weak ν_2 peaks were observed at around 800 cm^{-1} and 900 cm^{-1}. On further compression to 27 GPa, two peaks appeared at around 480 cm^{-1} and 500 cm^{-1}, as shown in Figure 5-3. Corresponding peaks were also investigated by Raman scattering from H_2S, [6] and the peak positions for H_2S and D_2S were found to be almost the same. Hence, these two peaks are assigned not to S–D vibration but to S–S or lattice vibrations. The color of the sample gradually changed from almost transparent to orange, dark red, and black above 27 GPa. Owing to the opaqueness, the incident laser beam could hardly penetrate the sample. Thus, all Raman peaks became weak.

The pressure shifts of the infrared and Raman frequencies are illustrated in Figure 5-4. The stretching peaks (ν_1, ν_3, and $2\nu_{SD}$) slightly shifted to the low frequency side, and the bending peaks ν_2 shifted to the high frequency side with increasing pressure. The pressure behavior of infrared and Raman peaks of D_2S was similar to that of H_2S.[8–10] The stretching ν_1 peak shifted at the ratio of –5.2 cm^{-1} / GPa in phase IV of D_2S. This pressure dependence is remarkably small compared with the value of –58 cm^{-1} / GPa for the O–H stretching ν_1 peak of solid ice, which suggests that the S–H covalent bonds weaken slightly and the hydrogen bonds become slightly stronger with compression.

As a result of the movement of a gasket hole in the culet, pressure

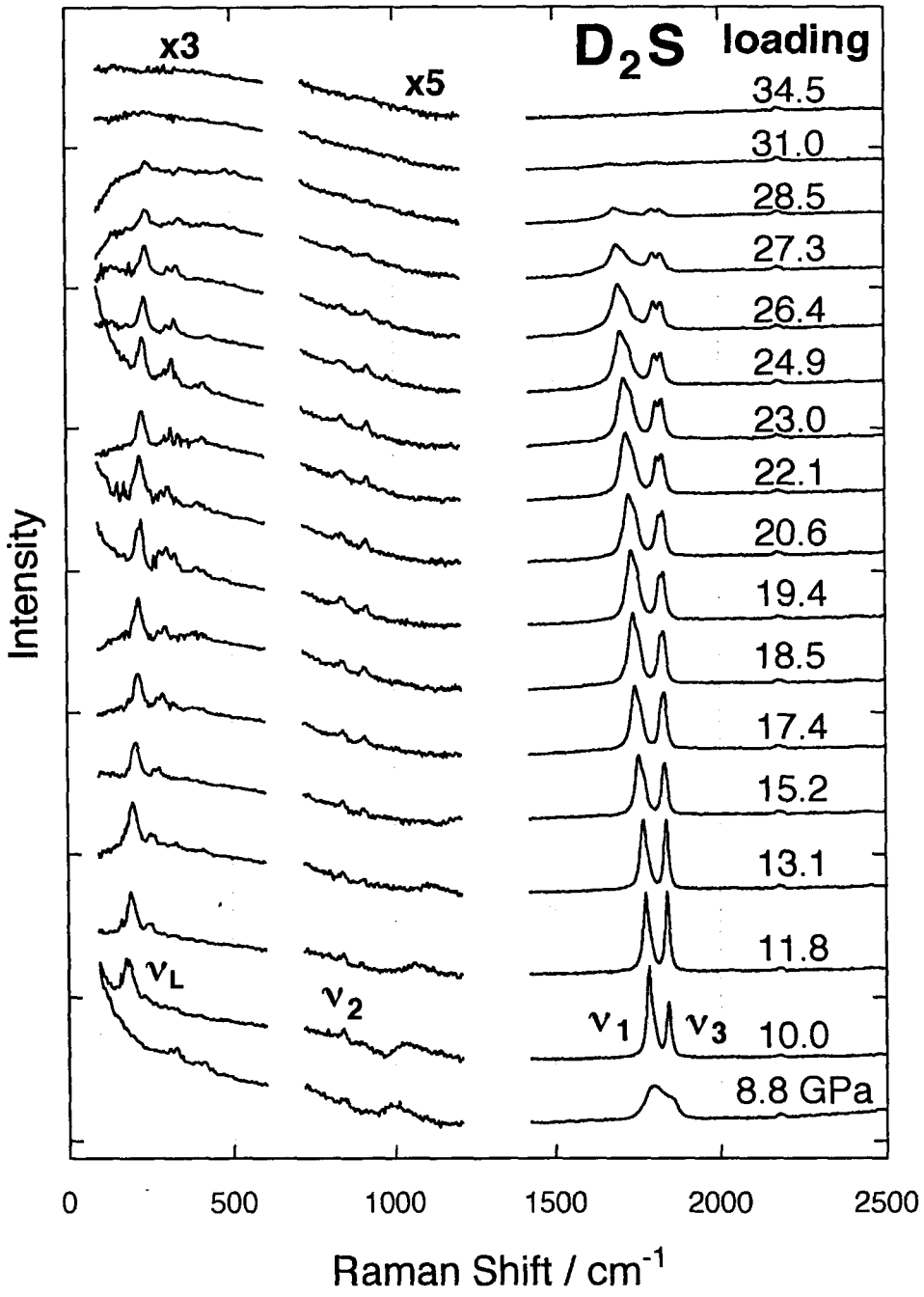

Figure 5-2. Raman spectra of solid D_2S up to 35 GPa at room temperature.

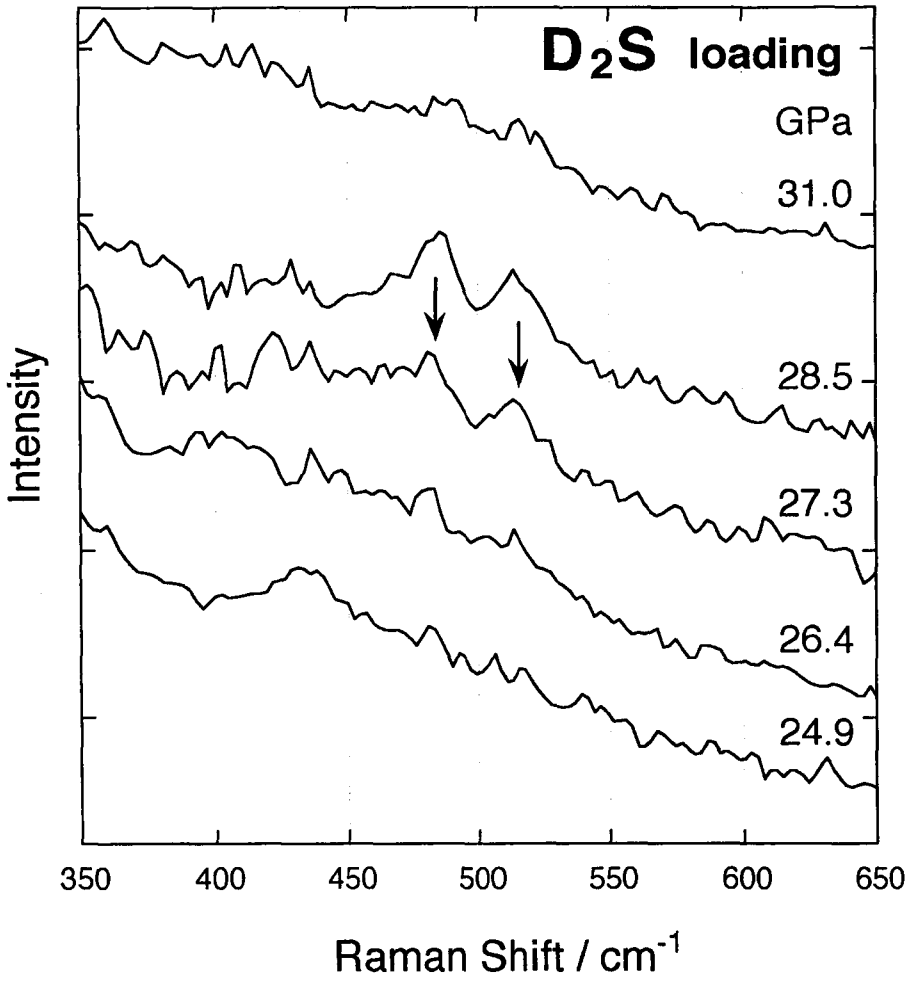

Figure 5-3. Magnification of Raman spectra of solid D_2S around 27 GPa. The arrows mark the new Raman peaks assigned to S–S stretching modes.

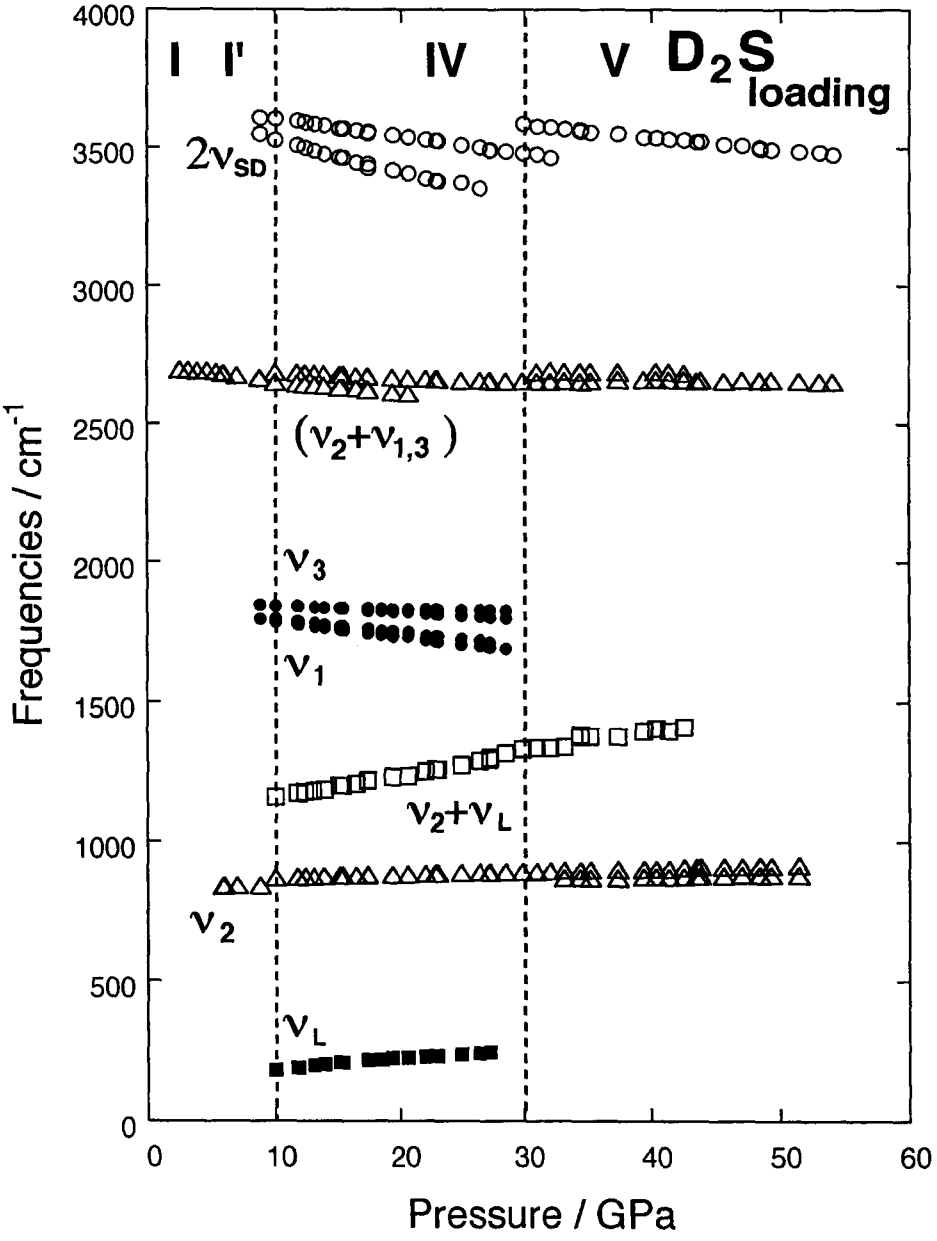

Figure 5-4. Variations in the vibrational frequencies of D_2S with pressure obtained by infrared (open symbols) and Raman (solid symbols) measurements. Two dashed vertical lines show phase boundaries.

gradients across the sample increased during pressure release. These pressure gradients led to different Raman spectral features, depending on the position of a specimen. In the part at higher pressure, several signals were detected mainly at 100–600 cm^{-1} (Figure 5-5-a) and should be assigned to the S–S stretching modes. Raman spectra observed in the pressure range from 25 to19 GPa resembled those of the high-pressure low-temperature (*hplt*) phase of sulfur, which was reported as a metastable phase obtained above 12 GPa by a low-power laser radiation for an ordinary crystalline sulfur.[11] The peak positions of the present sample, 221, 471 and 506 cm^{-1} at 19 GPa, correspond well to those of the *hplt* phase, 222, 469, and 504 cm^{-1} at the same pressure. One broad feature observed at 5.4 GPa at 100–600 cm^{-1} was similar to that of helical sulfur.[12] The Raman spectra dramatically changed at 0.1–0.2 GPa: six sharp peaks appeared at 100–600 cm^{-1}. All six peaks correspond well to intramolecular vibration of S_8 ring molecule, and the peaks centered at 154, 188, 220, 247, 439, 474 cm^{-1} are assigned to E_2, B_1, A_1, E_3, E_3, A_1 species, respectively.[13]

In the part at lower pressure, Raman peaks were observed in both S–D and the S–S stretching regions (Fig. 5-5-b), indicating that S–D and S–S bonds coexisted in the sample. The peaks observed at 1600–1900 cm^{-1} were different from those observed in the loading process: the ν_1 peak appeared to be much stronger than ν_3, and several peaks overlapped with the original ν_1 and ν_3 peaks. The additional peak observed at the low frequency side of ν_1 could be assigned to the S–D stretching peak of sulfanes (hydrogen polysulfides), D_2S_X. A broad peak observed around 1800 cm^{-1} in the pressure range of 5–0.1 GPa was at almost the same position as the peak in phase I, indicating that some D_2S molecules returned to phase I. Spectral changes in the 100–600 cm^{-1} region of Figure 5-5-b are similar to those of Figure 5-5-a.

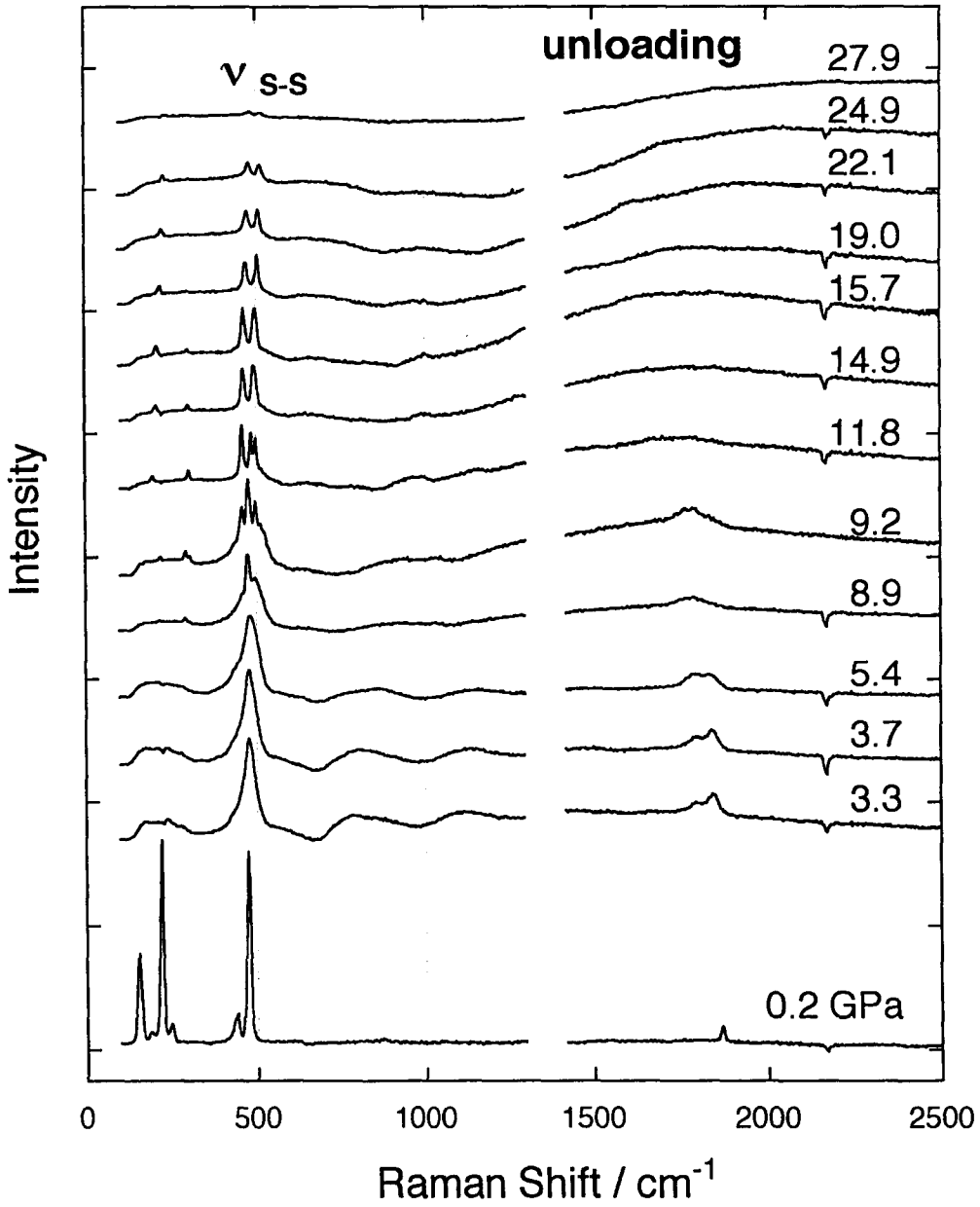

Figure 5-5-a. Raman spectra of D_2S measured for the part of the sample at higher pressure in the unloading process.

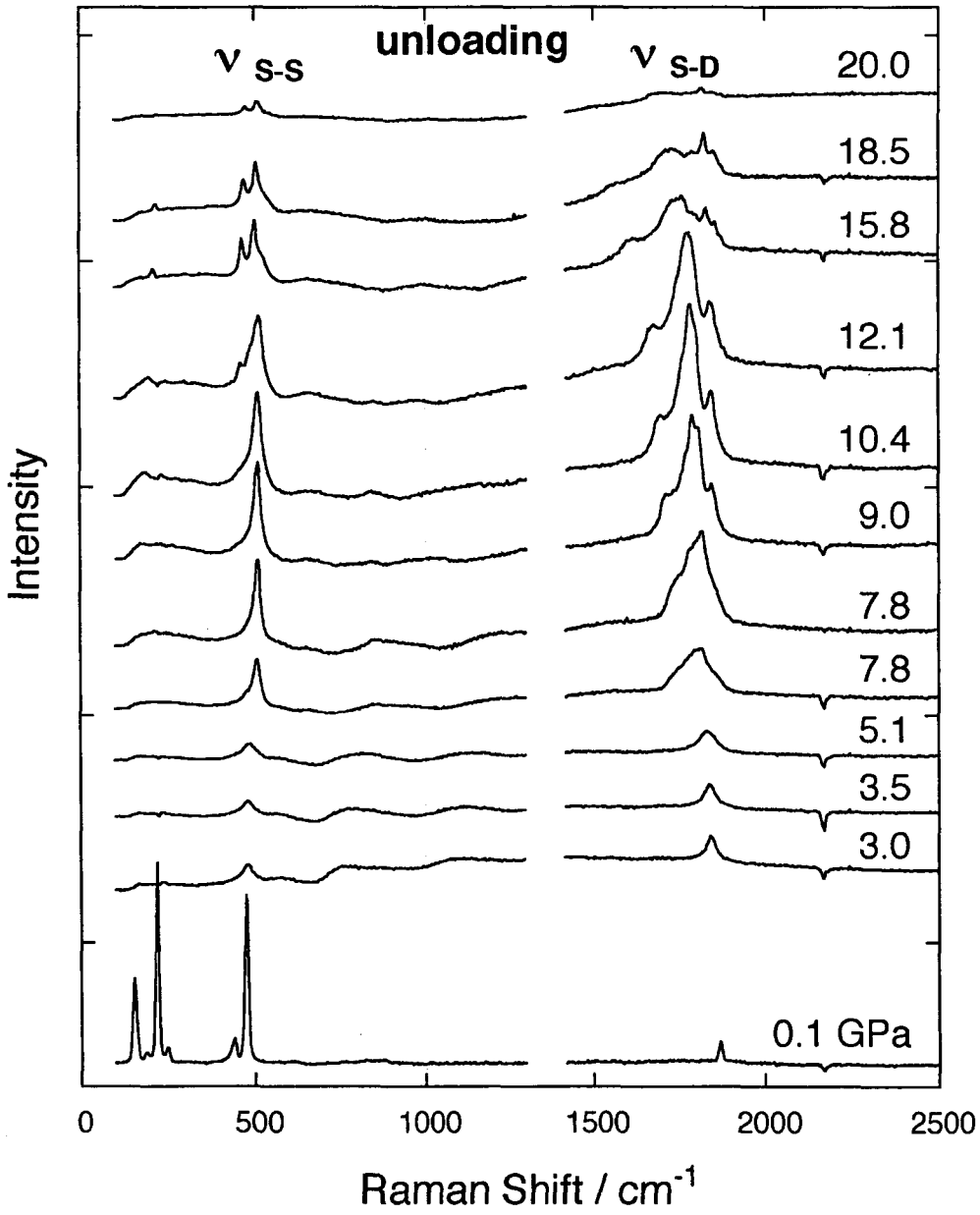

Figure 5-5-b. Raman spectra of D_2S measured for the part of the sample at lower pressure in the unloading process.

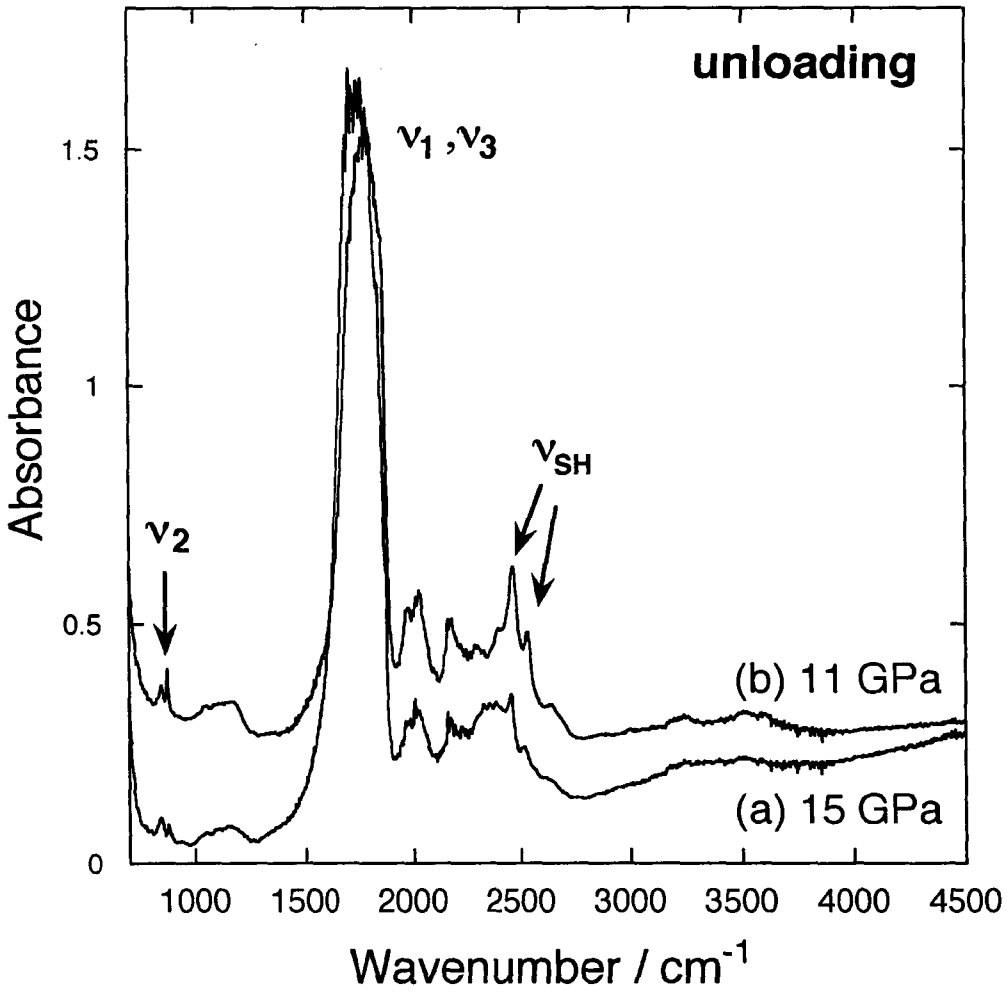

Figure 5-6. Infrared spectra of D_2S measured for the part of a sample at higher pressure (a) and at lower pressure (b) in the unloading process. The arrows indicate the peaks originating from phase IV.

Contrary to the Raman spectra, infrared spectra of solid H_2S did not show such significant spectral differences between the high-pressure and low-pressure parts. For example, the S–D stretching peaks, ν_1 and ν_3, with almost the same intensity were observed in both parts. This is because S–D bonds persisting inside the sample gave dominant features in the transmission spectra of the both parts. A smaller amount of the phase-IV peaks remaining in the part at higher pressure (Figure 5-6-a) only indicates dissociation that proceeded more in the part at higher pressure than at lower pressure. Unreacted D_2S evaporated when the sample was released to ambient pressure, and some solid remained. The solid showed no detectable peak in the mid-infrared region studied, although sulfur has an infrared peak ($2\nu_{10}$) at 870 cm^{-1} at ambient pressure.[14)]

Infrared absorption and Raman scattering are complementary techniques, and a comparison between vibrational frequencies of H_2S and those of D_2S helps to assign every peak of the spectra. We will interpret the observed infrared and Raman spectra and then propose a model which can consistently explain the molecular dissociation process in H_2S and D_2S on the basis of infrared, Raman, and X-ray diffraction data.[15)]

Two new infrared peaks observed at 3585 and 870 cm^{-1} above 27 GPa (Figure 5-1) suggest that some D_2S molecules are arranged in a different manner from those of phase IV in the pressure region above 27GPa. These peaks do not originate from a dissociated phase where the S–D bonds are lost, but should be assigned to the fundamental bending and overtone S–D stretching vibrations. The S–D stretching peak usually shifts to lower frequency with increasing pressure, since intermolecular hydrogen bonds become stronger as the molecules approach each other. Thus, the appearance of the new overtone at a higher frequency than the overtone band of phase IV

indicates that the hydrogen bonds of some molecules become weak around 27 GPa. Further, the continuous softening (low-frequency shift) of the overtone vibrations with pressure indicates that the S–D...S hydrogen-bond system still exists above 27 GPa, as in the case of H_2S.[10] The lower position of the bending peak also indicates weakened intermolecular interaction. Intensity changes in the infrared absorption peak reflect the change in volume of its related chemical species. Thus, the observed increase in the intensity of the two new peaks with pressure (Figure 5-1) suggests a gradual increase in the amount of an additional chemical species. The coexistence of the new peaks with the peaks of phase IV up to 54 GPa indicates that additional and original chemical species coexist from 27 to 54 GPa.

On the other hand, several Raman peaks observed in the 100–600 cm^{-1} region suggest that decomposition of D_2S to sulfur begins around 27 GPa. Those peaks probably originate from S–S covalent bonds, indicating formation of sulfur. The occurrence of sulfur also explains the drastic change in lattice vibrational peaks investigated by Raman experiment on H_2S.[6] The Raman spectral changes observed in the 100–600 cm^{-1} region during pressure release process suggest that the following structural changes take place in some parts of the sample; the *hplt* phase of sulfur appears at 25GPa, helical suffur around 5 GPa, and then S_8 rings near 1 atm. This interpretation is based on the similarity of the Raman spectra between the present sample and those of sulfur, although the Raman spectra of sulfur at high pressures have not been well defined yet. Helical sulfur was reported to have a chain structure, while the molecular structure of *hplt* phase is not clear. The S_8 molecule is a puckered eight-atom ring and is most stable at ambient pressure and temperature. It was reported that the characteristic features of the S_8 ring appear also from high-pressure phases of sulfur when unloading to 1 atm.[11]

Here we consider the process in which D_2S molecules dissociate under pressure to produce finally S_8 cyclic molecules. The structure of phase IV will yield useful information in explaining the process, since the molecular dissociation occurs around 27 GPa in phase IV. There is a weak interaction between the nearest sulfur atoms in phase IV in which the molecules form spiral chains along the c-axis,[5] and the first nearest S–S distance is 3.050 Å at 14.0 GPa, only 0.1 Å longer than the sum of "constant energy radii" of sulfur. Huggins introduced the concept of "constant energy radii" in an equation relating interatomic distances to bond energies.[16] When the interatomic distance is longer than the sum of "constant energy radii", there is no bonding nature between the atoms. It is natural to imagine that as S–S distances become shorter on further compression, S–S covalent bonds are formed. In addition, the similar transition pressures of H_2S and D_2S suggest that the approach of S atoms causes molecular dissociation to form helical sulfur with its chain structure. In the unloading process, the helical sulfur may not revert to D_2S but change to the S_8 cyclic molecule.

Very recently X-ray diffraction experiments on solid H_2S were performed up to 50 GPa.[15] The diffraction patterns indicate that several phases coexist above 28 GPa, which is consistent with the present infrared and Raman results on D_2S. These phases are: phase IV of H_2S, phase II of sulfur, amorphous phase, and undefined crystalline phase. The amorphous phase can involve both H_2S and sulfur molecules. No diffraction peaks of the undefined crystalline phase overlapped with peaks of α- sulfur or β- sulfur. On the basis of these X-ray results, it is inferred that the infrared peaks due to S–D bonds observed above 27 GPa correspond to the amorphous or undefined crystalline phase of D_2S, and the Raman peaks due to S–S bonds correspond to the phase II or amorphous phase of sulfur.

The outcome of the above discussion is summarized in Figure 5-7, which schematically shows changes in molecular structure and bonding manner of D_2S with increasing and decreasing pressure. When D_2S molecules in phase IV (a) are compressed above 27 GPa, S–S covalent bonds form between the nearest S atoms, resulting in $(D_2S)_X$ chains (b). Then, deuterium must be removed from $(D_2S)_X$ chains to produce S_X chains (c). In the unloading process, S_X chains change to S_8 cyclic molecules (d). Sulfur atoms could be tetracoordinated in the $(D_2S)_X$ chains (b) and bonded to two deuterium and two sulfur atoms like SF_4, where four bonding electron pairs and one lone pair together form a trigonal-bipyramidal molecule. The sulfur atoms are assumed to be at apical positions, and two deuterium atoms and one lone pair of electrons at equatorial positions, since the more electronegative ligand prefers to occupy the apical position [17] and the ligand which forms the covalent bond with a central atom such as hydrogen and methyl groups prefers to coordinate in the equatorial position.[18] The apical bonds have shown to be three-center four-electron bonds in a trigonal-bipyramidal molecule. When the $(D_2S)_X$ chains are formed, the deuterium atoms move from hydrogen-bond axes, resulting in the weakening of hydrogen bonds. Thus, the $(D_2S)_X$ chains (b) explain the infrared peaks observed above 27 GPa, which is consistent with the appearance of the Raman peaks due to S–S stretching modes.

5-4. Conclusion

Experiments using a diamond-anvil cell show that deuterium sulfide (D_2S) dissociates to form sulfur at pressures above 27 GPa and at room temperature. Raman-scattering spectroscopy indicates the presence of the S–S bonds of the high-pressure phase of sulfur above 27 GPa, although

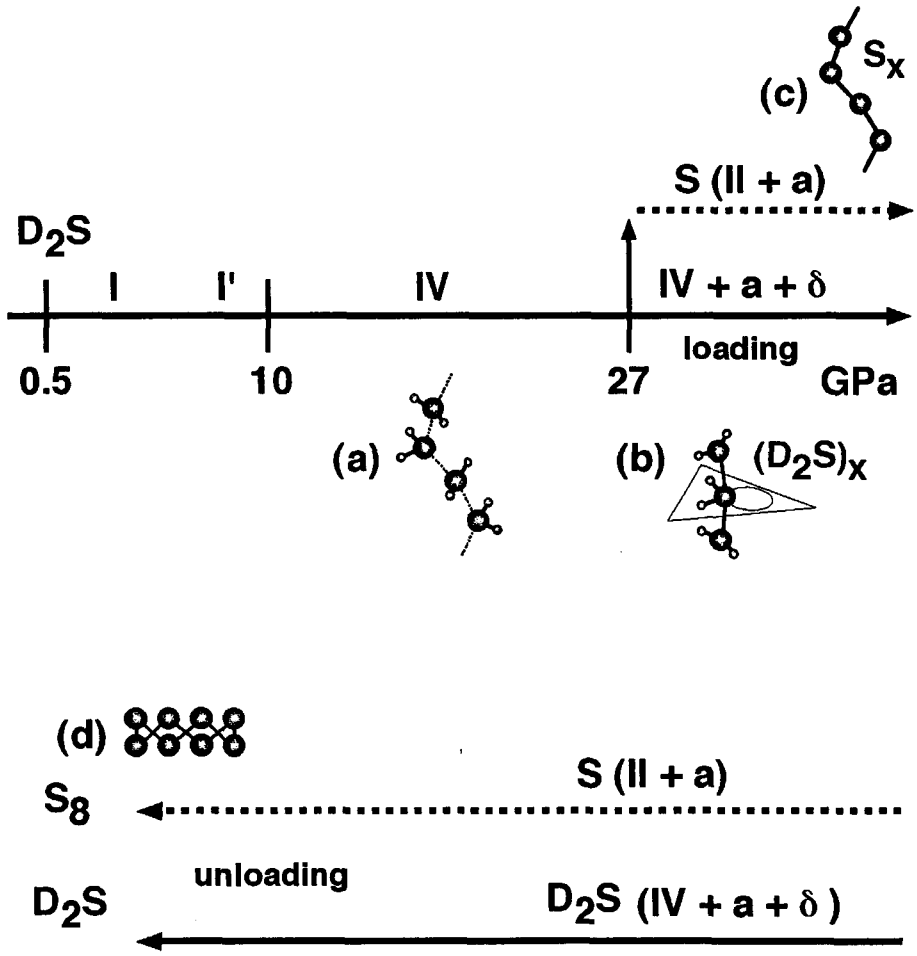

Figure 5-7 Schematic representation for changes in molecular structure and bonding manner of a sample. Part of D_2S dissociated to form sulfur above 27 GPa (dashed line). Both D_2S and sulfur persist in the sample in the unloading process. (a): amorphous and (δ): undefined crystalline phase.

infrared-absorption spectroscopy indicates the presence of the S–D bonds of both polymeric and unreacted D_2S. Judging from the experimental results of D_2S and the previous Raman data of H_2S, it is suggested that molecular dissociation begins in H_2S also around 27 GPa. Similarity in the dissociation pressure of H_2S and D_2S suggests that correlation between sulfur atoms has the key to the molecular dissociation process in H_2S and D_2S.

References

1) A. F. Goncharov, V. V. Struzhkin, M. S. Somayazulu, R. J. Hemley, H. K. Mao, *Science*, **273**, 218 (1996).

2) K. Aoki, H. Yamawaki, M. Sakashita, H. Fujihisa, *Phys. Rev. B*, **54**, 15673 (1996).

3) Ph. Pruzan, E. Wolanin, M. Gauthier, J. C. Chervin, B. Canny, D. Häusermann, M. Hanfland, *J. Phys. Chem. B*, **101**, 6230 (1997).

4) M. Sakashita, H. Yamawaki, H. Fujihisa, K. Aoki, S. Sasaki, H. Shimizu, *Phys. Rev. Lett.*, **79**, 1082 (1997).

5) H. Fujihisa, H. Yamawaki, M. Sakashita, K. Aoki, S. Sasaki, H. Shimizu, *Phys. Rev. B*, **57**, 2651 (1998).

6) M. Yamagishi, H. Furuta, S. Endo, M. Kobayashi, *Sci. and Technol. of High Pressure*, Proceedings of AIRAPT-17, edited by M.H. Manghnani, W.J. Nellis and M.F. Nicol, Univ. Press, Hyderabad, India, 391 (2000).

7) H. K. Mao, J. Xu, P. M. Bell, *J. Geophysical Res.*, **91**, 4673 (1986).

8) H. Shimizu, Y. Nakamichi, S. Sasaki, *J. Chem. Phys.*, **95**, 2036 (1991).

9) H. Shimizu, H. Murashima, S. Sasaki, *J. Chem. Phys.*, **97**, 7137 (1992).

10) H. Shimizu, T. Ushida, S. Sasaki, M. Sakashita, H. Yamawaki, K. Aoki,

Phys. Rev. B, **55**, 5538 (1997).

11) W. Häfner, H. Olijnyk, A. Wokaun, *High Pressure Res.*, **3**, 248 (1990).

12) B. Eckert, H. J. Jodl, H. O. Albert, P. Foggi, P. Frontiers of High-Pressure Research; Plenum Press: New York, 143 (1991).

13) D. W. Scott, J. P. McCullough, F. H. Kruse, *J. Mol. Spectrosc.*, **13**, 313 (1964).

14) G. W. Chantry, A. Anderson, H. A. Gebbie, *Spectrocheim. Acta*, **20**, 1223 (1964).

15) H. Fujihisa, H Yamawaki, M. Sakashita, A. Nakayama, T. Yamada, and K Aoki, *Phys. Rev. B*, **69**, 214102 (2004).

16) M. L. Huggins, *J. Am. Chem. Soc.*, **75**, 4126 (1953).

17) J. A. Deiters, R. R. Holmes, J. M. Holmes, *J. Am. Chem. Soc.*, **110**, 7672 (1988).

18) H. Wasada, K. Hirao, *J. Am. Chem. Soc.*, **114**, 16 (1992).

Chapter 6

Phase Transitions in Sulfur under Pressure

6-1. Introduction

Sulfur is a molecular crystal having the orthorhombic phase S-I, α-sulfur under ambient conditions. The molecules are crown-shaped rings consisting of eight sulfur atoms. Although the S-I phase of sulfur has no unsaturated bonds, reconstruction of molecular forms is expected to occur for sulfur under pressure, because it has a large number of allotropes and molecular forms including ring (S_6, S_8, S_{12}, etc.) and chain structures.[1] In addition, sulfur was formed from H_2S and D_2S at pressures above 27 GPa and room temperature as described in Chapters 4 and 5. When S–S distances become shorter on compression, reconstruction of S–S bonds will be expected to occur.

Pressure-induced structural transitions have been observed for sulfur under pressure and at room temperature using X-ray diffraction techniques. Akahama *et al.* found that the orthorhombic phase S-I transforms into a crystal phase S-II at 26.5–34 GPa via an amorphous phase, and further to a base-centered orthorhombic phase S-III at 83 GPa.[2] Luo and Ruoff reported the finding of similar phase transitions.[3,4] Optical transmission and reflection studies have shown that the transition to the S-III phase is near to the insulator–metal transition at 95 GPa.[5] On further compression at 162 GPa, sulfur transforms to a β- Polonium structure.[4] Neither crystal systems nor lattice constants are known for the S-II phase; only the pressure dependence of the interplanar spacings (d-values) were reported. For the S-III phase, the crystal system (base-centered orthorhombic structure) and the pressure

dependence of d-values were reported. Molecular structures, namely the atomic positions in the unit cell, have not yet been determined for both the S-II and S-III phases.

The crown-shaped S_8 rings are stable up to at least 12 GPa. Luo *et al.* showed by Raman spectroscopy with low laser power that the crown-shaped S rings remain intact under pressures of up to 12 GPa.[6] Anderson reported by infrared absorption spectroscopy that no breakdown of the S_8 ring molecules into chains occurs below 10 GPa.[7] The S_8 ring molecules can be broken, however, under very high pressures. The Raman spectrum of a sample that was compressed to 212 GPa and then decompressed to 0 GPa, was different from the spectrum of the original S_8 ring molecule.[4]

The Raman technique is very useful for understanding the molecular structure of sulfur, but it has the property of causing laser-triggered photoinduced transitions, especially under pressure. For example, Häfner *et al.* measured Raman spectra of sulfur at up to 50 GPa and found two different kinds of photoinduced transitions at about 12 GPa.[8] Luo *et al.* suggested that the absorption of energy to dissociate the S_8 units is a result of a pressure-induced narrowing of the band gap.[6] Yoshioka *et al.* reported that the use of a laser with sufficient power causes the dissociation of S_8 ring molecules and a transition to an S_6-featured phase at a pressure lower than the structural transition pressure.[9] Eckert summarized the effects of experimental conditions, such as the energy of the incident laser, on the phase transition phenomena of sulfur.[10]

One of the purposes of the present work is to understand, at the molecular level, the pressure-induced transitions of sulfur in the absence of laser excitation. Infrared spectroscopy should be able to probe the structure of sulfur without inducing photoinduced transitions, since the samples are

exposed to low-energy photons only. In this chapter, we report the changes that occur in S_8 ring molecules during the transitions from the S-I phase to amorphous and high-pressure S-II phases. We propose the molecular structure of the S-II phase on the basis of the present results and of the previously reported X-ray and Raman studies.

6-2. Experimental

Orthorhombic crystalline sulfur with a purity of 99.9999% was commercially obtained (from Wako Pure Chemical Industries, Ltd.) and used without further purification. The sample and small ruby chips were placed in the hole of a metal gasket (a spring steel, PK) sandwiched between diamond anvils. No pressure-transmitting media were used. Infrared absorption spectra of sulfur were measured at pressures in the range 1–58 GPa at room temperature using a micro FT-IR spectrometer (measuring range 450–4400 cm^{-1}). Pressures within the sample were determined from the pressure-induced shifts of the ruby fluorescence line.[11] The sample was exposed to laser power below 0.1 mW. The focusing spot of the laser on the sample was 5–10 μm in diameter.

To get additional information about molecular structure, Raman scattering spectra also were measured for the sample during the unloading process, but only at pressures lower than 3.1 GPa (see Chapter 2 for the experimental setup). To avoid a photoinduced transition, the laser power at the sample was kept below 1 mW.

6-3. Results and Discussion

The infrared spectra of sulfur changed during compression up to 57 GPa as shown in Figure 6-1. Two peaks were observed at 1.1 GPa: the ν_5

mode (S–S stretching) at 470 cm^{-1} and the $2\nu_{10}$ mode (the overtone of stretching) at 856 cm^{-1}. These peaks shifted continuously to higher frequencies upon loading (increasing pressure). The intensity of the signal of the $2\nu_{10}$ mode decreased with increasing pressure. In the pressure range between 20 and 35 GPa, where an amorphous phase was reported[2, 3] by an X-ray diffraction study, no absorption peaks were observed in the spectra other than broad features at around 500 cm^{-1}. This broad feature indicates a loss of a molecular structure with one characteristic S–S distance, and suggests that the S_8 ring molecules were broken. Because the sensitivity of an MCT detector drops precipitously at wavenumbers lower than 500 cm^{-1}, we could recognize the broad features around 500 cm^{-1} only above 10 GPa. Several absorption lines observed above 10 GPa in the range between 400 and 500 cm^{-1} must be noise. On compression above 37 GPa, the pressure range of the S-II phase,[2] four peaks appeared at around 530, 700, 800, and 1000 cm^{-1}. The sharp absorption peak at around 530 cm^{-1} indicates an occurrence of one characteristic S–S distance above 37 GPa. The special feature of the spectra above 37 GPa is the appearance of two strong peaks at around 700 and 800 cm^{-1}, which are absent in the spectra of S_8 ring molecules. The same infrared pattern was observed when the pressure was increased from 37 to 58 GPa.

The shifts of infrared frequency with pressure are shown in Figure 6-2. The data were fitted by second-order polynomials in pressure (p) up to 18 GPa as follows:

$$\nu_5 = 467 + 4.3\,p - 0.07\,p^2,$$

$$2\nu_{10} = 843 + 10.9\,p - 0.24\,p^2.$$

The observed data correspond well to the linear equations reported in the literature[7] at 0 – 8 GPa (see Figure 6-2), although the observed peak

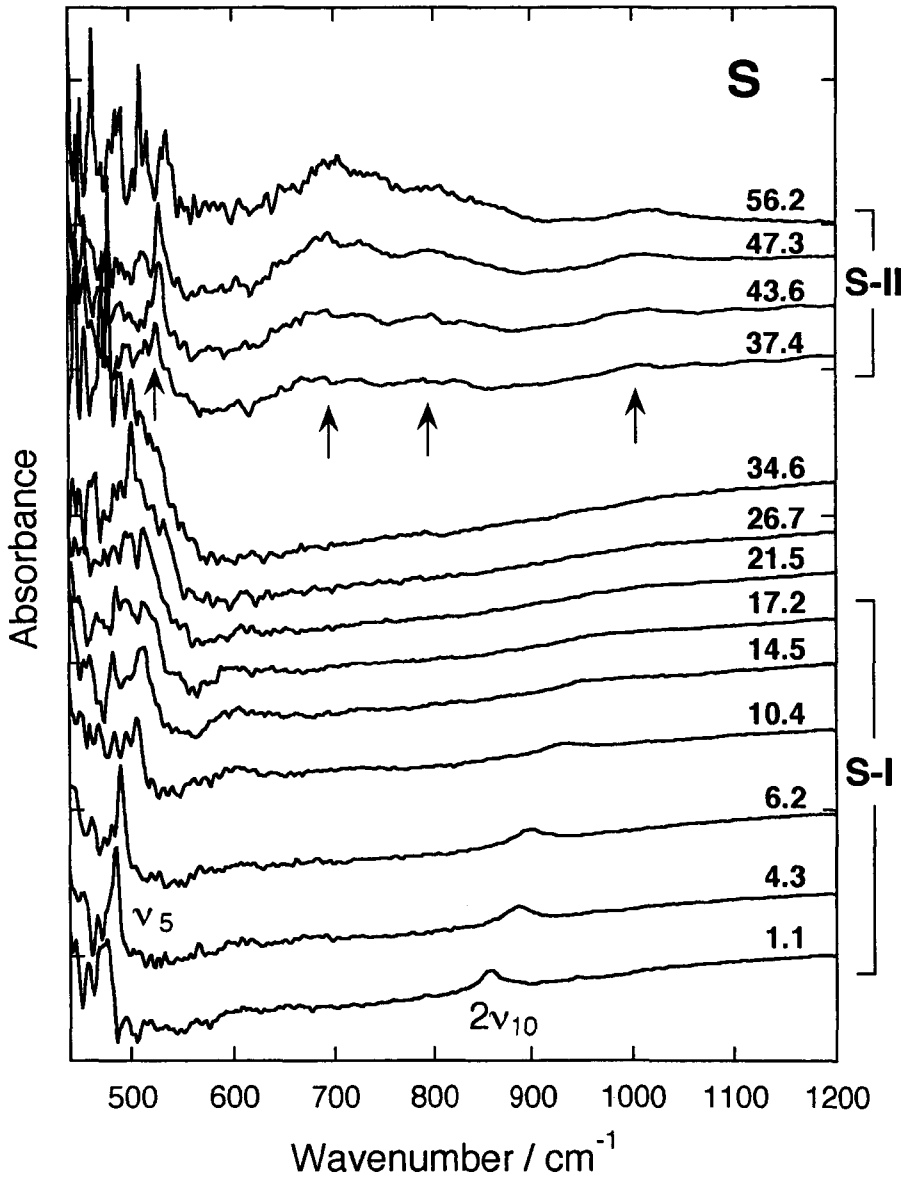

Figure 6-1. Infrared absorption spectra of sulfur at pressures up to 56 GPa at room temperature. New peaks marked with arrows appeared above 37 GPa. The curves are offset in the vertical direction for clarity.

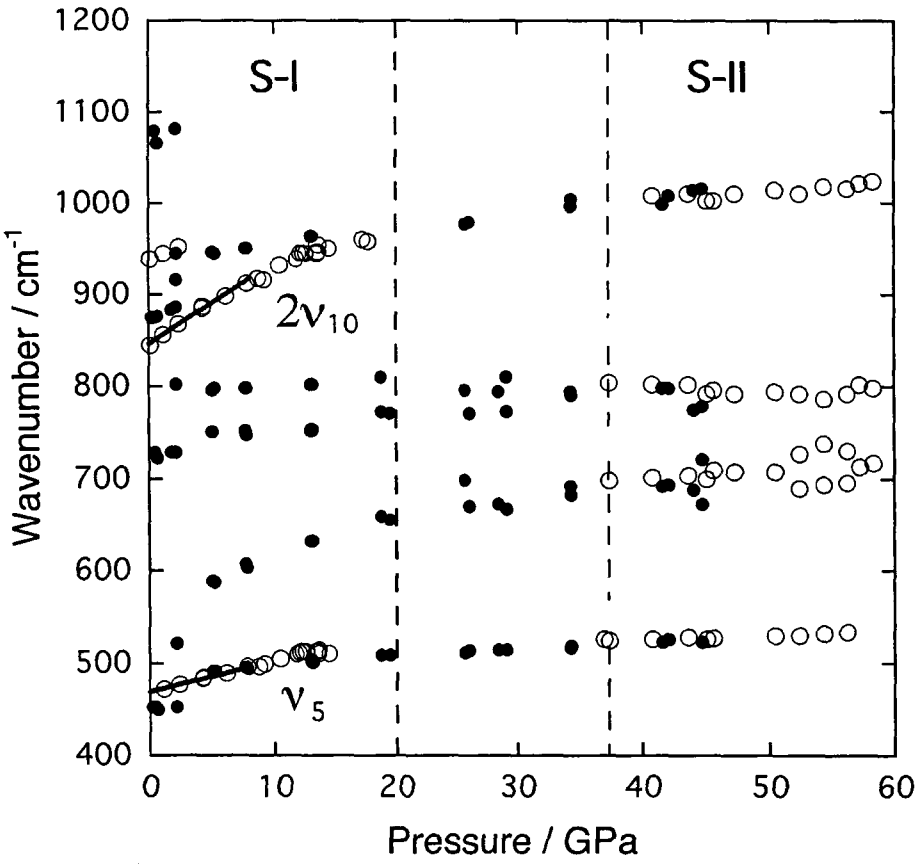

Figure 6-2. Variations of the infrared frequencies of sulfur with pressure, loading (open circles) and unloading (solid circles). The linear equations of ν_5 and $2\nu_{10}$ are drawn thorough the literature.[7] Two dashed vertical lines show phase boundaries.

positions of ν_5 have uncertainty because the spectral quality below 550 cm^{-1} was poor. Only very small pressure dependence was observed for the positions of the peaks that appeared above 37 GPa. These shifts are fitted by linear functions as follows:

$\nu_{(530)} = 510 + 0.4\,p$, $\nu_{(700)} = 667 + 0.8\,p$, $\nu_{(800)} = 813 - 0.3\,p$, and $\nu_{(1000)} = 964 + 1.0\,p$.

A strong hysteresis was observed in the infrared spectra of sulfur during the unloading process. The pattern observed only above 37GPa on loading remained during decompression down to 5 GPa, and then changed to one peak at 519 cm^{-1} at 3.1 GPa as shown in Figure 6-3-a. The Raman peak at this pressure (3.1 GPa, Figure 6-3-b) was very similar to the peak observed for amorphous sulfur at pressures above 5 GPa and temperatures below 200 K.[13] This amorphous sulfur is considered[12] to be a broken S_8 ring that adopts a helix-like structure. On further decompression to 1.8 GPa, two peaks appeared in the infrared spectra at around 450 and 880 cm^{-1} that are distinct from the frequencies for the ν_2 and $2\nu_{10}$ peaks of the S_8 ring molecules (see Figure 6-1, at 470 and 856 cm^{-1} at 1.1 GPa). This feature suggests that a molecular structure other than an S_8 ring appears at 1.8 GPa. In the Raman spectra at 1.8 GPa, we observed both the S–S stretching peaks at around 450 cm^{-1} and the weak bending peaks at 100–300 cm^{-1}. The stretching peaks had several components, probably of an S_8 ring and helical sulfur structures as mentioned below, while the bending peaks are characteristic of an S_8 ring molecule.

In the Raman spectra at 1 atm, the coexistence of two kinds of peaks was clearly observed (Figure 6-4): some belong to an S_8 ring, but others, namely four peaks at 262, 276, 426, and 459 cm^{-1}, do not. Both the relative intensities and positions of these four peaks correspond well to the helical

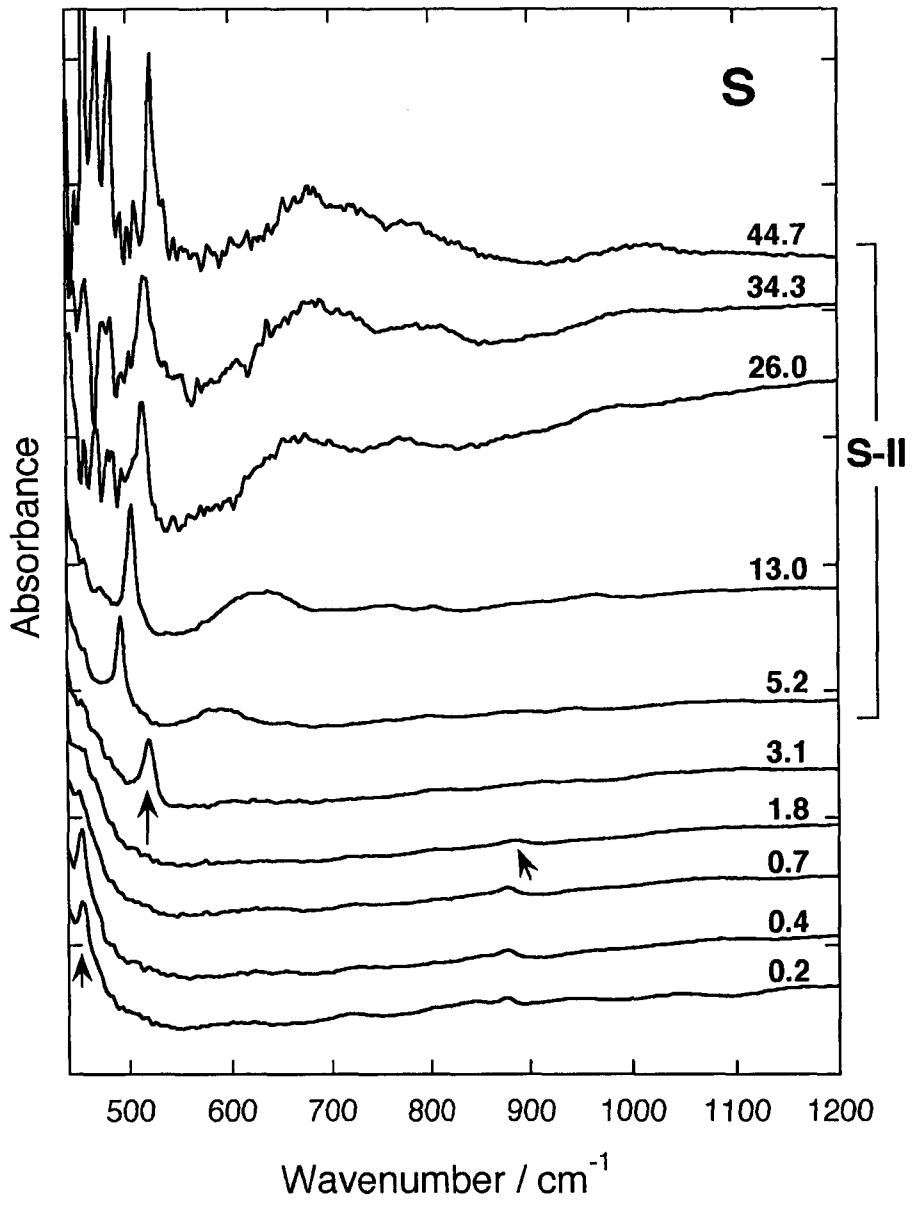

Figure 6-3-a. Infrared spectra of sulfur during the unloading process.

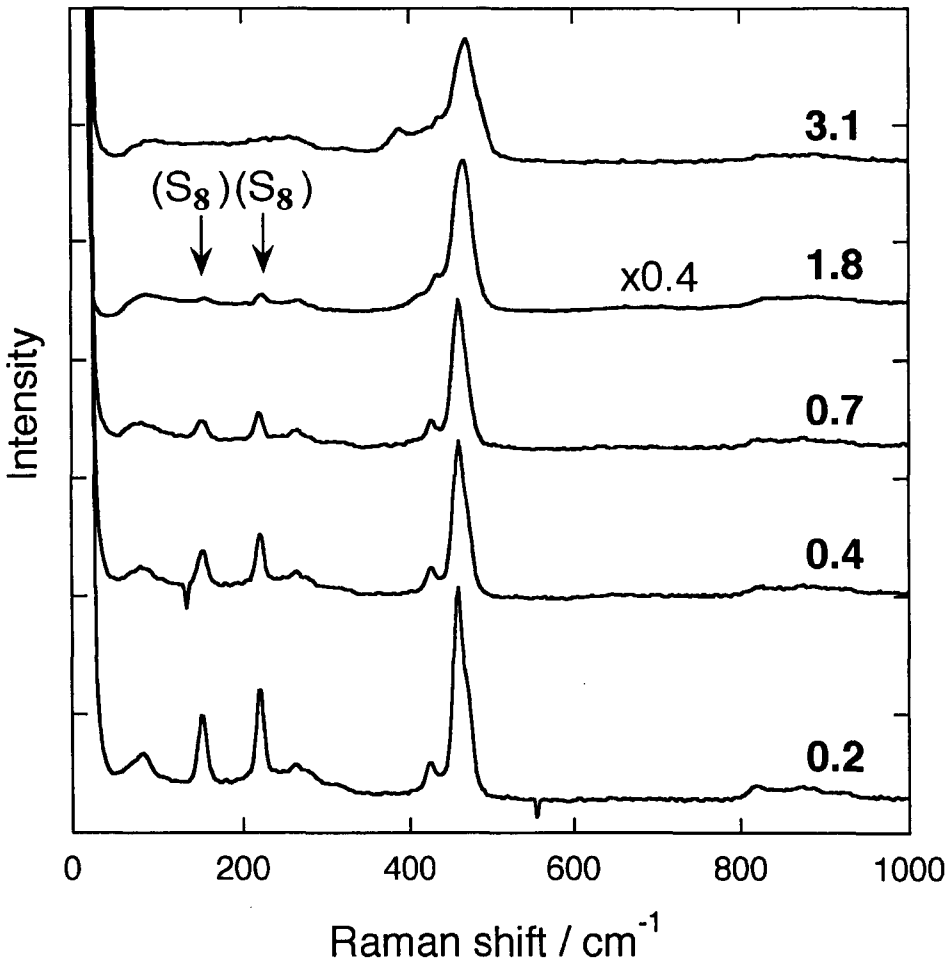

Figure 6-3-b. Raman spectra of sulfur during the unloading process.

sulfur structure S_μ reported by Eckert *et al.* (263, 276, 422, and 458 cm^{-1}).[12] They are also similar to the S*n* chains reported by Ward.[13] The Raman spectra (Figure 6-3-b) indicate that helical sulfur and S_8 ring molecules coexist at 1.8 GPa and that the helical molecules change to S_8 rings during decompression. That is to say, the intensity of the Raman peaks belonging to S_8-ring molecules increased when the recovered sample was kept at ambient temperature and pressure. This recovery of the intensity of S_8 peaks has been reported frequently for sulfur (e.g., see ref. 8).

We have obtained the following results based on our infrared and Raman experiments on sulfur:

(1) The infrared peaks from an original orthorhombic structure disappeared in the amorphous region, at 20–35 GPa, suggesting the decomposition of S_8 ring molecules within this range of pressures.

(2) New peaks appeared with the transition from the amorphous to the S-II phase (above 37 GPa). Their peak positions were different from those of S_8 ring molecules, suggesting another molecular structure.

(3) During the unloading process, helix-like sulfur appeared at 3.1 GPa and then helical sulfur and an S_8 ring molecules appeared at 1.8 GPa. The helical sulfur converted to an S_8 ring upon further decompression.

What is the molecular structure in the high-pressure phase S-II? The sharpness of the infrared peak observed at 530 cm^{-1} and the reported crystalline X-ray pattern of the S-II phase[2] indicate that the S-II phase consists of one molecular species with one characteristic S–S distance. One possible molecular structure is helical sulfur with different pitch from that of the helix-like sulfur that appeared at 3.1 GPa during decompression or that of the helical sulfur observed at 1.8 GPa. Another possible molecular structure is that of sulfur in a six-membered ring. It is difficult, however, to identify the

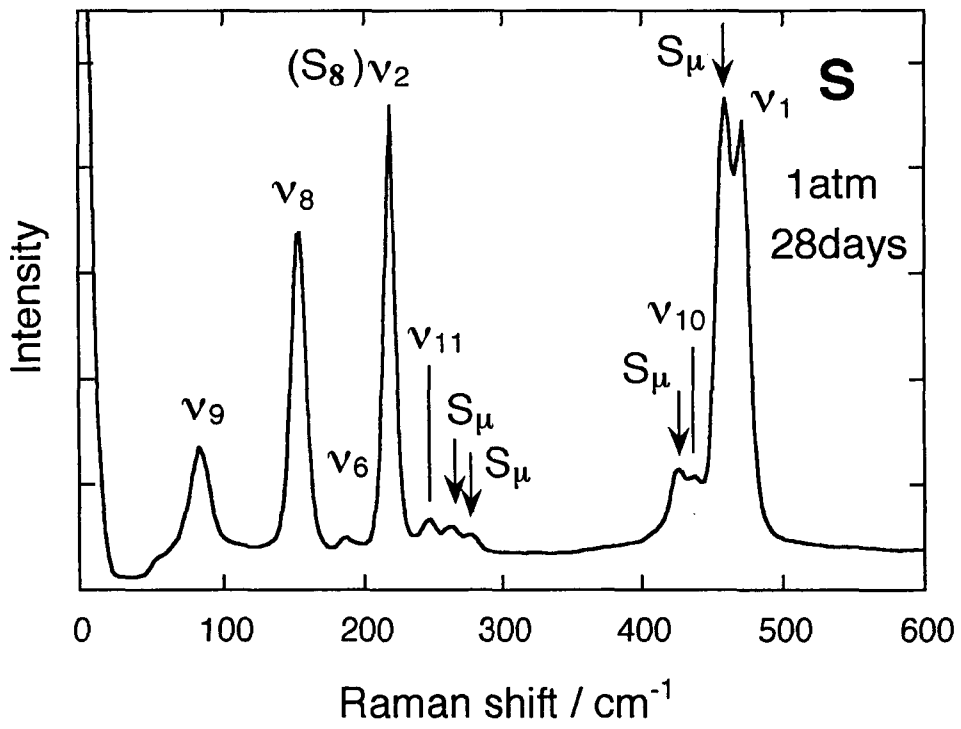

Figure 6-4. Raman spectra of sulfur after decompression to 1 atm.

molecular structure of phase II from the present data.

6-4. Conclusion

The vibrational spectra of solid sulfur have been studied at pressures up to 58 GPa at room temperature using a diamond anvil cell. The infrared peaks from an original orthorhombic structure disappeared in the 20–35 GPa region (in an amorphous region), suggesting the decomposition of S_8 ring molecules in this pressure range. New peaks appeared above 37 GPa (in a high-pressure S-II phase) with peak positions different from those of S_8 ring molecules. The S-II phase probably consists of molecules and not of atoms.

References

1) See, for example, B. Meyer, *Chem. Rev.* **76**, 367 (1976).

2) Y. Akahama, M. Kobayashi, and H. Kawamura, *Phys. Rev. B*, **48**, 6862 (1993).

3) H. Luo and A. L. Ruoff, *Phys. Rev. B*, **48**, 569 (1993).

4) H. Luo, R.G. Greene, and A.L. Ruoff, *Phys. Rev. Lett.*, **71**, 2943 (1993).

5) H. Luo, S. Desgreniers, Y.K. Vohra, and A.L. Ruoff, *Phys. Rev. Lett.*, **67**, 2998 (1991).

6) H. Luo and A.L. Ruoff, in High Pressure Science and Technology, edited by S.C. Schmidt, J.W. Shaner, G..A. Samara, and M. Ross (AIP Press, New York, 1994), p. 1527.

7) A. Anderson, W. Smith, and J.F. Wheeldon, *Chem. Phys. Lett.*, **263**, 133 (1996).

8) W. Häfner, H. Olijnyk, and A. Wokaun, *High Pressure Res.*, **3**, 248 (1990).

9) A. Yoshioka and K. Nagata, *J. Phys. Chem. Solids*, **56**, 581 (1995).

10) B. Eckert, R. Schumacher, H.J. Jodl, and P. Foggi, *High Pressure Research*, **17**, 113 (2000).

11) H.K. Mao, J. Xu, and P.M. Bell, *J. Geophys. Res.*, **91**, 4673 (1986).

12) B. Eckert, H.J. Jodl, H.O. Albert, and P. Foggi, in Frontiers of High-Pressure Research, edited by H. D. Hochheimer and R. D. Etters (Plenum Press, New York, 1991), p. 143.

13) A.T. Ward, *J. Phys. Chem.*, **72**, 4133 (1968).

14) B. Eckert, H.O. Albert, H.J. Jodl, and P. Foggi, *J. Phys. Chem.*, **100**, 8212 (1996).

Chapter 7

Phase Transitions and Chemical Reactions in C_2H_2 under Pressure

7-1. Introduction

High-pressure behavior of molecular solids is of fundamental significance to understand the nature of chemical bonds. Molecules weakly bonded by the van der Waals force approach each other rapidly by application of pressure and intermolecular interactions may become comparable in strength to intramolecular ones at sufficiently high pressure. Reconstruction of chemical bonding often takes place in molecular solids under such conditions. Polymerization, for instance, is expected for unsaturated molecules when they are pushed closer to threshold values of intermolecular distances. Pressure-induced polymerization has been observed for several kinds of molecules with triple bonds such as acetylene[1)], hydrogen cyanide[2)], cyanoacetylene[3)], and cyanogen[4)]. Among them, acetylene is the most appropriate molecule for a detailed investigation of the reaction mechanism because of the simplicity in its molecular structure and bonding nature.

In the acetylene molecule, the triple bond is constructed with one *s* and two *p* bonds. The hybridization of carbon atoms is considered to be the sp state, being expected to change into the sp^2 and further into the sp^3 state as polymerization proceeds. Previous Raman measurements revealed that the reaction occurs in the molecular–crystalline orthorhombic phase at room temperature and pressure above 3.5 GPa, accompanying a color change from colorless transparent to deep red[1)]. The major reaction products were *trans*- and *cis*-polyacetylene. X-ray diffraction suggested that the arrangement of acetylene molecules is favorable for formation of the *trans*-polymer through

the *trans*-opening of the triple bond[5]. These experimental results, however, are still insufficient to clarify the reaction mechanism. Resonance or surface effects on Raman spectra sometimes hide an overall structural feature of specimens owing to strong enhancement in scattering intensity of a particular species such as conjugated polymers.

In this chapter, we will describe the pressure-induced phase transition and polymerization in solid acetylene studied by infrared absorption spectroscopy. Infrared spectroscopy is another powerful technique to investigate reaction processes, and provides complementary structural data on reacting materials or reaction products. The polymerization mechanism in solid acetylene will be discussed on the basis of observed infrared spectra.

7-2. Experimental

7-2-1. Samples

Acetylene gas of 98 % purity was commercially obtained (from Kanto Acetylene Gas Kogyo Co., Ltd.). After removing acetone and water through a sodium hydrogen sulfite solution and granular calcium chloride, purified gas was condensed in a diamond-anvil cell (DAC) cooled with liquid nitrogen. The solidified acetylene was loaded in the small hole of a metal gasket and sandwiched between the opposing diamond anvils. The gasket was made of 50 μm-thick stainless steel or 100 μm-thick Inconel X-750, in which a 200–300 μm diameter hole was drilled with a microdrilling machine. Several ruby chips were enclosed together with the specimen in the gasket hole for pressure measurement. The cooled DAC was left in a glove chamber purged with nitrogen gas for an hour until it warmed up to room temperature.

7-2-2. Measurement of Infrared Spectra under Pressure

A small diamond anvil cell (DAC), 30 mm in diameter and 20 mm in thickness, was used for the high-pressure infrared absorption measurements[6]. The optical openings of the DAC were 60 degrees for both incident and transmitted infrared light, matching well those of the micro focusing optics of a FT-IR spectrometer. Type-IIa diamonds 1.2 mm thick were mounted in the cell, allowing spectral measurement over the whole frequency range from 700 cm^{-1} to 5000 cm^{-1}. Though diamond has strong absorptions due to two phonon bands around 1800–2400 cm^{-1}, such thin diamond anvils transmit ten percent of the incident light even for this absorption region.

Transmission infrared spectra were taken for a 100 μm x 100 μm area of the specimen with a microscope FT-IR spectrometer having an MCT detector (HORIBA FT-530). The spectral resolution was set to 0.5 cm^{-1} and the number of accumulations to 400. Spectra of acetylene were obtained by subtracting the reference spectrum of the empty DAC from the measured raw spectra. Pressures were determined using the frequency shift of the R_1 ruby fluorescence line (7.53 cm^{-1} / GPa) [7].

A liquid phase, cubic phase, and orthorhombic phase of acetylene could be produced as the pressure was increased to 1 GPa. Chemical reaction partly began at about 4 GPa and proceeded very slowly over the wide pressure range up to 14 GPa. It took about one day at each measuring pressure to complete the reaction. The reaction process was monitored by infrared spectra at a pressure interval of 1–2 GPa.

7-3. Results

7-3-1. Phase Transitions of Acetylene

The infrared spectra of three molecular phases — a liquid, cubic, and orthorhombic phases — were observed at pressures to 4 GPa. Measured absorption peaks were those associated with the fundamental and combination bands of intramolecular vibrations. A transition, for instance, from the cubic to the orthorhombic phase caused slight changes in peak position and width, but no significant variation in the spectral feature. Phase transitions were rather clearly detected by microscope observation, and hence we determined transition pressures for the coexisting two-phase states which were prepared by careful pressure tuning under a microscope. The determined pressures of 0.7 and 1.0 GPa for the liquid to cubic and the cubic to orthorhombic transitions, respectively, were in good agreement with those previously determined by Raman and X-ray measurements[1,5].

One typical spectrum measured for the orthorhombic phase is shown in Figure 7-1. The pressure was 1.1 GPa, just above the transition pressure. The observed peaks correspond well to those of polycrystalline films measured at 1 atm and 63 K[8]. At this low temperature, acetylene is known to form the orthorhombic structure. No additional peak was observed in the spectrum besides the absorption from acetylene. Acetone and water were completely removed through the purification process. The five major peaks were assigned to two fundamentals (ν_3 and ν_5) and three combination bands ($\nu_1 + \nu_5$, $\nu_3 + \nu_4$, and $\nu_4 + \nu_5$). The peak position and mode assignment of each peak are listed in Table 7-1.

Variations of the peak frequencies with pressure are plotted in Figure 7-2. Only the ν_3 band due to an anti–symmetric C–H stretching mode shows a negative frequency shift. The frequencies of the other peaks increase with pressure. A jump in frequency accompanied by the phase transitions was

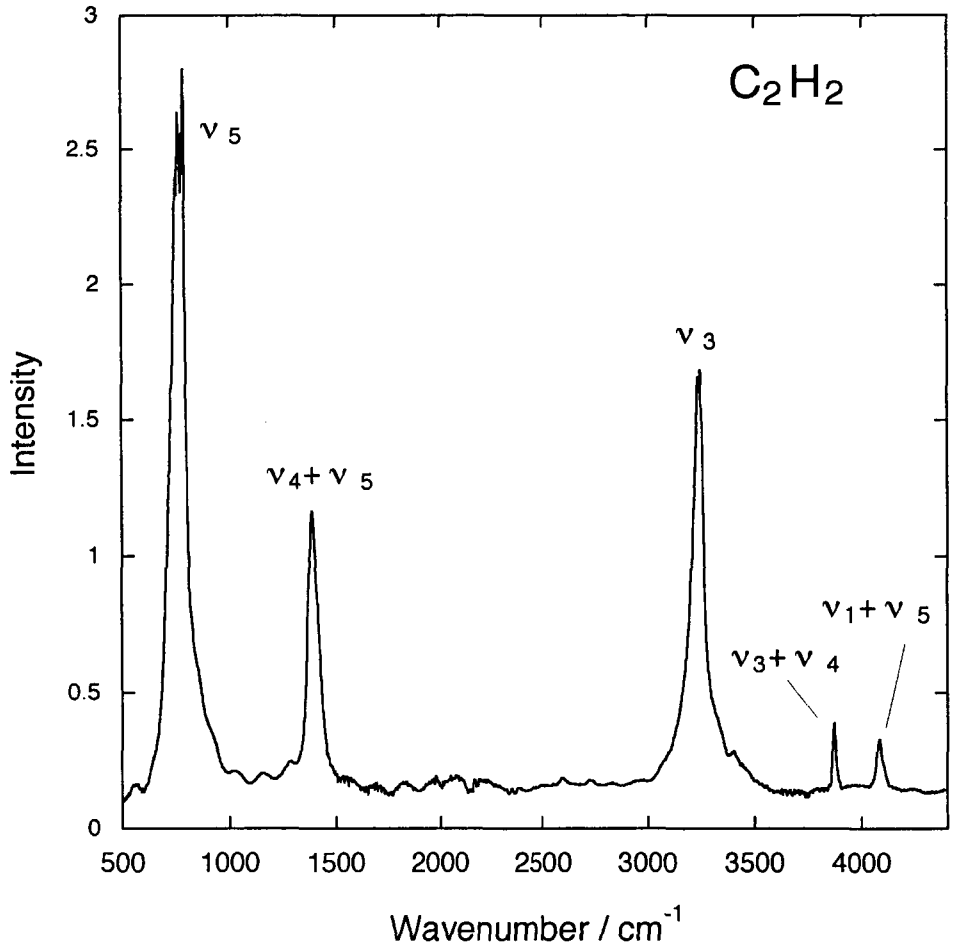

Figure 7-1. Infrared spectrum of orthorhombic acetylene measured at 1.1 GPa and at room temperature. Peak assignments are given in *Table 7-1.*

Table 7-1 Infrared frequencies of orthorhombic acetylene[a]

Crystalline 1.1GPa / cm^{-1}		Crystalline[b] 63K / cm^{-1}		Assignment[c]
4104.0	vw,sh	4094	w,sh	
4082.6	w	4076	w	$\nu_1 + \nu_5$
		3867	w,sh	
3868.3	w	3863	w	$\nu_3 + \nu_4$
		3857	w,sh	
3401.1	vw	3429	vw	$\nu_1 + \nu_T$
		3331	w	$\nu_2 + \nu_4 + \nu_5$
3236	s	3226.3	vs	ν_3
		3220.5	w,sh	ν_3 (C^{13})
		2726	vw	$\nu_2 + \nu_5$
		2064	vw	$\nu_2 + \nu_T$
		1422	m,sh	
1388	s	1390	s	$\nu_4 + \nu_5$
		1377	m,sh	
1282.0	w	1280	w	$2\ \nu_4$
		881	vw,b	$\nu_5 + \nu_R$
		847	vw,b	$\nu_5 + \nu_{R'}$
		768.8	vs	
762	vs	760.6	vs	ν_5
		747.5	s	

[a]Symbols: s=strong; m=medium; w=weak; v=very; b=broad; sh=shoulder.
[b]Reference 8. [c] ν_1: C–H symmetric stretch. ν_2: C≡C symmetric stretch. ν_3: C–H anti-symmetric stretch. ν_4: C–C–H symmetric deformation. ν_5: C–C–H anti-symmetric deformation.

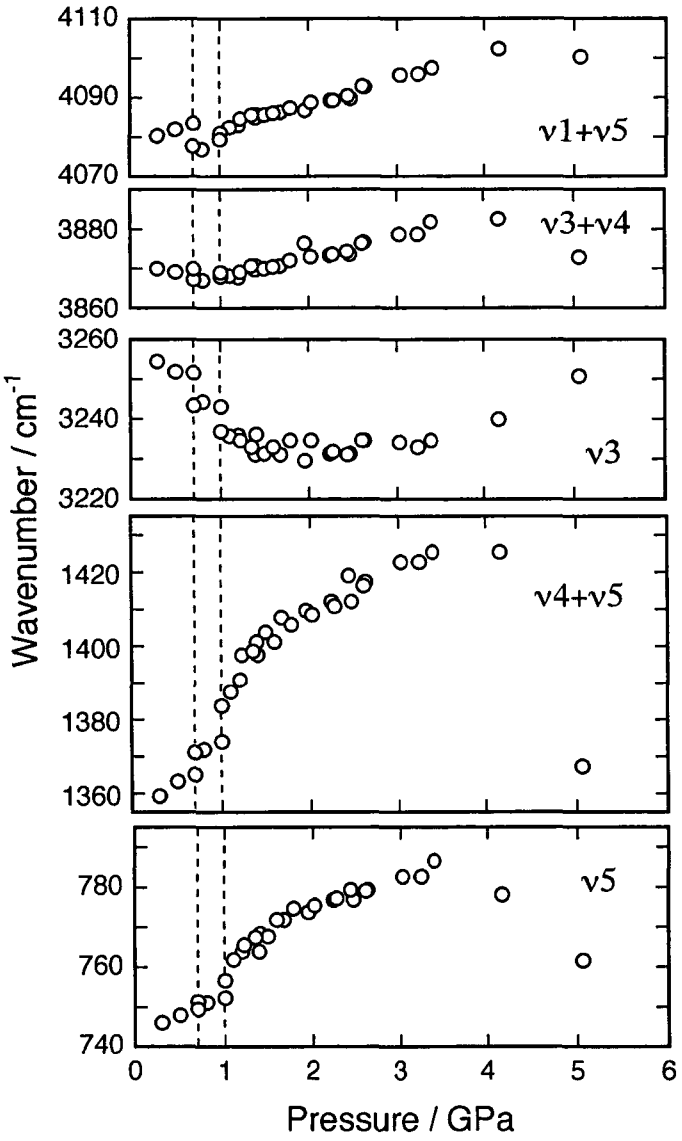

Figure 7-2. Pressure induced shifts of infrared peaks obtained for liquid and crystalline phases of acetylene. Two broken lines at 0.7 and 1.0 GPa indicate transition pressures for the liquid to cubic and cubic to orthorhombic phase, respectively.

clearly observed for the combination $\nu_4 + \nu_5$ and fundamental ν_3 bands. In the case of the $\nu_4 + \nu_5$ band, the magnitude of the frequency jump was about 6.0 cm^{-1} and 9.7 cm^{-1} at the liquid-cubic and cubic-orthorhombic phase transitions, respectively. Frequency decreases in the ν_3 mode at the transition points indicate successive strengthening of the intermolecular hydrogen bonding between neighboring molecules, whose molecular arrangement changes significantly with the phase transitions[9, 10]. There exists a weak hydrogen bond between the triple bond and hydrogen atom in adjacent acetylene molecules, and a T-shape configuration of dimers in the orthorhombic structure is preferable for formation of strong hydrogen bonding.

The frequencies of the infrared-inactive ν_1 and ν_4 modes were estimated from the observed frequencies of the infrared-active modes. Subtractions of the fundamental ν_5 and ν_3 frequencies from the combination $\nu_1 + \nu_5$ and $\nu_3 + \nu_4$ gave the ν_1 and ν_4 frequencies, respectively. They are plotted in Figure 7-3. The ν_1 band, a symmetric C–H stretching, showed a decrease in the frequency at the transition points and with increasing pressure, in a manner similar to the anti-symmetric C–H stretching (ν_3). This high-pressure behavior of the ν_1 band agrees with that measured by Raman scattering,[11] indicating again gradual strengthening of the hydrogen bonding. The estimated frequency of the C–C–H symmetric deformation (ν_4), also showed a pressure variation similar to that of the corresponding C–C–H anti-symmetric deformation (ν_5).

Significant frequency deviations were observed above 4 GPa of polymerization pressure (Figures 7-2 and 7-3). The observed peaks in this pressure range are due to unreacted acetylene molecules. It is notable that their frequencies deviated far from the extrapolated values in the

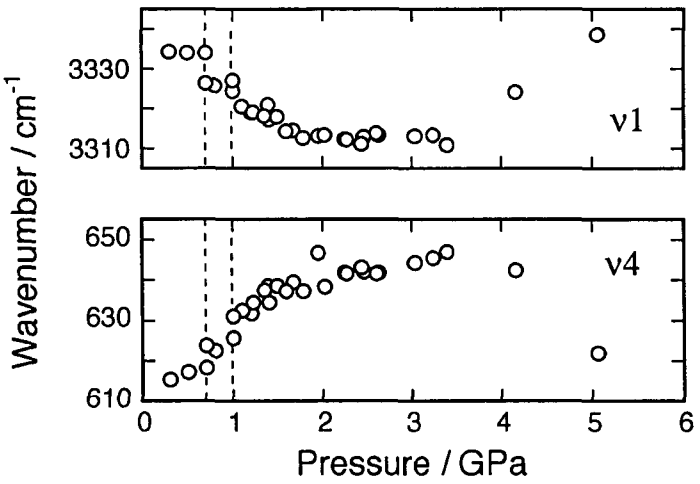

Figure 7-3. Pressure shifts of the two normal modes of acetylene, ν_1 and ν_4, which are calculated from the observed frequency shifts; $\nu_1 = (\nu_1 + \nu_5) - \nu_5$ and $\nu_4 = (\nu_3 + \nu_4) - \nu_3$.

orthorhombic phase and are close to those of the liquid phase. This tendency is very clearly seen in the fundamental ν_1, ν_3, ν_4, and ν_5 modes, and suggests that the molecular arrangement is not retained in the orthorhombic crystal. T-shaped configurations are broken to randomly oriented configurations in the neighborhood of the reaction sites at the beginning of the reaction and such disordered domains expand as the polymerization proceeds.

7-3-2. Polymerization of Acetylene

Polymerization was observed in the orthorhombic phase at 4.2 GPa. Figure 7-4 shows infrared spectra of the reacting specimen. The diamond windows of the pressure cell are nearly opaque in the frequency range from 1800 to 2400 cm^{-1}, so that the quality of the spectra was poor in this range. New peaks appearing at 3000 cm^{-1}, 1600 cm^{-1}, and 1000 cm^{-1} were assigned to C–H stretching, C=C stretching, and CH deformation vibrations, respectively. Their peak intensities increased very slowly with time. Peak growth stopped in several tens of hours after the appearance of the new peaks in the spectra.

The amount of the reacted monomer was estimated from the observed change in peak intensity. Two singlet peaks at 4102 and 3882 cm^{-1}, $\nu_1 + \nu_5$ and $\nu_3 + \nu_4$ combination bands, respectively, were chosen for this estimation. At 4.2 GPa these peaks showed a reduction by 24 % in the intensity, that is, 76 % of the monomers still remained. One reason for this incomlplete reaction is a pressure drop with the volume reduction accompanied by polymerization; the measured pressure decreased to 2.7 GPa from the initial value of 4.2 GPa after 70 hours. We increased pressure to recover the initial pressure of 4.2 GPa. However, no significant change in the spectral profile,

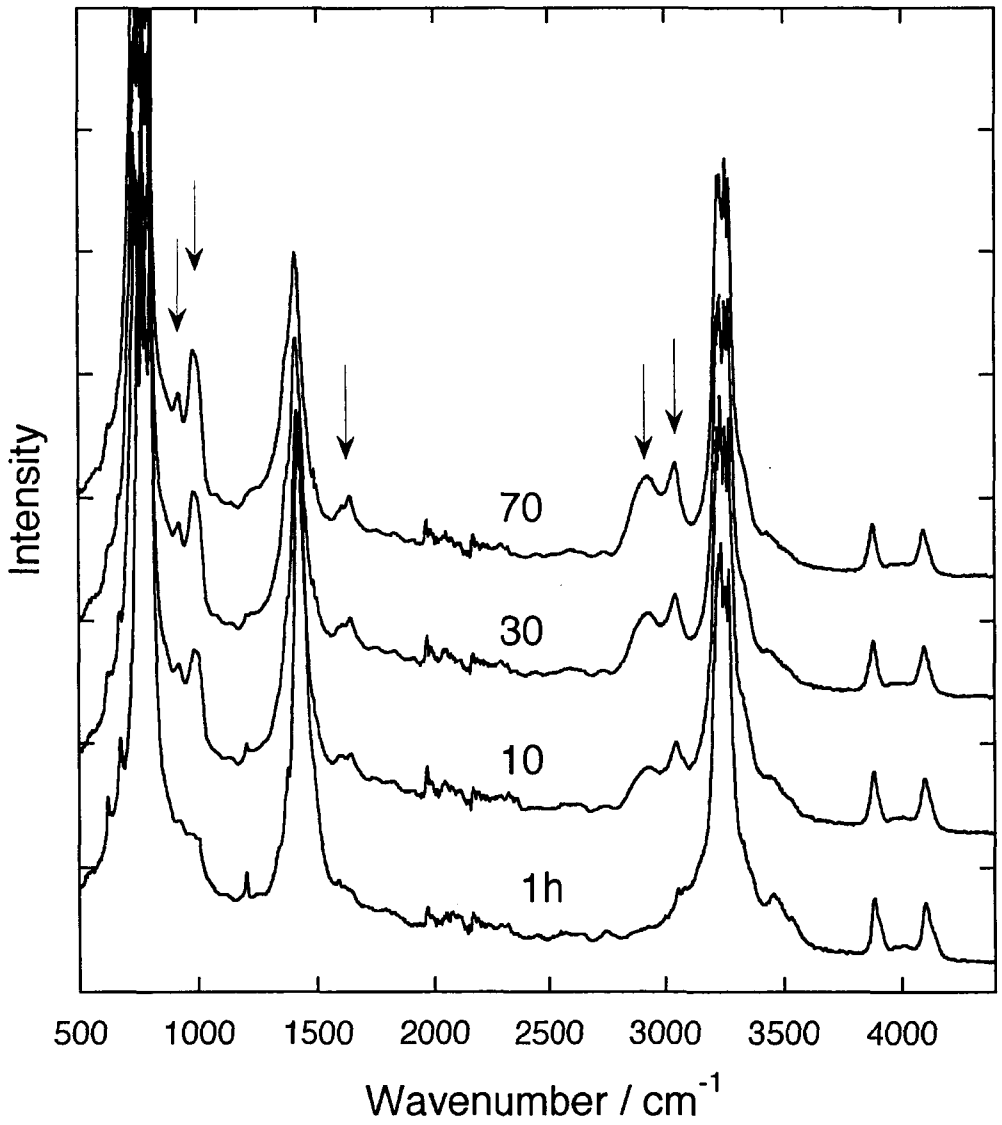

Figure 7-4. Infrared spectra taken for the reacting specimen at room temperature and 4.2 GPa. The number given to each spectrum indicates time in hours after pressurization to 4.2 GPa. Arrows show new peaks from the reacting part. The curves are offset in the vertical direction for clarity.

such as successive growth in the new peaks, was observed, and hence further compression beyond the initially reached pressure was required to restart the reaction.

Infrared spectra measured at various pressures are shown in Figure 7-5. The reaction was accelerated by further compression. The combination bands, $\nu_1 + \nu_5$ and $\nu_3 + \nu_4$, disappeared when the pressure was increased to about 10 GPa. Even the ν_3 and ν_5 fundamental bands that had shown saturated absorption at low pressures almost disappeared at about 14 GPa. Instead, the absorption from the reacted monomers such as the C–H stretching peaks around 3000 cm^{-1} increased with pressure. The polymer peaks seem to stop growing above 10 GPa, while the monomer peaks gradually disappear. The reaction still proceeds at such high pressures.

We turn our attention to the intensity change of two C–H stretching peaks of polymerized acetylene appearing around 3000 cm^{-1}; one peak at 2900 cm^{-1} can be assigned to a C–H stretching of saturated hydrocarbons and the other at 3100 cm^{-1} to that of unsaturated hydrocarbons with C–C double bonds. Their intensity changes with time and also with pressure provide a valuable insight into the reaction mechanism. As seen in Figure 7-4 the higher frequency peak appeared in advance of the lower frequency peak, then the two peaks grew gradually with time at almost the same rate. It suggests that double bonds were formed in the initial stage of polymerization at 4.2 GPa and successively saturated bonds were produced.

Pressure variations of the peak intensities obtained for the two C–H stretching modes are plotted in Figure 7-6. For two fully overlapped peaks measured above 6.8 GPa, we obtained the individual peak height and width by fitting the observed peak profiles with Lorentzian functions[12], wherein their peak widths were estimated from those obtained for the $\nu_1 + \nu_5$ or

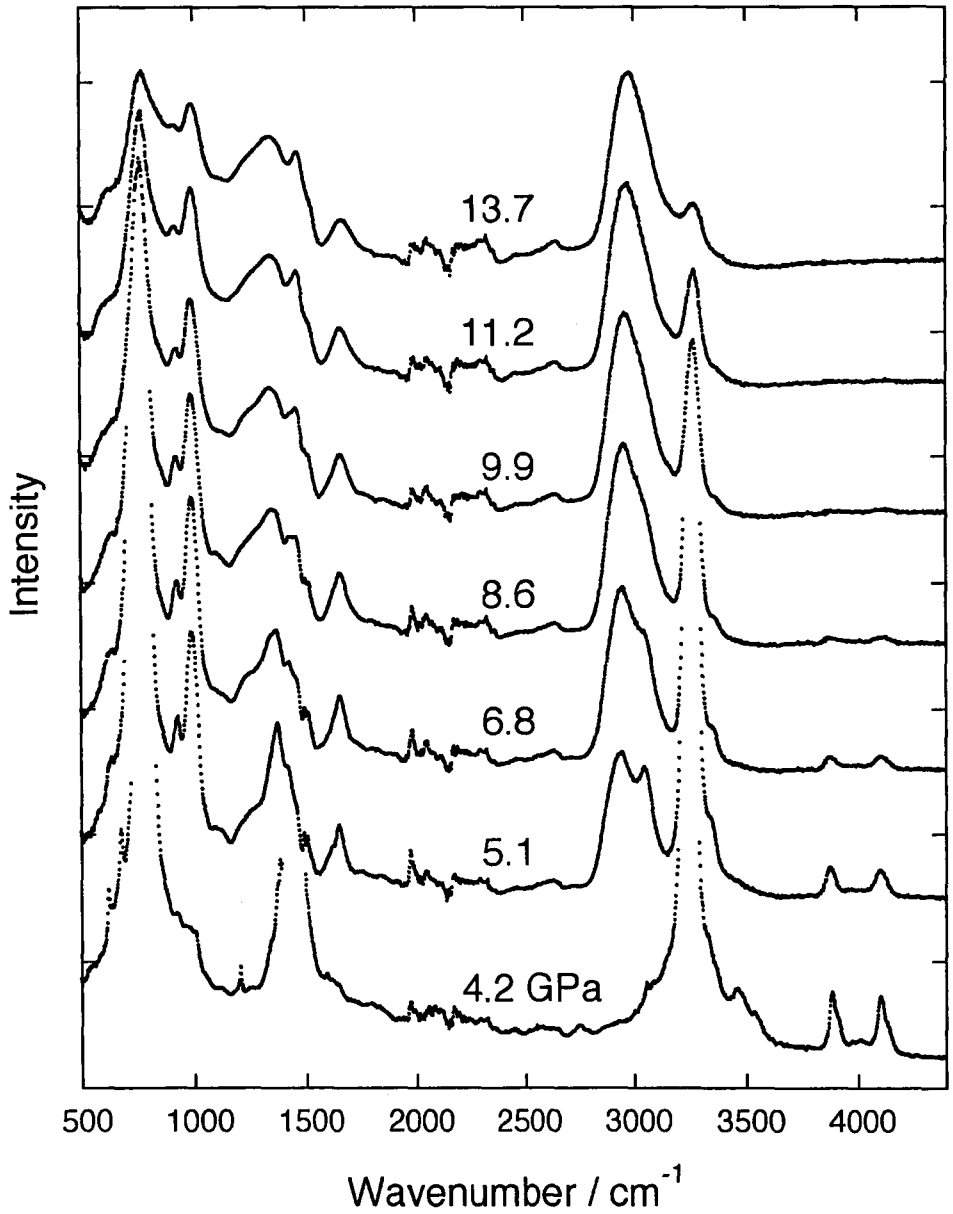

Figure 7-5. Changes in infrared spectra of the reacting specimen with pressure. Each spectrum was recorded after one hour on pressurization.

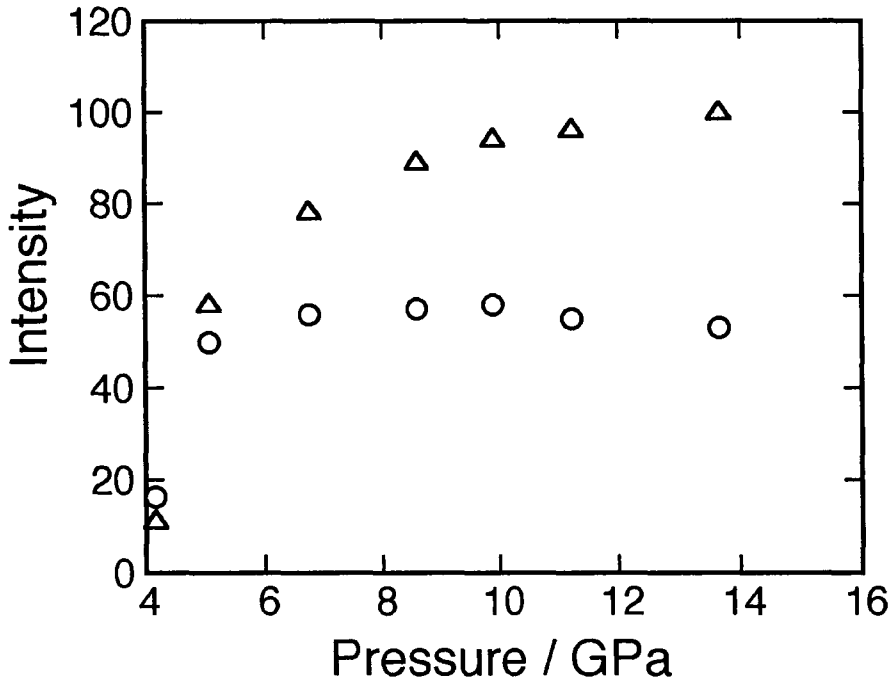

Figure 7-6. Variation of the infrared intensity of the two C–H stretching bands with pressure. Circles and triangles correspond to the peaks from unsaturated and saturated hydrocarbons, respectively.

$\nu_3 + \nu_4$ singlet peaks. As seen in Figure 7-6, the peak intensity for the saturated C–H stretching mode increased significantly with increasing pressure up to 14 GPa, whereas that for the unsaturated C–H stretching one stayed at an almost constant value. The intensity ratio increases from 1:1 at 4.2 GPa to about 2:1 at 14 GPa.

The infrared spectrum of the product at atmospheric pressure after release is shown in Figure 7-7. There were three kinds of C–C bonding, *trans-* C=C, *cis-* C=C, and saturated C–C bonds. The peak at 2917 cm^{-1} was assigned to the C–H stretching mode of saturated hydrocarbon and the shoulder at the higher frequency side of it was assigned to the C–H stretching of a *trans-* C=C bond. In the region below 2000 cm^{-1}, peaks related to the C–H out-of plane bending vibrations of *trans-* and *cis-* C=C bonds, and the C–H deformation vibration of saturated hydrocarbons were observed. The small peak from the monomer still remained at 3251 cm^{-1}. Tentative assignments of the observed peaks are listed in Table 7-2. The C-H bending mode of *trans*-C=C bond appeared at a low-frequency of 981 cm^{-1} compared with that of *trans*-polyacetylene, which suggests that no conjugated chains or only short conjugated chains were formed during compression.

7-4. Discussion

We summarize the experimental results obtained for the polymerization of acetylene.

1. Polymerization started at 4.2 GPa in the orthorhombic phase. C–C double bonds were formed at the initial stage of the reaction and soon the formation of saturated C–C bonds was followed.

2. Upon further compression beyond 4.2 GPa, the amount of saturated C–C bonds predominantly increased, while that of C=C bonds remained constant.

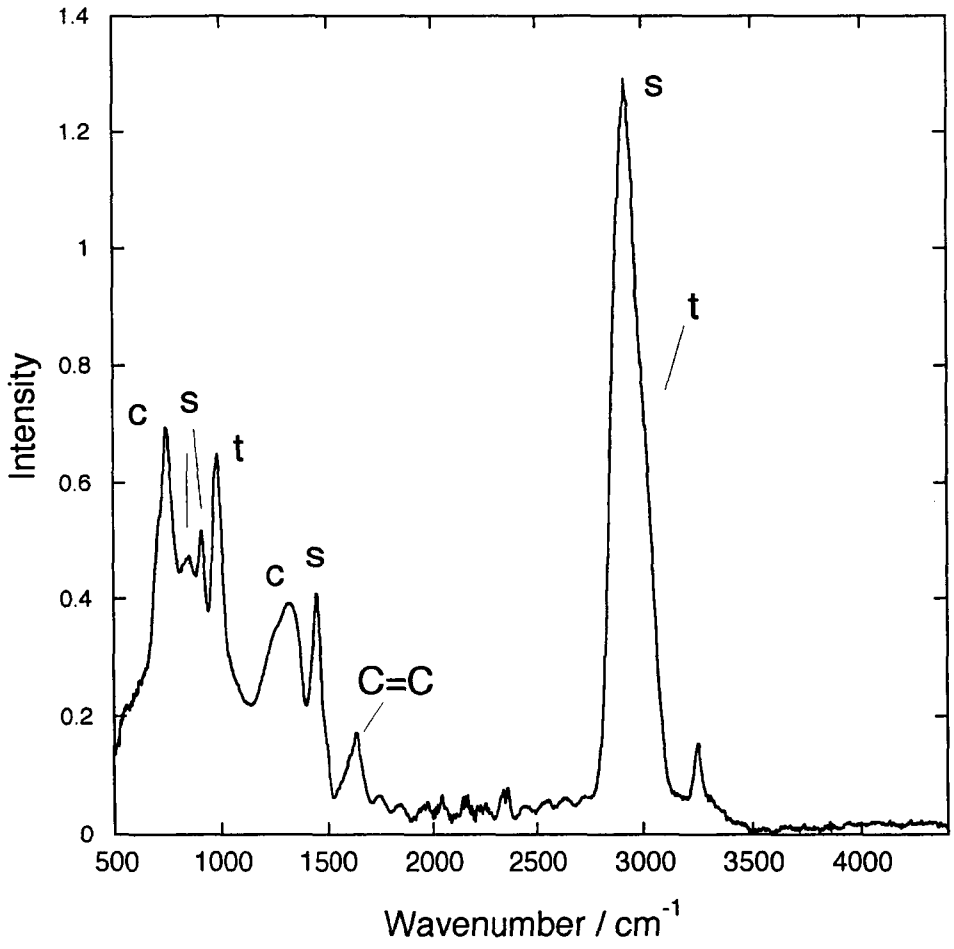

Figure 7-7. Infrared spectrum of the polymer product measured at room temperature and atmospheric pressure. Symbols : *t* ; *trans*-C=C, *c* ; *cis*- C=C, and s ; saturated hydrocarbons.

Table 7-2 Infrared frequencies of polymerization product at 1 atm

Frequency / cm^{-1}		Mode description	
polymer[a]	polyacetylene[b]		
3250.7		C–H anti-symmetric stretch of	acetylene
shoulder	3013(t)	C–H stretch	*trans*-C=C
2917.1		C–H stretch	saturated C–C
1635.6		C=C stretch	C=C
1448.3		C–H deformation	saturated C–C
1330.4	1329(c)	C–H in-plane deformation	*cis*-C=C
981.1	1015(t)	C–H out-of-plane deformation	*trans* C=C
908.3		C–H deformation	saturated C–C
845.6		C–C stretch	chain molecule
746.1	740(c)	C–H out of plain deformation	*cis*- C=C

[a]This work. [b]Reference 13.

The amount of monomer decreased as polymerization proceeded, but small amounts of the pristine monomer still remained at 14 GPa.

3. The reaction product contained *trans*- C=C, *cis*- C=C, and saturated C–C bond. Polymers with long conjugated chains were not produced.

Some possible reaction paths for the solid-state polymerization are drawn in Figure 7-8. Through these reaction paths C≡C triple bonds are converted successively to C=C or C–C bonds. First, a reaction takes place between two neighboring molecules to form a diene backbone. There are two possible reaction sites for the following attack of acetylene monomer. An addition reaction at the end site extends the conjugated backbone and no saturated C–C bond is formed (path a). On the other hand, additions at b site develop a side chain attached to the saturated carbons (paths b). Thus the following addition reactions would extend conjugated chains or form cross-linked networks depending on the reaction sites. Trans-type reactions are demonstrated in Figure 7-8; similar reaction paths are expected also for *cis*-type reactions.

It is interesting to see how the numbers of double and single bonds change along these reaction paths. In paths b, the number of single bonds increases by two, while that of double bond does not change; one consumed double bond is compensated with one new double bond formed in an attached monomer. In contrast, the number of double bonds increases one by one along with an extension of conjugated chains in path a. The present infrared results indicate that the polymerization proceeds along path b in solid acetylene. The single bond increases in number with pressure, while the double bond shows no significant increase (Figure 7-6). Such reaction paths allow formation of cross-linked polymers consisting of double and single C–C bonds and limit the extension of the conjugated linear chains. The

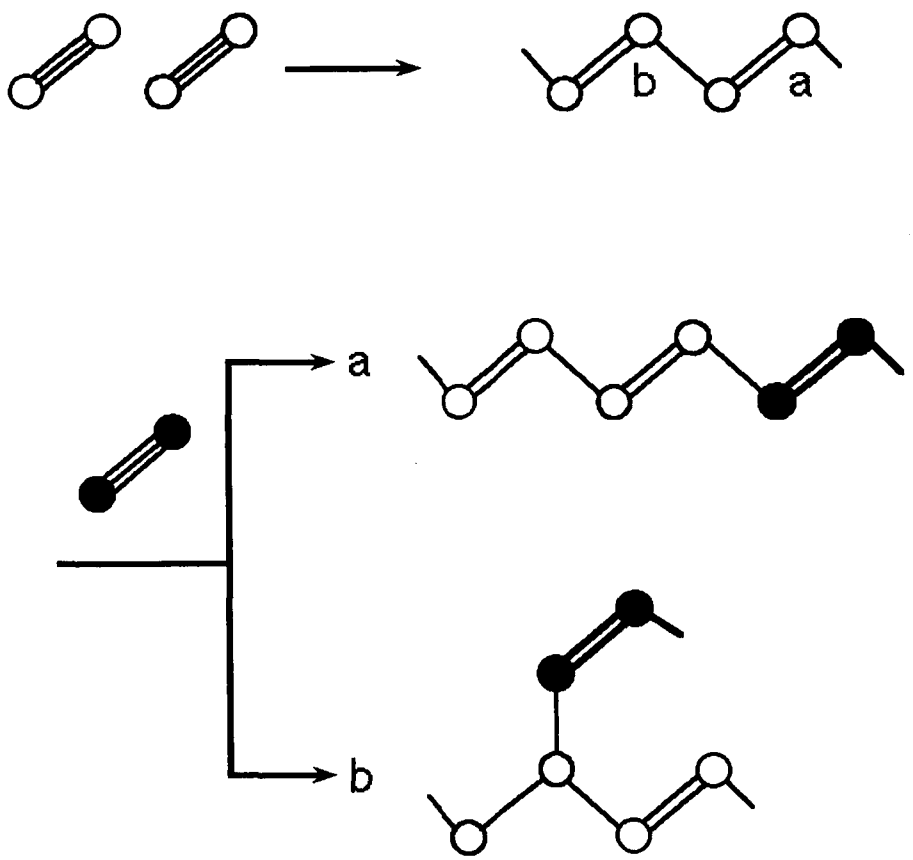

Figure 7-8. Some possible paths for the polymerization reaction of acetylene. Path a and b illustrate the reaction between acetylene molecule and a part of the already formed chain.

structures of a polymer thus prepared through the speculated reaction paths seem to agree with the observed infrared spectra; the spectrum of the recovered specimen showed presence of *trans*- C=C, *cis*- C=C, and saturated C–C bonds. Cross-linked polymers consisting of sp^2 and sp^3 hybrid orbitals are formed by solid-state polymerization of acetylene.

Polymerization would proceed in such a way that the acetylene molecules participate in addition reactions one by one to construct disordered cross-linked polymers. It is not a cooperative reaction in which every molecule polymerizes simultaneously along preferable reaction paths in the crystal; a cooperative reaction may lead to formation of linear polymers. The frequency shifts in molecular vibrations observed for the reacting specimen above 4 GPa (see Figures 7-2 and 7-3) indicate that the molecular arrangement in the orthorhombic crystal was broken during the polymerization. Hence, a well-ordered reaction, which sometimes produces crystalline polymers as observed in diacetylene crystals[14], is no longer expected for acetylene.

Here, we compare the results of the high-pressure infrared absorption measurement with those obtained by Raman scattering, and show that the infrared spectra provide an overall structural feature for the polymerization process. In the previous Raman study by Aoki *et al.*,[1] a sequential reaction process (i.e., the formation of conjugated polymers above 3.5 GPa and further polymerization of saturated polymers by compression beyond 6 GPa) was suggested. The infrared spectra observed in the present study, however, indicate that both conjugated and saturated polymers were formed simultaneously when the reaction was initiated at 4.2 GPa. This difference between Raman and infrared experiments can be attributed to the resonance effect in Raman scattering, which significantly enhances the Raman

intensities of conjugated polymers through the coupling of excitation light with the electronic state[15]. The scattering intensity for non-resonant saturated polymers is so weak that their Raman peaks were not detectable.

Finally, we may point out the difference between the solid-state polymerizations of acetylene and benzene, which both have the same atomic composition, $(CH)_n$; n=2 for acetylene and n=6 for benzene. Benzene compressed to 30 GPa transforms to a disordered cross-linked polymer by opening the aromatic rings[16]. Unlike acetylene, benzene showed no significant change in infrared pattern during a pressure increase; the polymerization reaction was recognized in the course of decreasing pressure. Polymerized benzene was shown to have activated C-terminals. C=O or C–O stretching peaks were observed in the infrared spectrum of polymerized benzene exposed to air at atmospheric pressure. For the polymerized acetylene the intensity of C–H stretching peaks remained almost constant and neither C=O nor C–O stretching peaks were observed (Figure 7-7). The amount of activated terminals should be very small in polymerized acetylene compared with that in benzene. These differences may be related to the mobility of a molecule in association with solid-state reaction. Acetylene is so small that it can move to an activated site even in the dense solid and form a covalent bond. A broken benzene ring, on the other hand, seems too large to have enough flexibility for the formation of a bond at the reaction site.

7-5. Conclusion

High-pressure infrared spectra of acetylene were measured with a diamond-anvil cell at room temperature and pressures up to 13.7 GPa. Transitions from a liquid to a crystalline cubic and to a crystalline orthorhombic phase were observed in the molecular phase at 0.7 GPa and 1.0

GPa, respectively. Polymerization occurred in the orthorhombic phase at 4.2 GPa, accompanied by the appearance of new peaks indicating the formation of C=C double and saturated C–C single bonds. The saturated single bonds showed an increase in quantity on further compression beyond 4 GPa, while the double bonds showed no significant change. The spectrum of the reaction product recovered from 14 GPa indicated formation of cross-linked polymers containing *trans*- and *cis*- C=C, and saturated C–C single bonds.

References

1) K. Aoki, S. Usuba, M. Yoshida, Y. Kakudate, K. Tanaka, S. Fujiwara, *J. Chem. Phys.*, **89**, 529 (1988).

2) K. Aoki, B. J. Baer, H. C. Cynn, M. Nicol, *Phys. Rev. B*, **42**, 4298 (1990).

3) K. Aoki, Y. Kakudate, M. Yoshida, S. Usuba, S. Fujiwara, *J. Chem. Phys.*, **91**, 778, 2814 (1989).

4) C. S. Yoo, M. Nicol, *J. Phys. Chem.*, **90**, 6726, 6732 (1986).

5) K. Aoki, Y. Kakudate, M. Yoshida, S. Usuba, K. Tanaka, S. Fujiwara, *Synth. Met.*, **28**, D91 (1989).

6) K. Aoki, Y. Kakudate, M. Yoshida, S. Usuba, K. Tanaka, S. Fujiwara, *Jpn. J. Appl. Phys.*, **26**, 2107 (1987).

7) G. J. Piermarini, S. Block, J. D. Barnett, R. A. Forman, *J. Appl. Phys.*, **46**, 2774 (1975).

8) G. L. Bottger, D. F. Eggers, Jr., *J. Chem. Phys.*, **40**, 2010 (1963).

9) G. J. H. Van Nes, F. Van Bolhuis, *Acta Crystallogr. B*, **35**, 2580 (1979).

10) H. K. Koski, E. Sandor, *Acta Crystallogr.* **B**, 31, 350 (1975).

11) K. Aoki, Y. Kakudate, S. Usuba, M. Yoshida, K. Tanaka, S. Fujiwara, *J. Chem. Phys.*, **88**, 4565 (1988).

12) I. Kojima, N. Fukumoto, M. Kurahashi, *Bunseki Kagaku*, **35**, T96 (1986).

13) M. Gussoni, C. Castiglioni, M. Miragoli, G. Lugli, G.; Zerbi, *Spectrochem Acta.*, **41A**, 371 (1985).

14) G. Wegner, *Macromol. Chem.*, **154**, 35 (1972).

15) G. P. Brivio, E. Mulazzi, *Phys. Rev. B*, **30**, 876 (1984).

16) Ph. Pruzan, J. C. Chervin, M. M. Thiery, J. P. Ltie, J. M. Besson, J. P. Forgerit, M. Revault, *J. Chem. Phys.*, **92**, 6910 (1990).

Chapter 8

Summary and Conclusions

The present thesis has dealt with the phase transitions and chemical reactions that occur in simple hydrogen-bonded molecular solids of H_2O, H_2S, and C_2H_2 under pressure. Intermolecular interactions may become comparable in strength to intramolecular ones at sufficiently high pressure. Thus, the compression of the molecular solids induces several phase transitions and chemical reactions including hydrogen-bond symmmetrization, molecular dissociation, and polymerization. Such high-pressure behavior was investigated from the viewpoint of the competition destabilization of intramolecular bonds by infrared and Raman spectroscopy, with much attention paid to hydrogen-bonds. The conclusions or findings obtained are summarized below.

* * *

Chapter 2

Experimental technique of infrared microspectrscopy at high pressure is described. A small diamond anvil cell was designed and built to meet precise requirements simultaneously, regarding its optical characteristics and its high-pressure performance. On-axis Cassegrain-type beam condensers and a liquid nitrogen cooled MCT (HgCdTe) photoconductive detector are used for infrared system. A reference spectrum is subtracted from a raw spectrum of each test sample to improve the quality of the infrared spectra.

Chapter 3

Ice is the most typical hydrogen-bonded molecular solid, in which strong hydrogen bonding and intramolecular interactions become comparable at around 60 GPa; the hydrogen-bond symmetrization occurs in ice at 62.1 GPa. The OH stretching infrared frequency initially located at 3500 cm^{-1} at ambient pressure falls toward zero around 60 GPa. A new absorption band appears in the low frequency region below 800 cm^{-1} at about 65 GPa, growing a definite peak with a shift to a high frequency by further compression. Such a turn in the pressure dependence of the stretching frequency evidences the transition from ice VII to symmetric ice X. The OH bending peak disappears before the transition. Two absorption peaks, which are originated from the OH stretching and librational vibrations in ice VII, persist above the transition pressure, being assigned to a translational and distortional lattice vibrations in ice X.

Chapter 4

Hydrogen sulfide is a sister molecule of ice having weaker hydrogen bonds than ice. Infrared spectra at high pressure and room temperature reveal that molecular dissociation and metallization occur in solid H_2S near 46 and 96 GPa, respectively. The molecular dissociation was signaled to be the disappearance of SH stretching bands in the 2300–2500 cm^{-1} region and simultaneous appearance of a lattice vibrational mode around 1300 cm^{-1}. At higher pressures, a low-energy electronic absorption band develops and eventually extends throughout the infrared region studied (700–6000 cm^{-1}). Thus, metallization seems to occur by closing a band gap originating from S–S bond formation in the dissociated phase. The molecular dissociation of H_2S is a first-order transition with the protons moving from the axes of the

hydrogen bonds. This differs from the second-order like dissociation of H_2O molecules that occurs in ice when those hydrogen bonds symmetrize.

Chapter 5

High-pressure behavior of deuterium sulfide was investigated in order to clarify the mechanism of molecular dissociation in H_2S. Experiments with a diamond-anvil cell show that D_2S dissociates to form sulfur at pressures above 27 GPa and room temperature. Raman-scattering spectroscopy indicates the presence of S–S bonds of a high-pressure phase sulfur, helical sulfur, and eight-membered cyclic sulfur. On the other hand, infrared-absorption spectroscopy indicates the presence of S–D bonds of both polymeric and unreacted D_2S. The formation of sulfur from D_2S can be interpreted as reconstruction of chemical bonds at high pressures.

Chapter 6

Sulfur is a molecular crystal having the orthorhombic form and the molecules are crown-shaped rings consisting of eight sulfur atoms at ambient temperature and pressure. The vibrational spectra of solid sulfur have been studied at pressures up to 58 GPa at room temperature using a diamond anvil cell. The infrared peaks from an original orthorhombic structure disappeared at 20–35 GPa (in an amorphous region), suggesting the decomposition of S_8 ring molecules at this pressure range. New peaks appeared above 37 GPa (in a high-pressure S-II phase) with peak positions different from those of S_8 ring molecules. The S-II phase most likely consists of molecules and not of atoms. In conclusion, S_8 ring molecules are broken at 20–35 GPa (amorphization pressure), and then changed to another form in the high-pressure S-II phase. Further spectroscopic studies will clarify the molecular or atomic structure at

the insulator–metal transition (95 GPa).

Chapter 7

Acetylene is a very simple molecule having C≡C triple bond and very weak hydrogen bond. High-pressure infrared spectra were measured in a diamond-anvil cell at room temperature and pressures up to 13.7 GPa. Transitions from a liquid to a crystalline cubic and to a crystalline orthorhombic phase were observed in the molecular phase at 0.7 GPa and 1.0 GPa, respectively. Polymerization occurred in the orthorhombic phase at 4.2 GPa, accompanied by the appearance of new peaks indicating formation of C=C double and saturated C–C single bonds. The saturated single bonds showed an increase in quantity on further compression beyond 4 GPa, while the double bonds showed no significant change. The spectrum of the reaction product recovered from 14 GPa indicated formation of cross-linked polymers containing *trans*- C=C, *cis*- C=C, and saturated C–C single bonds.

*　　*　　*

As described in the present thesis, high-pressure behavior of H_2O, H_2S, and C_2H_2 are clarified. Strong hydrogen-bond restricts the intermolecular geometry in H_2O and induces hydrogen-bond symmetrization. On the other hand, weak hydrogen-bond induces reconstruction of chemical bonds in H_2S and C_2H_2. The author hopes that high-pressure techniques will be widely used in the creation of new materials and new chemical reaction, including novel polymers and polymerization.

List of Publications

1) FT-IR study of the solid state polymerization of acetylene under pressure.
M. Sakashita, H. Yamawaki, K. Aoki, *J. Phys. Chem.*, **100,** 9943-9947 (1996).

2) Observation of Fano interference in high-pressure ice VII.
K. Aoki, H. Yamawaki, and M. Sakashita, *Phys. Rev. Lett.*, **76**, 784-786 (1996).

3) Infrared absorption study of the hydrogen-bond symmetrization in ice to 110 GPa.
K. Aoki, H. Yamawaki, M. Sakashita, and H. Fujihisa, *Phys. Rev. B*, **54**, 15673-15677 (1996).

4) Pressure-induced molecular dissociation and metallization in hydrogen-bonded H_2S solid.
M. Sakashita, H. Yamawaki, H. Fujihisa, and K. Aoki, *Phys. Rev. Lett.*, **79,** 1082-1085 (1997).

5) Infrared Spectroscopy under High Pressure.
M. Sakashita, H. Yamawaki, and K. Aoki, *Rev. High Pressure Sci. Technol.*, **8**, 33-40 (1998) (in Japanese).

6) Structures of H_2S: Phases I ' and IV under high pressure.
H. Fujihisa, H. Yamawaki, M. Sakashita, K. Aoki, S. Sasaki, and H. Shimizu, *Phys. Rev. B*, **57**, 2651-2654 (1998).

7) Molecular dissociation in deuterium sulfide under high pressure: Infrared and Raman study.
Mami Sakashita, H. Fujihisa, H. Yamawaki, and K. Aoki, *J. Phys. Chem. A*, **104**, 8838-8842 (2000).

8) Infrared analysis of the molecular structure of sulfur at up to 58 GPa.

M. Sakashita, H. Fujihisa, H. Yamawaki, K. Aoki, submitted to *Phys. Rev. B.*

The Related Papers

1) Infrared and Raman spectra of macrocyclic poly(oxymethylene).
Masamichi Kobayashi, Mami Sakashita, and Masaki Hasegawa, *Macromolecules*, **24**, 4796-4800 (1991).

2) Morphology dependent anomalous frequency shifts of infrared absorption bands of polymer crystals: Interpretation in terms of transition dipole-dipole coupling theory.
Masamichi Kobayashi and Mami Sakashita, *J. Chem. Phys.*, **96**, 748-760 (1992)

3) Phase study of solid CO_2 to 20 GPa by infrared-absorption spectroscopy.
K. Aoki, H. Yamawaki, and M. Sakashita, *Phys. Rev. B*, **48**, 9231-9234 (1993).

4) Crystal Structure of the High-Pressure Phase of Solid CO_2.
K. Aoki, H. Yamawaki, M. Sakashita, Y. Gotoh, and K. Takemura, *Science*, **263**, 356-358 (1994).

5) Pressure-Tuned Fermi Resonance in Ice VII.
K. Aoki, H. Yamawaki, and M. Sakashita, *Science*, **268**, 1322-1324 (1995).

6) Morphology-Dependent Anomalous Frequency Shifts of Infrared Absorption Bands: Poly(tetrafluoroethylene) and Its Linear Oligomers Perfluoroeiocosane and Perfluorotetracosane.
Masamichi Kobayashi, Mami Sakashita, Toshihisa Adachi, and Mitsue Kobayashi, *Macromolecules*, **28**, 316-324 (1995).

7) High-Pressure FT-IR Spectra of Liquid and Crystalline CH_2F_2 up to 13 GPa.

Youhong Wu, Shigeo Sasaki, Hiroyasu Shimizu, Mami Sakashita, Horoshi Yamawaki, and Katsutoshi Aoki, *J. Phys. Soc. Jpn.*, **64**, 1038-1039 (1995).

8) Reversible phase transition between the metastable phases of tetracyanoethylene under high pressure.

H. Yamawaki, M. Sakashita, K. Aoki, and K. Takemura, *Phys. Rev. B*, **53**, 11403-11407 (1996).

9) High-pressure phase transitions of solid H_2S probed by Fourier-transform infrared spectroscopy.

H. Shimizu, T. Ushida, S. Sasaki, M. Sakashita, H. Yamawaki, and K. Aoki, *Phys. Rev. B*, **55**, 5538-5541 (1997).

10) Mutual incommensurability and interlayer interaction in $(MX)xTX_2$-type ternary chalcogenides with layered composite crystal structure.

Y. Gotoh, J. Akimoto, Y. Oosawa, H. Yamawaki, M. Sakashita and K. Aoki, *Physica B*, **237**, 177-178 (1997).

11) Phase Study of NH_3 to 100GPa by Infrared Absorption.

M. Sakashita, H. Yamawaki, H. Fujihisa, and K. Aoki, *Rev. High Pressure Sci. Technol.*, **7**, 796-798 (1997).

12) Hydrogen-bond symmetrization and molecular dissociation in hydrogen halids.

K. Aoki, E. Katoh, H. Yamawaki, M. Sakashita and H. Fujihisa, *Physica B*, 265, 83-86 (1999).

13) Raman and infrared study of phase transitions in solid HBr under pressure.

E. Katoh, H. Yamawaki, H. Fujihisa, M. Sakashita, and K. Aoki, *Phys. Rev.*

B, **59**, 11244-11250, (1999).

14) Infrared absorption study of Fermi resonance and hydrogen-bond symmetrization of ice up to 141 GPa.

M. Song, H. Yamawaki, H. Fujihisa, M. Sakashita, and K. Aoki, *Phys. Rev. B*, **60**, 12644-12650 (1999).

15) Raman study of phase transition and hydrogen bond symmetrization in solid DCl at high pressure.

E. Katoh, H. Yamawaki, H. Fujihisa, M. Sakashita, and K. Aoki, *Phys. Rev. B*, **61**, 119-124 (2000).

16) Methane Hydrate Behavior under High Pressure.

Hisako Hirai, Tadashi Kondo, Masashi Hasegawa, Takehiko Yagi, Yoshitaka Yamamoto, Takeshi Komai, Kazushige Nagashima, Mami Sakashita, Hiroyuki Fujihisa, and Katsutoshi Aoki, *J. Phys. Chem. B*, **104**, 1429-1433 (2000).

17) Infrared spectroscopic study of H_2O-D_2O mixed ice up to 100 GPa.

Eriko Katoh, M. Song, H. Yamawaki, H. Fujihisa, M. Sakashita, and K. Aoki, *Phys. Rev. B*, **62**, 2976-2979 (2000).

18) Methane hydrate, amoeba or a sponge made of water molecules.

Hisako Hirai, Masashi Hasegawa, Takehiko Yagi, Yoshitaka Yamamoto, Kazushige Nagashima, Mami Sakashita, Katsutosi Aoki and Takumi Kikegawa, *Chem. Phys. Lett.*, **325**, 490-498 (2000).

19) High-pressure structures of methane hydrate observed up to 8 GPa at room temperature.

H. Hirai, Y. Uchihara, H. Fujihisa, M. Sakashita, E. Katoh, K. Aoki, K. Nagashima, Y. Yamamoto, and T. Yagi, *J. Chem. Phys.*, **115**, 7066-7070 (2001).

20) Protonic diffusion in high-pressure ice VII.

Eriko Katoh, H. Yamawaki, H. Fujihisa, M. Sakashita, and K. Aoki, *Science*, **295**, 1264-1266 (2002).

21) Proton Diffusion in High Pressure Ice.

K. Aoki, Eriko Katoh, H. Yamawaki, H. Fujihisa, and M. Sakashita, *High Pressure Res.*, **22**, 9-11 (2002).

22) High-pressure structures of methane hydrate.

H. Hirai, Y. Uchihara, H. Fujihisa, M. Sakashita, E. Katoh, K. Aoki, Y. Yamamoto, K. Nagashima and T. Yagi, *J. Phys.: Condens. Matter*, **14**, 11443-11446 (2002).

23) High-pressure spectroscopic measurement on diffusion with a diamond-anvil cell.

K. Aoki, E. Katoh, H. Yamawaki, H. Fujihisa, and M. Sakashita, *Rev. Sci. Instrum*, **74**, 2472-2476 (2003).

24) Infrared investigation on ice VIII and the phase diagram of dense ices.

M. Song M, H. Yamawaki, H. Fujihisa, M. Sakashita, and K. Aoki, *Phys. Rev. B*, **68**, 014106 (2003).

25) Infrared observation of the phase transitions of ice at low temperatures and pressures up to 50 GPa and the metastability of low-temperature ice VII.

M. Song M, H. Yamawaki, H. Fujihisa, M. Sakashita, and K. Aoki, *Phys. Rev. B*, **68**, 024108 (2003).

26) Raman spectroscopy and heat capacity measurement of calcium ferrite type $MgAl_2O_4$ and $CaAl_2O_4$.

H. Kojitani, K. Nishimura, A. Kubo, M. Sakashita, K. Aoki, and M. Akaogi, *Phys. Chem. Minerals*, **30**, 409-415 (2003).

27) Powder X-ray diffraction study of the volume change of ice VIII under high pressure.

H. Yamawaki, H. Fujihisa, M. Sakashita, A. Nakayama, and K. Aoki,

Physica B*: Condens. Matter*, **344**, 260-264 (2004).

28) Microscopic structure of nanometer-sized silica particles.

T. Uchino, A. Aboshi, S. Kohara, Y. Ohishi, M. Sakashita, and K. Aoki, *Phys. Rev. B*, **69**, 155409 (2004).

29) Molecular dissociation and two low-temperature high-pressure phases of H_2S.

H. Fujihisa, H Yamawaki, M. Sakashita, A. Nakayama, T. Yamada, and K. Aoki, *Phys. Rev. B*, **69**, 214102 (2004)